



Measurement of W^\pm boson production in Pb+Pb collisions at $\sqrt{s_{NN}} = 5.02$ TeV with the ATLAS detector

ATLAS Collaboration*

CERN, 1211 Geneva 23, Switzerland

Received: 25 July 2019 / Accepted: 25 October 2019 / Published online: 18 November 2019
© CERN for the benefit of the ATLAS collaboration 2019

Abstract A measurement of W^\pm boson production in Pb+Pb collisions at $\sqrt{s_{NN}} = 5.02$ TeV is reported using data recorded by the ATLAS experiment at the LHC in 2015, corresponding to a total integrated luminosity of 0.49 nb^{-1} . The W^\pm bosons are reconstructed in the electron or muon leptonic decay channels. Production yields of leptonically decaying W^\pm bosons, normalised by the total number of minimum-bias events and the nuclear thickness function, are measured within a fiducial region defined by the detector acceptance and the main kinematic requirements. These normalised yields are measured separately for W^+ and W^- bosons, and are presented as a function of the absolute value of pseudorapidity of the charged lepton and of the collision centrality. The lepton charge asymmetry is also measured as a function of the absolute value of lepton pseudorapidity. In addition, nuclear modification factors are calculated using the W^\pm boson production cross-sections measured in pp collisions. The results are compared with predictions based on next-to-leading-order calculations with CT14 parton distribution functions as well as with predictions obtained with the EPPS16 and nCTEQ15 nuclear parton distribution functions. No dependence of normalised production yields on centrality and a good agreement with predictions are observed for mid-central and central collisions. For peripheral collisions, the data agree with predictions within 1.7 (0.9) standard deviations for W^- (W^+) bosons.

1 Introduction

Collisions of lead ions in the Large Hadron Collider (LHC) allow the formation of a hot and dense medium with temperatures significantly exceeding the critical temperature for a phase transition from ordinary to strongly interacting matter [1]. Experiments at the Relativistic Heavy Ion Collider (RHIC) at lower energies than the LHC established that strongly interacting matter takes the form of a quark–gluon plasma (QGP) [2–5]. Particles carrying colour charge pro-

duced in hard interactions of quarks and gluons in the initial stages of a nuclear collision lose energy while traversing the QGP, leading to the phenomenon of jet quenching [6, 7]. This phenomenon was established by the observation of the suppression of charged-hadron yields in heavy-ion collisions, which was reported by experiments both at RHIC and the LHC, see e.g. Refs. [8–12]. Other studies related to jet quenching include LHC measurements of the suppression of inclusive jet yields [13, 14], dijet transverse momentum imbalance [15, 16] and modifications to the jet fragmentation [17, 18].

At all stages of QGP evolution, colourless elementary particles created in hard scatterings are expected to interact only weakly with the medium, which makes them excellent probes of the very initial stage of the collision. Moreover, in heavy-ion collisions energetic particles are produced in the interaction between nucleons in the nuclei. The latter are complex objects, so the geometry of the collision plays a central role in the interpretation of the experimental results. The RHIC experiments measured the properties of highly energetic (virtual) photons [19, 20] in Au+Au collisions and found that their production rates scale with the nuclear thickness. At the LHC, the ATLAS and CMS experiments measured the production of isolated prompt photons [21, 22], Z [23, 24] and W^\pm bosons [25, 26] in lead–lead (Pb+Pb) collisions at $\sqrt{s_{NN}} = 2.76$ TeV. In addition, the forward production of Z bosons was measured by the ALICE experiment in Pb + Pb collisions at $\sqrt{s_{NN}} = 5.02$ TeV [27]. The production rates of electroweak (EW) vector bosons were found to be unaffected by the presence of the QGP, and in agreement with the expectations from the collision geometry.

Production of EW bosons is an important benchmark process at hadron colliders. Measurements in proton–proton (pp) collisions at $\sqrt{s} = 5.02, 7, 8$ and 13 TeV at the LHC [28–33] and at previous colliders at lower energies [34, 35] are well described by calculations based on higher-order perturbative quantum chromodynamics (QCD) and the theory of EW interactions. At leading order, W^\pm bosons are preferentially produced in $u\bar{d} \rightarrow W^+$ and $d\bar{u} \rightarrow W^-$ processes [36].

* e-mail: atlas.publications@cern.ch

In Pb + Pb collisions, due to the different proportions of u and d quarks in the proton compared to the lead nucleus, the individual W^+ and W^- production rates are expected to be modified – which is often referred to as the isospin effect – but not their sum. Furthermore, EW boson production is sensitive to the parton distribution functions (PDF) which define the initial kinematics of the hard process. In Pb + Pb collisions, production of W^\pm bosons may differ from that in pp collisions due to effects arising from the presence of the bound nucleons in the nucleus. The measurements of W^\pm boson production in heavy-ion collisions therefore offer an opportunity to extract valuable information about nuclear modifications to the free-nucleon PDF [37–40].

Leptonic W^\pm boson decays are of particular interest, since the charged leptons are expected to not interact substantially with the QGP. Differences between the angular distributions of the W^+ and W^- boson decay products and the different relative yields of W^+ and W^- bosons produced in Pb+Pb and pp collisions can be explored using lepton charge asymmetry. This observable is defined as the difference between the differential yields of positively and negatively charged leptons divided by their sum, expressed as a function of the charged-lepton pseudorapidity (η_ℓ ¹):

$$A_\ell(\eta_\ell) = \frac{dN_{W^+ \rightarrow \ell^+ \nu} / d\eta_\ell - dN_{W^- \rightarrow \ell^- \bar{\nu}} / d\eta_\ell}{dN_{W^+ \rightarrow \ell^+ \nu} / d\eta_\ell + dN_{W^- \rightarrow \ell^- \bar{\nu}} / d\eta_\ell}.$$

In the measurement of the asymmetry as a function of η_ℓ , several systematic effects are reduced significantly in the ratio.

In a nucleus–nucleus (A+A) collision in the absence of nuclear effects, the number of events of a hard process X (N_X) is proportional to the pp cross-section for this process (σ_X^{pp}) scaled by factors related to the A+A collision geometry. These geometric parameters can be estimated using the Glauber approach [41, 42] as detailed in Sect. 3.1. An effective nucleon–nucleon (NN) cross-section for the process X in A+A collisions, further referred to as normalised production yield, can be defined using the total number of inelastic A+A collisions (N_{evt}) and the mean nuclear thickness function ($\langle T_{AA} \rangle$) (defined as the mean number of binary collisions divided by the total inelastic NN cross-section):

$$\sigma_X^{\text{NN}} = \frac{N_X}{N_{\text{evt}} \cdot \langle T_{AA} \rangle}. \quad (1)$$

This expression allows a direct comparison between the production yields in heavy-ion collisions and the pp cross-

section for the same hard process. Differences between σ_X^{NN} and σ_X^{pp} may arise due to nuclear effects including the isospin effect and inaccuracies in the description of the nuclear geometry. These differences are usually quantified using the nuclear modification factor defined as:

$$R_{AA} = \sigma_X^{\text{NN}} / \sigma_X^{pp}. \quad (2)$$

In this paper, the first measurement of W^\pm boson production yields in the electron and muon decay channels in Pb + Pb collisions at $\sqrt{s_{\text{NN}}} = 5.02$ TeV is presented. The data sample was collected in 2015 and corresponds to an integrated luminosity of 0.49 ± 0.03 nb⁻¹. The normalised fiducial production yields are measured separately for W^+ and W^- bosons. Then, the nuclear modification factors are extracted using production cross-sections in pp collisions at the same centre-of-mass energy taken from Ref. [28]. The lepton charge asymmetry is measured as a function of the absolute value of the charged-lepton pseudorapidity. The results are compared with predictions based on next-to-leading-order (NLO) QCD calculations with the use of CT14 NLO [43] PDFs (accounting for the isospin effect) and two sets of predictions including nuclear modifications: EPPS16 [44] and nCTEQ15 [45].

This paper is organised as follows. The ATLAS detector is introduced in Sect. 2. The data and simulated event samples are described in Sect. 3. A brief discussion of the data analysis procedure and systematic uncertainties is given in Sect. 4. The results are presented in Sect. 5 and the paper is summarised in Sect. 6.

2 The ATLAS detector

The ATLAS detector [46] at the LHC covers nearly the entire solid angle around the collision point. It consists of an inner tracking detector surrounded by a thin superconducting solenoid, electromagnetic and hadronic calorimeters and a muon spectrometer incorporating three large superconducting toroidal magnets.

The inner-detector system (ID) is immersed in a 2 T axial magnetic field and provides charged-particle tracking in the range $|\eta| < 2.5$. A high-granularity silicon pixel detector including the insertable B-layer installed before Run 2 [47, 48] covers the vertex region and is followed by a silicon microstrip tracker. These silicon detectors are complemented by a transition radiation tracker, which enables radially extended track reconstruction up to $|\eta| = 2.0$.

The calorimeter system covers the pseudorapidity range $|\eta| < 4.9$. Within the region $|\eta| < 3.2$, electromagnetic (EM) calorimetry is provided by high-granularity lead/liquid-argon (LAr) calorimeters, with an additional thin LAr pre-sampler covering $|\eta| < 1.8$ to correct for energy loss in

¹ ATLAS uses a right-handed coordinate system with its origin at the nominal interaction point (IP) in the centre of the detector and the z -axis along the beam pipe. The x -axis points from the IP to the centre of the LHC ring, and the y -axis points upward. Cylindrical coordinates (r, ϕ) are used in the transverse plane, ϕ being the azimuthal angle around the z -axis. The pseudorapidity is defined in terms of the polar angle θ as $\eta = -\ln \tan(\theta/2)$.

material upstream of the calorimeters. The EM calorimeter is divided into a barrel section covering $|\eta| < 1.475$ and two endcap sections covering $1.375 < |\eta| < 3.2$. Hadronic calorimetry is provided by a steel/scintillator-tile calorimeter, segmented into three barrel structures within $|\eta| < 1.7$ and two copper/LAr hadronic endcap calorimeters. The solid-angle coverage is completed with copper/LAr and tungsten/LAr forward calorimeter modules (FCal) in $3.1 < |\eta| < 4.9$, optimised for electromagnetic and hadronic measurements, respectively.

The muon spectrometer (MS) comprises separate trigger and high-precision tracking chambers measuring the deflection of muons in the magnetic field generated by the toroidal magnets. The field integral of the toroids ranges between 2.0 and 6.0 Tm across most of the detector. A set of precision chambers covers the region $|\eta| < 2.7$ with three layers of monitored drift tubes, complemented by cathode-strip chambers in the forward region. The muon trigger system uses resistive-plate chambers in the barrel ($|\eta| < 1.05$), and thin-gap chambers in the endcap ($1.05 < |\eta| < 2.4$) regions.

Two zero-degree calorimeters (ZDC), situated at approximately ± 140 m from the nominal IP, detect neutral particles, mostly neutrons and photons, with $|\eta| > 8.3$. The ZDC use tungsten plates as absorbers, and quartz rods sandwiched between the tungsten plates as the active medium.

In 2015, the ATLAS detector had a two-level trigger system [49]. The level-1 trigger is implemented in custom hardware and uses a subset of detector information to reduce the event rate to a value of at most 100 kHz. This is followed by a software-based high-level trigger which further reduces the rate in order to record events to disk at about 1 kHz.

3 Data and simulated event samples

3.1 Data sample and event centrality

This analysis is based on the full set of Pb + Pb collision data collected by the ATLAS experiment in 2015 at a centre-of-mass energy of $\sqrt{s_{\text{NN}}} = 5.02$ TeV and corresponds to an integrated luminosity of 0.49 nb^{-1} .

In heavy-ion measurements, centrality classes represent the percentiles of the total inelastic non-Coulombic cross-section excluding diffractive contributions [50], and reflect the overlap volume of the two colliding nuclei. In the ATLAS experiment, the centrality of Pb + Pb events is defined using the total transverse energy measured in the FCal, which is evaluated at the electromagnetic scale and denoted by $\text{FCal } \Sigma E_{\text{T}}$. Geometric parameters, such as the average number of inelastically interacting nucleons in both colliding nuclei, $\langle N_{\text{part}} \rangle$, and the average nuclear thickness function, $\langle T_{\text{AA}} \rangle$, and their systematic uncertainties are obtained from

Table 1 Geometric parameters extracted from the MC Glauber code v2.4 for different centrality classes in 2015 Pb + Pb data. Average numbers of inelastically interacting nucleons $\langle N_{\text{part}} \rangle$ and mean values of the nuclear thickness function (T_{AA}) are listed with their absolute and relative uncertainties

Centrality (%)	$\langle N_{\text{part}} \rangle$	$\delta \langle N_{\text{part}} \rangle$ (%)	$\langle T_{\text{AA}} \rangle$ [1/mb]	$\delta \langle T_{\text{AA}} \rangle$ (%)
0–2	399.0 ± 1.2	0.30	28.30 ± 0.25	0.88
2–4	380.2 ± 2.0	0.53	25.47 ± 0.21	0.82
4–6	358.9 ± 2.4	0.67	23.07 ± 0.21	0.91
6–8	338.1 ± 2.7	0.80	20.93 ± 0.20	0.96
8–10	317.8 ± 2.9	0.91	18.99 ± 0.19	1.0
10–15	285.2 ± 2.9	1.0	16.08 ± 0.18	1.1
15–20	242.9 ± 2.9	1.2	12.59 ± 0.18	1.4
20–25	205.6 ± 2.9	1.4	9.77 ± 0.18	1.8
25–30	172.8 ± 2.8	1.6	7.50 ± 0.17	2.3
30–40	131.4 ± 2.6	2.0	4.95 ± 0.15	3.0
40–50	87.0 ± 2.4	2.8	2.63 ± 0.11	4.2
50–60	53.9 ± 2.0	3.7	1.28 ± 0.07	5.8
60–80	23.0 ± 1.3	5.7	0.39 ± 0.03	8.2
0–80	141.3 ± 2.1	1.5	7.00 ± 0.11	1.6

the Glauber model [42] and assigned to each centrality class by matching them to the modelled FCal ΣE_{T} distribution.

The centrality determination for the 2015 Pb + Pb dataset follows a procedure similar to that used for lower-energy Pb + Pb data in ATLAS, which is described in Ref. [51]. In that procedure, the set of Pb + Pb collision geometries is defined via the Glauber model, using the Monte Carlo Glauber (MC Glauber) code v2.4 [52], an inelastic nucleon–nucleon cross-section of $\sigma_{\text{tot}}^{\text{NN}} = 70 \pm 5$ mb at $\sqrt{s_{\text{NN}}} = 5.02$ TeV, and a single Woods–Saxon distribution for the nucleon radial profile. The modelled FCal ΣE_{T} distribution is matched with the distribution measured in minimum-bias (MB) data selected with $\text{FCal } \Sigma E_{\text{T}} > 40$ GeV. This FCal ΣE_{T} selection ensures that contributions from photonuclear and diffractive events in the fit range are negligible. Table 1 lists the values of the $\langle N_{\text{part}} \rangle$ and $\langle T_{\text{AA}} \rangle$ parameters with their uncertainties in different centrality classes used in this analysis.

For consistency with other heavy-ion measurements from the ATLAS Collaboration, this analysis uses the binning in FCal ΣE_{T} and geometric parameters determined from the MC Glauber code v2.4 as the default. Recently, an updated version of the MC Glauber code, v3.2, became available with several suggested improvements in the geometric modelling. These improvements are described in Ref. [53] and include a lower value of $\sigma_{\text{tot}}^{\text{NN}}$ at $\sqrt{s_{\text{NN}}} = 5.02$ TeV with a smaller uncertainty (67.6 ± 0.5 mb), separate radial distributions for protons and neutrons in the nucleus, and other improvements in the determination of nucleon positions within the nucleus.

To reassess the scaling of boson yields within this improved model of the Pb + Pb collision geometry, the centrality determination is performed following the same procedure as described in Ref. [51] but using an alternative set of Pb + Pb events generated with the MCGlauber code v3.2. The fit to the FCal ΣE_T distribution in data results in a larger estimate (by 0.6%) for the fraction of inelastic Pb + Pb events being contained in MB events selected with FCal $\Sigma E_T > 40$ GeV. Because of the increased fraction of inelastic Pb + Pb events in the FCal ΣE_T range used for the fit, each centrality range is mapped to a systematically higher range of FCal ΣE_T values, and the number of MB Pb + Pb events in each centrality selection is lower by approximately 0.6%. Furthermore, the estimated value of $\langle T_{AA} \rangle$ in the centrality classes is lower by 1% in the most central events but higher by 6–7% in the most peripheral classes, consistent with the change in $\langle T_{AA} \rangle$ found in Ref. [53]. The systematic uncertainties of $\langle T_{AA} \rangle$ are determined following procedures identical to the MCGlauber code v2.4 case [51], but with a smaller $\sigma_{\text{tot}}^{\text{NN}}$ variation of ± 0.5 mb. The binning in FCal ΣE_T and geometric parameters determined from the MCGlauber code v3.2 are used only for comparison with the MCGlauber code v2.4.

3.2 Monte Carlo simulation of signal and background events

Samples of Monte Carlo (MC) simulated events were used to evaluate the selection efficiencies and to model the properties of signal and background processes. The response of the ATLAS detector was simulated using the GEANT4 framework [54,55]. Signal processes, i.e. the W^\pm boson production and leptonic decays, were modelled with the POWHEG-BOX v2 event generator [56,57] interfaced to PYTHIA 8.186 [58] to model parton showering and fragmentation processes. The CT10 PDF set [59] evaluated with NLO accuracy was used to set the initial kinematics for the matrix-element calculation. Events produced in EW background processes ($W^\pm \rightarrow \tau^\pm \nu$, $Z \rightarrow \mu^+ \mu^-$, $Z \rightarrow e^+ e^-$, $Z \rightarrow \tau^+ \tau^-$) were generated with the same generator set-up. To model the production of top-quark pairs ($t\bar{t}$), the POWHEG-BOX v2 event generator [60] was used with the CT10f4 PDF set [59] in the matrix element. For $t\bar{t}$ production, the parton shower and fragmentation were simulated using PYTHIA 6.428 [61]. More details of the event generator set-up for all considered processes can be found in Ref. [28], where the same configurations were used.

MC subsamples were produced separately for pp , pn , np , and nn collisions and a weighting procedure was applied to combine all subsamples as described here. For each subprocess of interest, a global event weight was derived: it is based on the mass ($A = 208$) and atomic ($Z = 82$) numbers of the colliding lead nuclei, and on the total number of generated events. This corresponds to a fraction of all

nucleon-nucleon collisions of $f_{pp} = (Z/A)^2 = 15.5\%$ for pp , $f_{pn} = f_{np} = Z(A-Z)/A^2 = 23.9\%$ for pn or np , and $f_{nn} = [(A-Z)/A]^2 = 36.7\%$ for nn . The global event weight for each subprocess is calculated as the ratio of the number of expected events to the number of generated events:

$$w = \frac{\langle T_{AA} \rangle^{0-80\%} \cdot N_{\text{evt, MB}}^{0-80\%} \cdot \sigma_{ij}}{N_{\text{gen, ij}}^{0-80\%}} f_{ij},$$

where f_{ij} stands for f_{pp} , $f_{pn,np}$ or f_{nn} , $N_{\text{gen, ij}}^{0-80\%}$ is the number of generated events for the given subprocess in the 0–80% centrality class (see Sect. 3.1), $N_{\text{evt, MB}}^{0-80\%}$ is the total number of MB events in the 0–80% centrality class, and σ_{ij} is the production cross-section for the given subprocess. If not stated otherwise, theoretical predictions presented in this paper are calculated using fixed fractions of pp , pn , np , and nn collisions. For the background subtraction procedure, W^\pm and Z boson production cross-sections are scaled to NNLO accuracy using DYNNLO [62,63] calculations with the CT14 NNLO PDF set [43]. The scaling factors take the following values: 1.026 for W^+ , 1.046 for W^- , and 1.007 for Z boson production. It should be noted that the DYNNLO code supports calculations only for the pp isospin combination. For other isospin combinations, the same scaling as for pp collisions is assumed.

In order to study detector performance in conditions that match the data, the simulated events were embedded into experimental data taken during the 2015 Pb + Pb run. This data-overlay procedure ensures an accurate description of the underlying event in the MC simulation, and additionally provides detector conditions matching those of Pb+Pb data-taking periods. Events used in the overlay procedure were recorded using a dedicated set of MB triggers and total ΣE_T triggers, which were used to enhance the rate of more central events.

4 Data analysis

4.1 Object definitions and event selection

Candidate events with W^\pm boson production are required to have only one primary vertex reconstructed from at least three tracks with a transverse momentum, p_T , larger than 400 MeV, and to pass a trigger selection, which requires a single electron or muon candidate with a p_T threshold of 15 GeV or 8 GeV, respectively. In addition, the electron trigger applies a loose identification requirement [64] and the underlying-event contribution to the energy deposits in calorimeter cells is subtracted [65].

In events assigned to the 50–80% centrality classes, an additional selection is made using the ZDC in order to sup-

press EM background contributions. Events with at least one neutron detected in each arm of the ZDC are accepted, and the fraction of rejected events is about 0.4% in both the electron and muon channels.

A small fraction of the selected events contain more than one inelastic interaction (pile-up). The anti-correlation between the FCal ΣE_T and the number of neutrons detected in the ZDC is used to suppress pile-up events. Events with a number of ZDC neutrons much higher than the number expected from the bulk of events for a given value of FCal ΣE_T are rejected. The fraction of rejected events is about 0.4% in both the electron and muon channels, and is constant across centrality classes.

The electron trigger efficiency is 99% for peripheral events and slowly decreases to 96% for central events. The muon trigger efficiency in the endcap region of the detector is $\sim 90\%$ and in the barrel region it varies from 60 to 80%. No dependence on detector occupancy (centrality) is found.

Electron candidates are reconstructed using information from tracking detectors and the EM calorimeter [64]. They are required to have $p_T^\ell > 25$ GeV and $|\eta_\ell| < 2.47$. Candidates falling in the transition region between barrel and endcap calorimeters ($1.37 < |\eta_\ell| < 1.52$) are rejected. In addition, isolation and ‘medium’ likelihood-based identification requirements [64] optimised for Pb + Pb collisions as a function of centrality are applied. Muon candidates are reconstructed by combining tracks measured in the ID with tracks measured in the MS [66], and must satisfy $p_T^\ell > 25$ GeV and $|\eta_\ell| < 2.4$. In addition, muons have to pass the requirements of ‘medium’ identification and of a dedicated isolation selection [66].

The electron energy calibration is primarily obtained from the simulation by employing multivariate techniques [67]. Residual corrections to the energy scale and resolution are determined from data by comparing the measured $Z \rightarrow e^+e^-$ invariant mass distribution to the one predicted by the simulation [67]. This procedure was found to be sensitive to the pile-up distribution in data due to different settings used for the signal readout from the EM calorimeters [68]. Therefore, a special set of energy scale correction factors was derived for the 2015 Pb+Pb dataset. Measurements of muon momenta can be biased by the detector alignment and resolution, distortions of the magnetic field or imprecise estimates of the amount of passive material in the detector. Corrections of the muon momentum scale and resolution, which are applied to the simulation, are derived using $Z \rightarrow \mu^+\mu^-$ events [66].

Events with W^\pm boson candidates are selected by requiring an electron or a muon that is matched to a lepton selected at the trigger level. The (anti-)neutrinos from $W^\pm \rightarrow \ell^\pm\nu$ decays escape direct detection. A measure of the neutrino transverse momentum, p_T^ν , can be inferred from the global event momentum imbalance in the plane transverse to the

beam axis. In heavy-ion collisions, low- p_T particle production is significantly enhanced compared to pp collisions, thereby resulting in a resolution of missing transverse momentum obtained from calorimeter cells that is much worse than in pp collisions. In the most central Pb + Pb collisions at $\sqrt{s_{NN}} = 2.76$ TeV, the resolution reaches as much as 45 GeV [25] due to enhanced contributions from the underlying event, while for $\sqrt{s_{NN}} = 5.02$ TeV, it is expected to be even larger because of increased underlying-event activity. Therefore, tracks are used instead of calorimeter cells, as low- p_T tracks from the underlying event can be suppressed more easily. The missing transverse momentum vector, p_T^{miss} , is defined as the negative vector sum of the ID-track transverse momenta, excluding good leptons with a poor-quality ID track. In the case of electrons, the calorimeter energy measurement is used, while for muons the p_T determined from a combined reconstruction using ID and MS hits is used. This approach is analogous to the one developed in pp collisions [69]. In order to minimise the noise contribution from the underlying event while retaining sensitivity to the contribution from the hard-scattering process, only tracks with $p_T > 4$ GeV are used in the calculation of p_T^{miss} . The transverse mass of the lepton– p_T^{miss} system is defined as:

$$m_T = \sqrt{2p_T^\ell p_T^{\text{miss}} (1 - \cos \Delta\phi)},$$

where $\Delta\phi$ is the azimuthal angle between p_T^ℓ and p_T^{miss} vectors. The W^\pm boson candidates are required to have $p_T^{\text{miss}} > 25$ GeV and $m_T > 40$ GeV.

The background contribution from $Z \rightarrow \ell^+\ell^-$ decays is further suppressed by imposing a Z-veto requirement. Events with at least two leptons of the same flavour which form an opposite-charge pair with an invariant mass above 66 GeV are rejected. These events are selected by requiring that one lepton in the pair has $p_T > 25$ GeV and fulfils all other quality criteria discussed above, while the other lepton in the pair passes a lower p_T threshold of 20 GeV with looser quality requirements.

4.2 Background estimation

Background processes that contribute to the W^\pm boson production measurement are EW processes producing $W^\pm \rightarrow \tau^\pm\nu$, $Z \rightarrow \ell^+\ell^-$ and $Z \rightarrow \tau^+\tau^-$ decays, as well as top-quark production and multi-jet processes. The multi-jet background includes various processes such as semileptonic decays of heavy-flavour hadrons or in-flight decays of kaons and pions for the muon channel, and photon conversions or misidentified hadrons for the electron channel.

The background contributions from EW production are evaluated using simulated event samples described in Sect. 3. They are normalised according to their expected number of

events in the data evaluated from Eq. (1) using production cross-sections scaled to NNLO accuracy. It is found that the contributions from $Z \rightarrow \ell^+\ell^-$ and $W^\pm \rightarrow \tau^\pm\nu$ processes dominate. In the electron channel, they amount to 4.1% and 1.6%, respectively, for electrons, while for positrons, these fractions are 4.2% and 1.5%, respectively. In the muon channel, they amount to 3.0% and 1.9%, respectively, of the event sample selected with negative muons, while for positive muons, these fractions are 3.1% and 1.8%, respectively.

The background contributions from $t\bar{t}$ production are also evaluated using MC simulation. They are estimated to be at the level of 0.1% for electrons and 0.2% for muons. Contributions from the production of single top quarks and dibosons, which are even smaller, are neglected.

A large fraction of multi-jet background events are rejected by the lepton isolation requirement and the p_T^{miss} selection. However, the very large production cross-sections for multi-jet processes make their contribution to the selected event sample significant. This contribution is estimated using template fits to p_T^ℓ distributions for $p_T^\ell > 20$ GeV following a method similar to the one described in Refs. [28, 70]. Template distributions enriched in events from multi-jet background processes are taken from data by selecting events with non-isolated leptons, while templates for the signal and other background processes are extracted from the MC simulation. The variable used to determine the isolation of electrons and muons is, however, correlated with p_T^ℓ for multi-jet events, modifying the p_T^ℓ distribution shape for non-isolated leptons relative to that for isolated leptons. Therefore, prior to the fit, the shape of the multi-jet background template in p_T^ℓ is corrected, so that it more closely matches the shape of the multi-jet background distribution passing the signal isolation selection. The correction procedure is given below for the muon channel. In the case of the electron channel, all steps of the procedure are similar.

The events with non-isolated muons are divided into subsamples defined by ranges of 0.1 unit in a track-based isolation variable, p_T^{iso}/p_T^μ , where p_T^{iso} is the sum of track transverse momenta in a cone around the muon. From each of the subsamples, a multi-jet background template is extracted. The evolution of the template shapes is summarised in Fig. 1, which shows ratios of self-normalised p_T^μ distributions for different templates. The ratios are taken between templates from ranges of p_T^{iso}/p_T^μ which have centres separated by 0.3 units. The average of the ratios, r , is then used as a weight to correct the distribution shape of the multi-jet background:

$$N_{\text{MJ}}^{\text{template}}(p_T^\mu) = N_{\text{MJ}}^{\text{uncorrected}}(p_T^\mu) \cdot r (p_T^\mu)^{d/0.3}.$$

The weight r is modified using the ratio of the distance d between the centre of a given p_T^{iso}/p_T^μ range and the mean value of the signal isolation (determined from MC simulation) to the distance of 0.3 units between centres of p_T^{iso}/p_T^μ

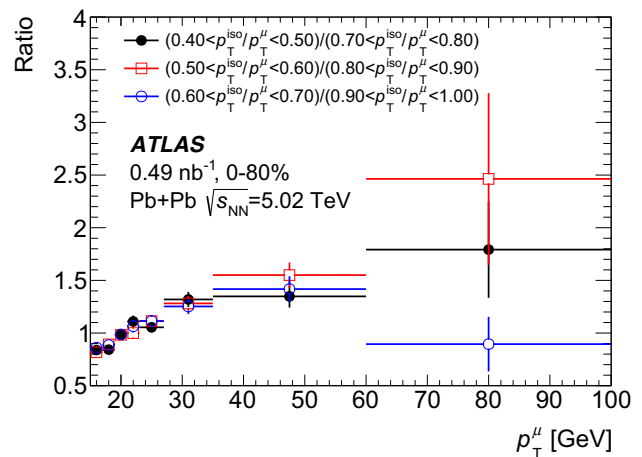


Fig. 1 Ratios of the p_T^μ distribution shape for multi-jet background templates extracted from different ranges of p_T^{iso}/p_T^μ . The ratios are taken between templates from ranges of p_T^{iso}/p_T^μ which have centres separated by 0.3 units. The error bars represent the statistical uncertainties

ranges used to determine the weight. This procedure ensures that the extracted multi-jet background yields are stable regardless of the exact definition of the non-isolated muons used to construct a template. In order to estimate the multi-jet background yield differentially in η_μ , the template fits are performed separately for each η_μ bin.

Events from multi-jet background processes are estimated to contribute up to about 20% and 12% to the event samples selected in the electron and muon channels, respectively. The multi-jet background fraction increases by about 10% of the total in central collisions compared with peripheral collisions in both electron and muon channels.

Figures 2 and 3 show the detector-level distributions of W^+ and W^- event candidates decaying in the electron and muon channels, respectively, as a function of lepton pseudorapidity, η_ℓ , and as a function of lepton transverse momentum, p_T^ℓ . Background contributions from QCD multi-jet production and from EW processes discussed above are also shown in the plots. Fairly good agreement is found between data and the sum of signal and background contributions. The non-smooth behaviour of the multi-jet background distributions is related to large statistical uncertainties of the templates, which are propagated through the background subtraction procedure to the final results.

4.3 Experimental corrections

The $W^\pm \rightarrow \ell^\pm\nu$ production yields in the electron and muon decay channels are measured in a fiducial phase-space region defined as:

$$p_T^\ell > 25 \text{ GeV}, |\eta_\ell| < 2.5, p_T^\nu > 25 \text{ GeV}, m_T > 40 \text{ GeV},$$

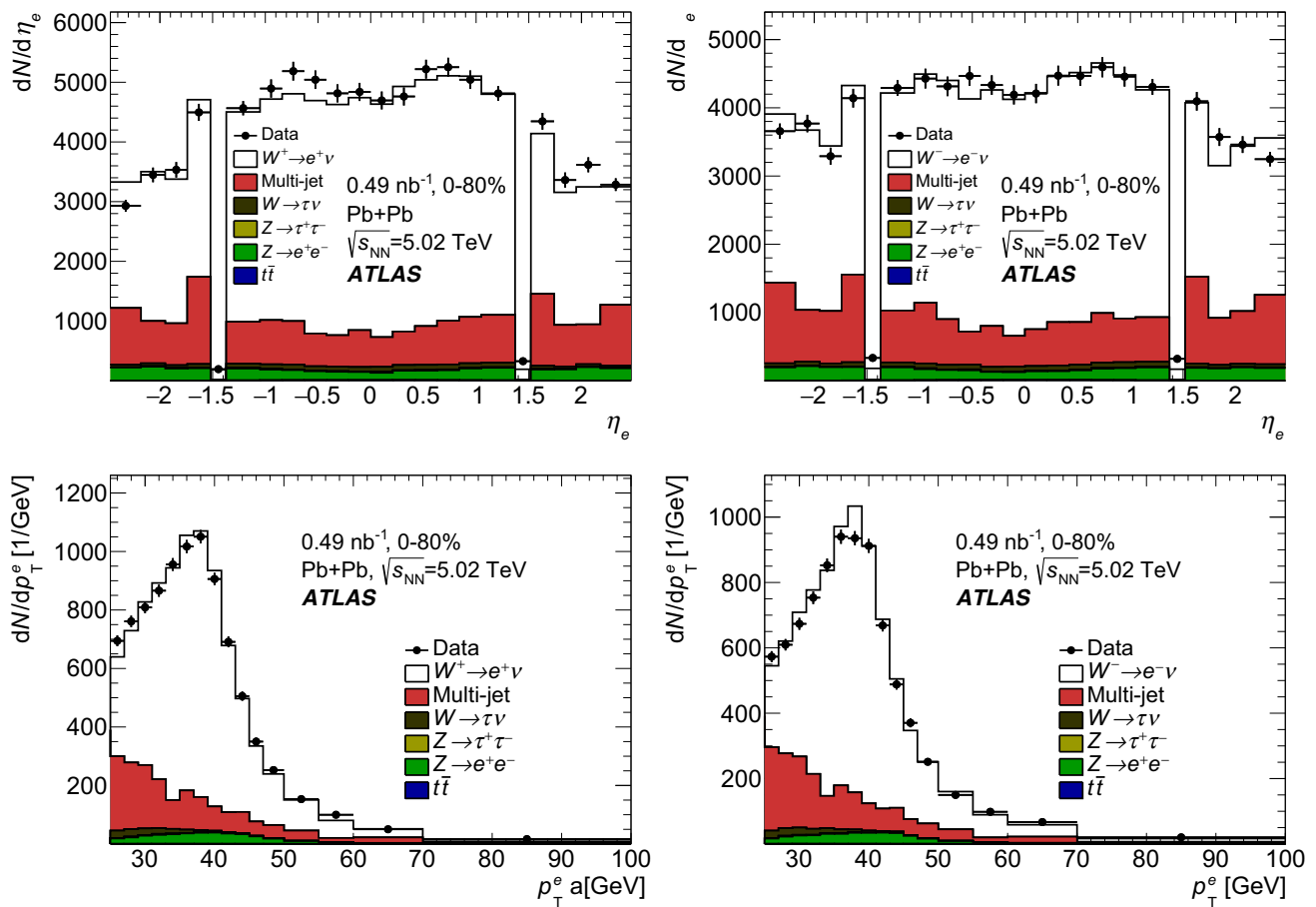


Fig. 2 Detector-level distributions of W^+ (left) and W^- (right) event candidates decaying in the electron channels after all selection requirements as a function of the electron pseudorapidity (top) and transverse momentum (bottom). The contributions of EW and top-quark backgrounds are normalised according to their expected number of events

in the data, while the contribution of QCD multi-jet background is normalised using a template fit to the p_T^e distribution. Distributions are presented for the 0–80% centrality class. The error bars represent the statistical uncertainties

where $\ell = e, \mu$ stands for the electron or muon, p_T^ν is the transverse momentum of the respective (anti)neutrino and m_T is the transverse mass of the lepton and neutrino system. To correct for QED final-state emissions, the lepton kinematics are evaluated before photon radiation.

The $W^\pm \rightarrow \ell^\pm \nu$ event yields are extracted in each bin of η_ℓ and centrality using the formula:

$$N_W = \frac{N_W^{\text{obs}} - N_W^{\text{bkg}}}{C_W},$$

where N_W^{obs} and N_W^{bkg} are the numbers of observed and background events, respectively, and C_W denotes bin-by-bin correction factors, which are evaluated using the signal MC simulation in bins of η_ℓ and centrality, accounting for differences between data and MC simulation as described below. The correction factors are determined separately for each lepton charge and each decay channel, and are defined as:

$$C_W(\eta_\ell^{\text{reco}}, \text{centrality}) = \frac{N_W^{\text{sel, pass}}(\eta_\ell^{\text{reco}}, \text{centrality})}{N_W^{\text{sel, gen}}(\eta_\ell^{\text{true}}, \text{centrality})},$$

with $N_W^{\text{sel, pass}}$ being the sum of event weights for events that fulfil the detector-level selection criteria described in Sect. 4.1, while $N_W^{\text{sel, gen}}$ denotes the sum of event weights for events selected in the generator-level fiducial phase space. The C_W correction factors account for differences between selections applied to the reconstructed lepton pseudorapidity, η_ℓ^{reco} , and the true pseudorapidity, η_ℓ^{true} . These factors account also for the lepton reconstruction, identification, isolation, and trigger efficiencies, which are evaluated separately, as well as for the p_T^{miss} selection efficiency. Lepton efficiencies are measured in the data and determined in MC simulation using the tag-and-probe method in $Z \rightarrow \ell^+ \ell^-$ events in the Pb + Pb system [49, 64, 66]. They are evaluated as a function of the reconstructed η_ℓ and p_T^ℓ in the electron channel, while in the muon channel, they depend only on η_ℓ . Differences

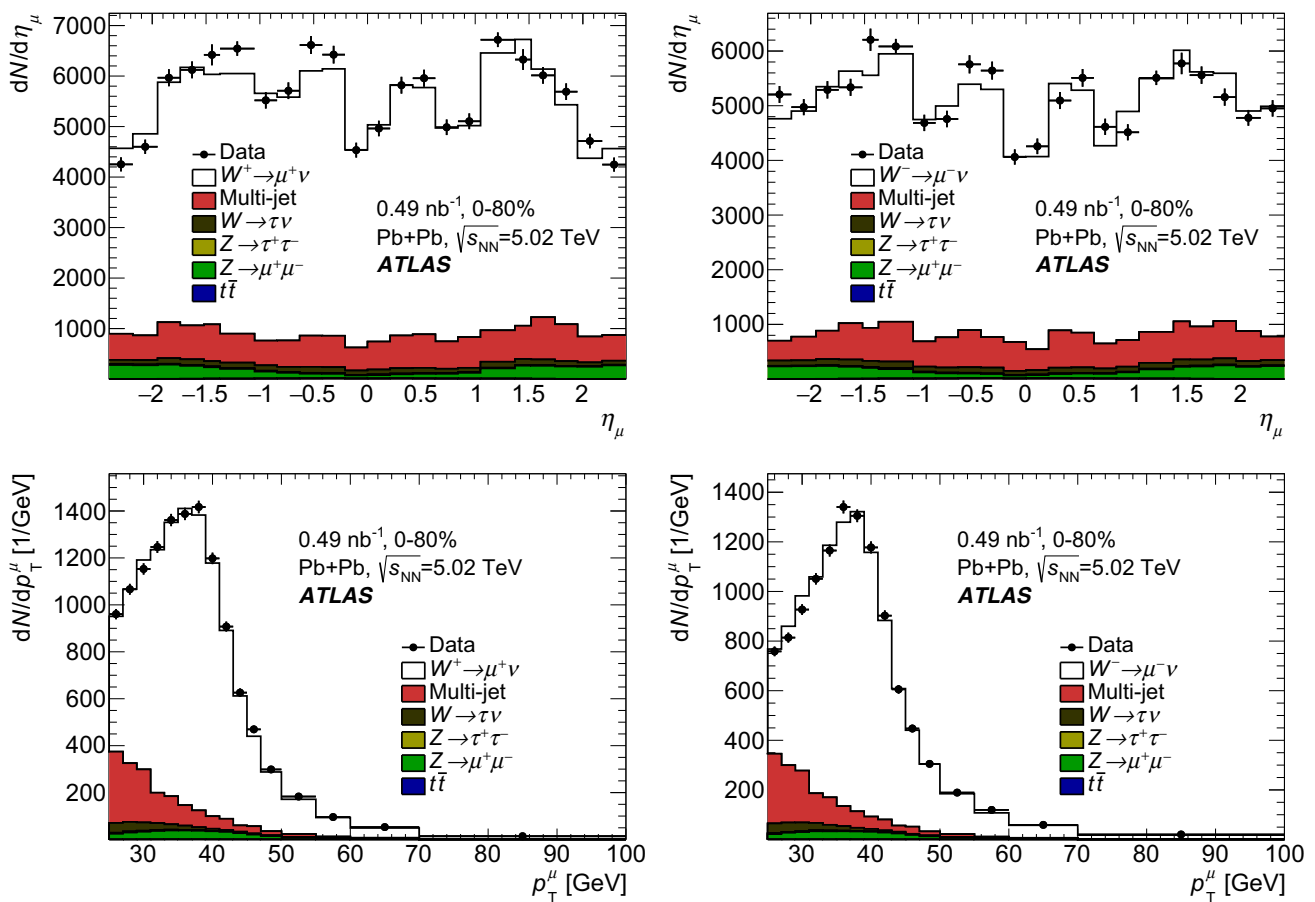


Fig. 3 Detector-level distributions of W^+ (left) and W^- (right) event candidates decaying in the muon channels after all selection requirements as a function of the muon pseudorapidity (top) and transverse momentum (bottom). The contributions of EW and top-quark backgrounds are normalised according to their expected number of events

in the data, while the contribution of QCD multi-jet background is normalised using a template fit to the p_T^μ distribution. Distributions are presented for the 0–80% centrality class. The error bars represent the statistical uncertainties

between efficiencies extracted from the data and MC simulation do not exceed a few percent. Scale factors used to correct the MC simulation are derived as ratios of efficiencies determined in data and simulation. Within the precision of the tag-and-probe method, no dependence of scale factors on centrality is observed. The reconstructed sum of event weights, $N_W^{\text{sel,pass}}$, is evaluated after correcting the simulation, such that the simulated detector response matches the response observed in data.

Figure 4 shows the C_W correction factors evaluated for positive electrons and muons as a function of η_ℓ and centrality in events from selected centrality ranges. A sizeable evolution with event centrality is observed for both channels. The centrality dependence is mainly driven by the p_T^{miss} resolution which deteriorates with increasing event activity. The usage of the data overlay procedure in production of the MC samples ensures a good description of the underlying event in the simulation. The p_T^{miss} resolution is also tested

with $Z \rightarrow \ell^+ \ell^-$ events as a function of centrality, and reasonably good agreement between p_T^{miss} distributions in the data and MC simulation is found. Residual differences are due to a misalignment of the ID. They are covered by the systematic uncertainty discussed in Sect. 4.4. The veto on $Z \rightarrow \ell^+ \ell^-$ decays also contributes to the change of the C_W correction factor in the most central events, where the rate of ‘loose’ quality leptons increases. The muon reconstruction and identification efficiencies are measured to be above 90% and not dependent on centrality. The efficiency of the muon isolation selection is measured to be $\sim 90\%$ in the barrel region and $\sim 96\%$ in the endcap region. This selection was optimised as a function of centrality, and therefore no dependence on detector occupancy is observed. The electron isolation efficiency depends on centrality and varies from $\sim 90\%$ in peripheral events to $\sim 75\%$ in the most central events. In the electron channel, a significant difference in the evolution of the C_W correction factor can be noticed

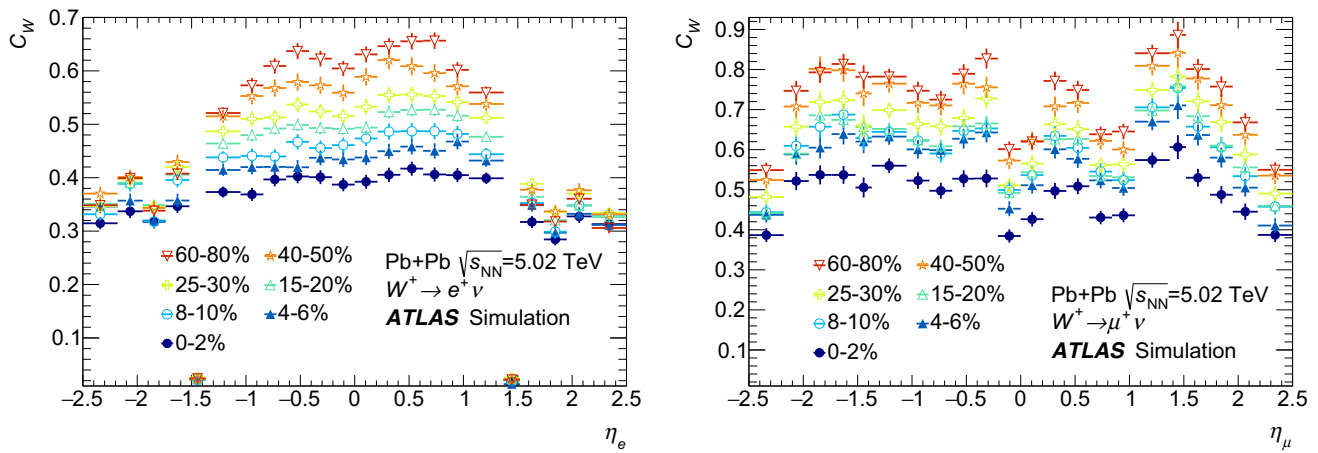


Fig. 4 Correction factor C_W for positive electrons (left) and positive muons (right) as a function of η_ℓ evaluated in selected centrality classes. The error bars represent the statistical uncertainties

between the central ($|\eta| < 1.37$) and forward pseudorapidities ($1.52 < |\eta| < 2.47$). That behaviour can be attributed to the electron reconstruction efficiency, which increases in the forward region as a function of centrality from $\sim 75\%$ to $\sim 95\%$ almost compensating for other effects, while in the barrel region it changes from ~ 90 to $\sim 95\%$. The increase in the reconstruction efficiency is caused by the increasing number of charged-particle tracks and a loose requirement on matching the track to the EM cluster. Finally, the electron identification is optimised to have a constant efficiency as a function of centrality and its value is above 80% . For negative electrons and muons, the C_W correction factors (not shown in the figure) are sensitive to the same effects and result in similar behaviour as a function of η_ℓ and centrality.

As shown in Eq. (1), particle production yields in heavy-ion collisions are often presented in terms of the number of counts per MB collision. The total number of MB collisions corresponding to the analysed dataset is extracted from a MB data sample as described in Ref. [51] and is equal to 2.99×10^9 collisions for the 0–80% centrality class. The N_{evt} values for centrality classes used in this analysis are derived as corresponding fractions of this number.

4.4 Systematic uncertainties

Systematic uncertainties of the measured observables are determined separately for electron and muon decay channels as well as for positive and negative lepton electric charges. They are estimated for each pseudorapidity bin and centrality class. The sources of systematic uncertainties considered are described below.

The uncertainties in the measurement of lepton reconstruction, identification, trigger and isolation efficiency scale factors are separated into statistical and systematic components. The statistical uncertainties of the scale factors are

propagated to the final results using a toy MC approach, while the systematic uncertainties are propagated in a fully correlated way across all lepton η_ℓ and p_T^ℓ bins. In the electron channel, the largest of these uncertainties is related to the electron identification efficiency measurement, which is limited by statistical precision and is at most 4% for yields measured as a function of η_ℓ . The dominant uncertainty in the muon channel comes from the measurement of muon trigger efficiency and varies between 2 and 4% for yields measured as a function of η_ℓ .

Systematic uncertainties related to electron energy calibration and muon momentum calibration are evaluated by varying scale and resolution corrections applied to the lepton candidates. The corresponding variations of measured yields are $\sim 0.1\%$ and their contribution to the systematic uncertainty is, therefore, neglected.

The resolution and background rejection power of the reconstructed p_T^{miss} depends on the contribution from low- p_T particles produced in the underlying event. In order to assess the impact of this contribution, the threshold for the p_T of ID tracks used in the p_T^{miss} calculation is varied in both the data and MC simulation from its nominal value of 4 GeV up and down by 1 GeV , and the full analysis is repeated. The higher track p_T threshold minimises the impact of the underlying event on the p_T^{miss} resolution but also removes tracks required to balance the transverse energy of the event. Studies performed in MB events showed that the 3 GeV p_T threshold introduces a bias in the mean values of the x and y components of p_T^{miss} . Therefore, the lower track p_T threshold introduces sources of spurious p_T^{miss} related to a larger contribution of soft particles from the underlying event. In addition, misalignment of the ID produces a charge-dependent bias in the measured p_T of tracks, which is specific to the analysed dataset. The bias is evaluated to be 2% for tracks with a p_T of about 40 GeV . Since the signal lepton track drives the

value of reconstructed p_T^{miss} , an uncertainty due to this bias is evaluated by varying the p_T^{miss} scale in data by $\pm 2\%$. This variation is applied in a correlated way to events with leptons of positive and negative charge. If an anti-correlated variation is used instead, the impact on the charge asymmetry measurement is found to be negligible. The total uncertainty in measured yields due to the p_T^{miss} reconstruction and ID misalignment varies as a function of centrality between 2 and 4% for the electron channel and between 1 and 3% for the muon channel.

An uncertainty varying from 2 to 8% in the electron channel and $\sim 2\%$ in the muon channel is associated with the data-driven estimation of the multi-jet background. The variation in the electron channel is η -dependent. A smaller effect is observed in the barrel region, while the 8% variation is observed in the endcap region where the fraction of the multi-jet background is significant. This uncertainty is partially estimated using systematic variations of the correction applied to the shape of the multi-jet background template. By default, the distance, d , used in the shape reweighting procedure described in Sect. 4.2 is defined relative to the mean value of the signal isolation. However, the width of the signal isolation region in $p_T^{\text{iso}}/p_T^{\mu}$ is non-negligible, and for systematic variations, d is recalculated relative to the boundaries of this region. In addition, the shape of the multi-jet background template is found to be dependent on η . The uncertainty due to this effect is estimated by comparing templates constructed using leptons from separate η regions (either barrel or endcap) to the nominal template. The contribution from residual differences in shapes to the total systematic uncertainty related to the multi-jet background estimation is 1–3% in the electron channel and $\sim 1\%$ in the muon channel. An additional uncertainty is related to the statistical precision of multi-jet background templates extracted from data. It is evaluated to be $\sim 2\%$ (barrel) and $\sim 4\%$ (endcap) in the electron channel and $\sim 2\%$ in the muon channel. The two independent components, representing systematic and statistical contributions to the uncertainty, are added in quadrature while reporting the total uncertainty.

Uncertainties in the estimation of EW and top-quark backgrounds are evaluated by varying their normalisation within the error of their cross-sections. These variations result in up to 0.5% uncertainty in the electron channel and up to 0.2% uncertainty in the muon channel.

The average nuclear thickness function, $\langle T_{AA} \rangle$, is used to normalise the W^{\pm} boson production yields. The $\langle T_{AA} \rangle$ uncertainties listed in Table 1 are used to vary the normalised yields. The resulting normalisation uncertainty ranges from 0.9% in the most central collisions to 8.2% in the 60–80% centrality class, while for the 0–80% centrality class, it is 1.6%.

The simulated event samples produced for different isospin combinations of colliding nucleons are normalised

assuming a fixed collision rate for each combination. The impact of this assumption is checked by correcting the data after background subtraction using C_W correction factors evaluated from the signal simulation produced for either pp collisions or nn collisions. No significant difference is observed compared to the application of nominal corrections.

A summary of systematic uncertainties as a function of $\langle N_{\text{part}} \rangle$ is shown in Figs. 5 and 6 for the electron and muon channels, respectively. The total systematic uncertainty of the W^{\pm} boson yields obtained in the electron decay channel varies as a function of η_{ℓ} in the barrel region between 4 and 5%. This uncertainty is affected by the statistical precision of the efficiency scale factors measured in bins of η_{ℓ} . Total systematic uncertainties in the endcap regions are much larger and reach 10%. This is caused by the significant multi-jet background contamination and significantly lower statistical precision of the efficiency scale factor estimation. The total systematic uncertainty for η_{ℓ} -integrated yields is largely independent of centrality and amounts to about 5%. In the muon channel, the precision of the measurement for all η_{ℓ} values is similar to the precision of the electron channel measurement in the barrel region. As a function of centrality, the total systematic uncertainty in the muon channel is approximately constant at about 3%.

4.5 Channel combination

The corrected electron and muon channel measurements are combined using the best linear unbiased estimate (BLUE) method [71], accounting for correlations of systematic uncertainties across the channels and measurement bins. For some systematic errors, no covariance matrix is available, and therefore some assumptions about correlations between bins and production channels need to be made. The $\langle T_{AA} \rangle$ uncertainty and theoretical uncertainty in the background production cross-sections for simulated processes are assumed to be fully correlated between bins and channels. This approach is justified as they are used as simple normalisation factors which are common to both channels and across all analysis bins. The uncertainties in the multi-jet background estimation are assumed to be fully correlated between analysis bins and uncorrelated between the decay channels. Finally, the uncertainties related to the p_T^{miss} reconstruction are conservatively assumed to be correlated between both the analysis bins and the decay channels.

5 Results

Figure 7 shows a comparison between the differential normalised production yields for W^+ and W^- bosons obtained for the electron and muon decay channels as a function of the absolute value of the charged-lepton pseudorapidity, $|\eta_{\ell}|$.

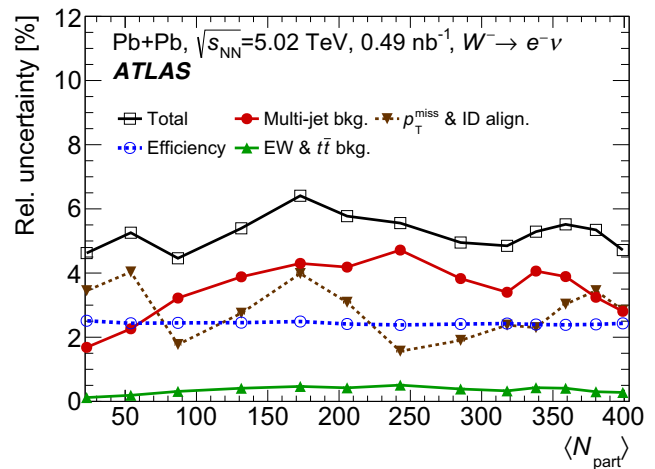
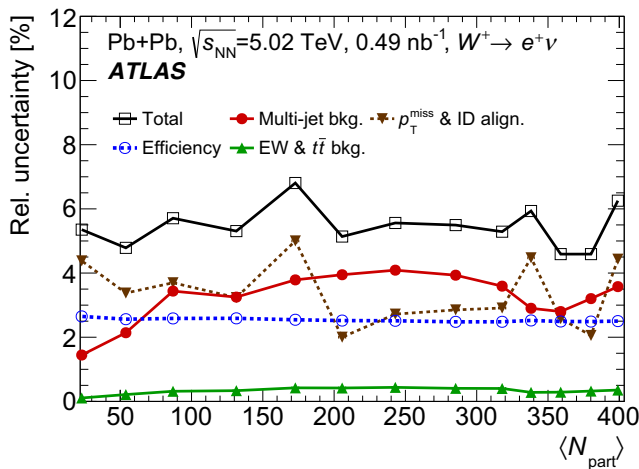


Fig. 5 Relative systematic uncertainties of W^+ (left) and W^- (right) boson production yields measured in the electron decay channel evaluated as a function of $\langle N_{part} \rangle$. The total systematic uncertainty is represented by open squares, while other markers represent contributions from individual sources of uncertainty. The uncertainties related

to electron efficiency corrections (“Efficiency”), p_T^{miss} reconstruction and ID misalignment uncertainties (“ p_T^{miss} and ID align”), as well as the uncertainties related to the estimation of EW and top-quark backgrounds (“EW and $t\bar{t}$ bkg”), are added in quadrature

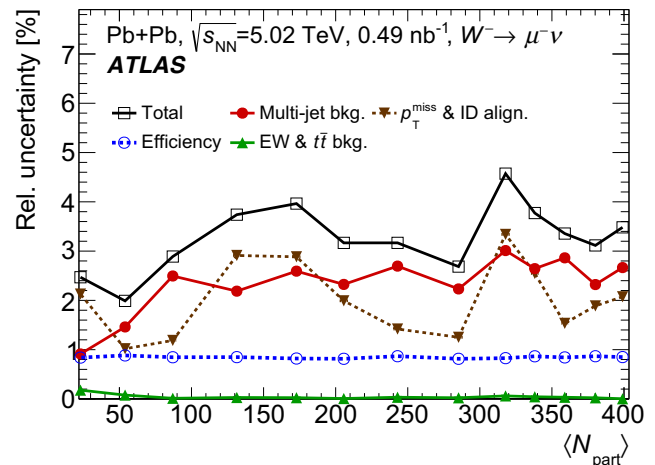
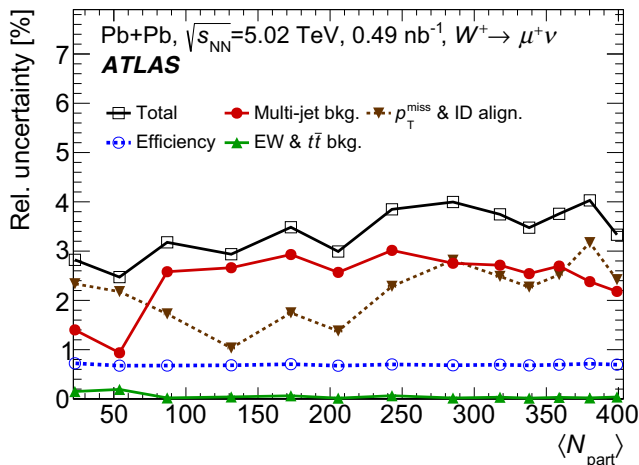


Fig. 6 Relative systematic uncertainties of W^+ (left) and W^- (right) boson production yields measured in the muon decay channel evaluated as a function of $\langle N_{part} \rangle$. The total systematic uncertainty is represented by open squares, while other markers represent contributions from individual sources of uncertainty. The uncertainties related to muon effi-

ciency corrections (“Efficiency”), p_T^{miss} reconstruction and ID misalignment uncertainties (“ p_T^{miss} and ID align”), as well as the uncertainties related to the estimation of EW and top-quark backgrounds (“EW and $t\bar{t}$ bkg”), are added in quadrature

The combined dataset is also shown on the same figure. Good agreement is found between the two decay modes, supporting the combination of the measurements. The distribution for W^+ bosons falls steeply at large $|\eta_\ell|$, whereas for W^- bosons, it tends to be flat with $|\eta_\ell|$. This is attributed to the fact that high- p_T W^\pm bosons are mostly left-handed [72] and preferentially produced in the valence-quark direction, thus towards non-zero pseudorapidity. The W^+ boson decays into a right-handed positive lepton, which is thus boosted back towards lower $|\eta_\ell|$, while the W^- boson decays into a left-handed negative lepton which is boosted towards higher $|\eta_\ell|$.

Figure 8 shows a comparison between lepton charge asymmetries obtained for the electron and muon decay channels as a function of the charged-lepton absolute pseudorapidity. Good agreement is found between the two decay modes, which supports the combination of the two datasets. The resulting combined data points are also shown on the same figure.

Figure 9 shows a comparison of the normalised production yields for W^+ and W^- bosons obtained for the electron and muon decay channels, as well as their combination, as a function of the event centrality (represented by $\langle N_{part} \rangle$).

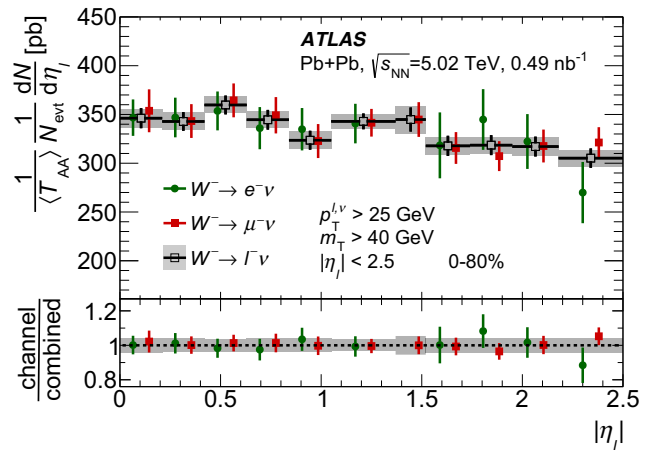
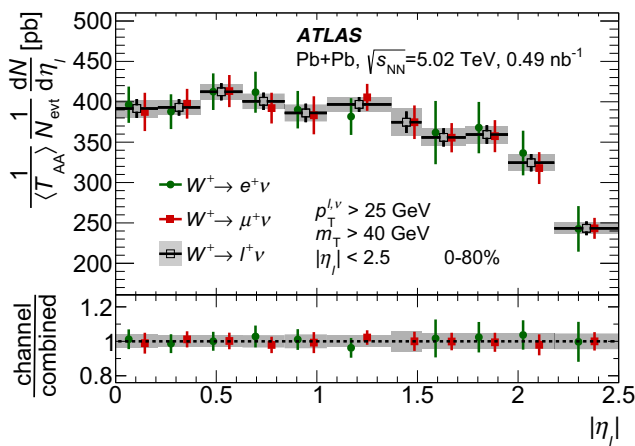


Fig. 7 Differential normalised production yields for W^+ (left) and W^- (right) bosons as a function of absolute pseudorapidity of the charged lepton shown separately for electron and muon decay channels as well as for their combination. Statistical and systematic uncertainties of the combined yields are shown as bars and shaded boxes, respectively. For the individual channels, only the total uncertainties are shown as

error bars. Systematic uncertainties related to $\langle T_{AA} \rangle$ are not included. The lower panels show the ratios of channels to combined yields in each bin with error bars and shaded boxes representing the total uncertainties of the channels and combined yields, respectively. The points for individual channels are shifted horizontally for better visibility

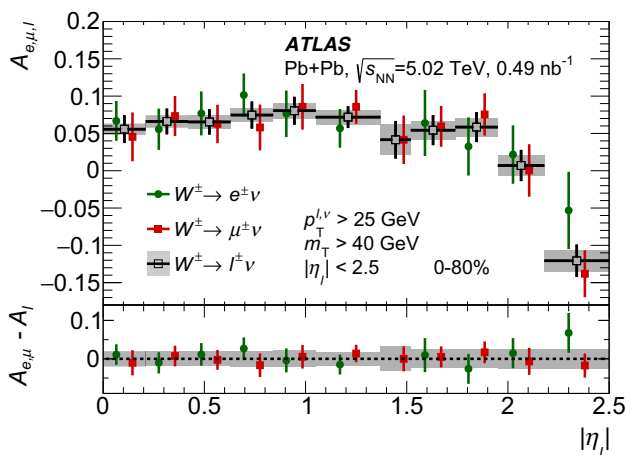


Fig. 8 Lepton charge asymmetry as a function of absolute pseudorapidity of the charged lepton, $|\eta_\ell|$, measured for W^\pm bosons decaying into electrons and muons as well as for the combination of the two channels. Statistical and systematic uncertainties of the combined charge asymmetry are shown as bars and shaded boxes, respectively. For the individual channels, only the total uncertainties are shown as error bars. The lower panel shows the differences between the asymmetries measured for each channel separately and their combination with error bars and shaded boxes representing the total uncertainties of the channels and combined asymmetry, respectively. The points for individual channels are shifted horizontally for better visibility

Here, also, good agreement between the two decay modes is observed.

Figure 10 shows a comparison of combined differential normalised production yields for W^+ and W^- bosons with theoretical predictions as a function of charged-lepton pseudorapidity. The predictions are calculated using the MCFM

code [73] at NLO accuracy in QCD. The calculations are performed using either the free-nucleon CT14 NLO PDF set or one of two PDF sets including nuclear modifications (nPDFs): EPPS16 or nCTEQ15. All predictions account for the isospin effect. Uncertainties in the theoretical predictions include contributions from PDF uncertainties, variations of the renormalisation and factorisation scales and variations of the strong coupling constant α_S . All predictions provide a good description of the shapes of the measured $|\eta_\ell|$ distributions. The prediction based on the CT14 NLO PDF set differs by 2–3% in normalisation compared with the data, while the predictions based on nPDFs underestimate the measured yields by 10–20%. It should also be noted that the W^+ (W^-) boson production cross-sections measured in the pp system [28] are larger by 5% (4%) than the CT14 NLO theory predictions for pp collisions, corresponding to a difference of about one standard deviation.

The combined lepton charge asymmetry is compared with theoretical predictions in Fig. 11. All three predictions agree with the data within systematic uncertainties, except for the most forward $|\eta_\ell|$ bin. The isospin effect, which yields a larger fraction of $W^- \rightarrow \ell^- \nu$ events in Pb + Pb compared to pp collisions in the forward region, results in a sign-change of the asymmetry that is observed within the $|\eta_\ell|$ acceptance of the measurement.

Figure 12 compares the normalised production yields of W^+ and W^- bosons as a function of $\langle N_{part} \rangle$ for the combined electron and muon channels. The normalised production yields for W^+ bosons are about 10% higher than the yields for W^- bosons. The data are also compared with theoretical predictions based on the CT14 NLO PDF set, which

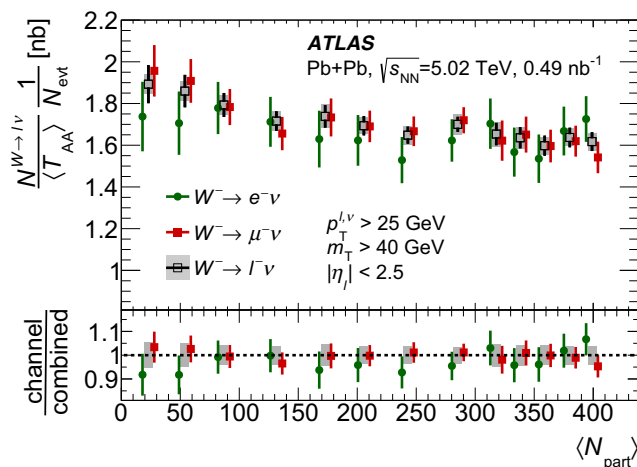
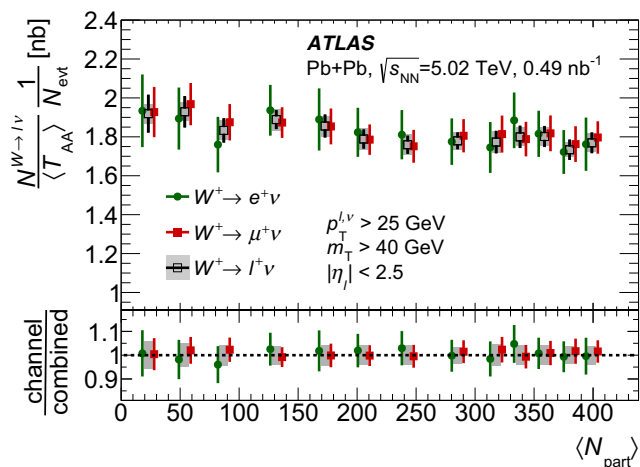


Fig. 9 Normalised production yields for W^+ (left) and W^- (right) bosons as a function of $\langle N_{\text{part}} \rangle$ shown separately for electron and muon decay channels as well as for their combination. Statistical and systematic uncertainties of the combined yields are shown as bars and shaded boxes, respectively. For the individual channels, only the total uncertainties are shown as error bars. Systematic uncertainties related

to $\langle T_{AA} \rangle$ are not included. The lower panels show the ratios of channels to combined yields in each bin with error bars and shaded boxes representing the total uncertainties of the channels and combined yields, respectively. The points for individual channels are shifted horizontally for better visibility

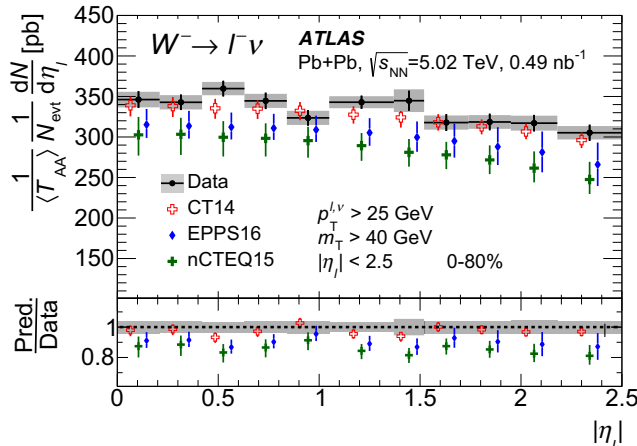
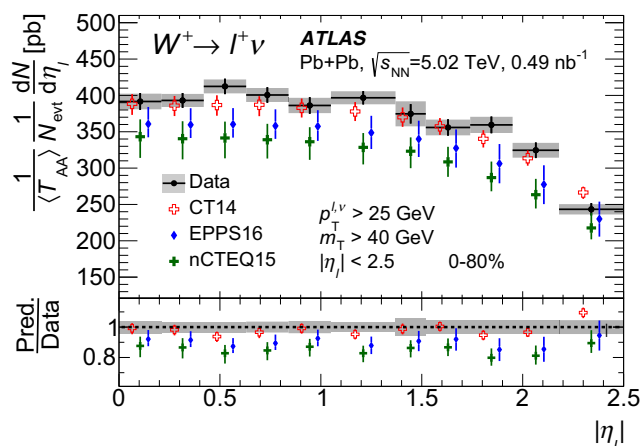


Fig. 10 Differential normalised production yields for W^+ (left) and W^- (right) bosons as a function of absolute pseudorapidity of the charged lepton for the combined electron and muon channels. Error bars show statistical uncertainties, whereas systematic uncertainties are shown as shaded boxes. Systematic uncertainties related to $\langle T_{AA} \rangle$ are not included. The measured distributions are compared with theory predictions calculated with the CT14 NLO PDF set as well as with EPPS16

and nCTEQ15 nPDF sets. For the theory predictions, the error bars represent total uncertainties due to PDF uncertainties, scale variations and α_S variations. The lower panels show the ratios of predicted yields to the measured ones, and the shaded band shows the sum in quadrature of statistical and systematic uncertainties of the data. The points for theory predictions are shifted horizontally for better visibility

include the isospin effect. The normalised production yields for W^\pm bosons do not change with $\langle N_{\text{part}} \rangle$ for mid-central and central collisions represented by $\langle N_{\text{part}} \rangle$ values above 200. In this range of centralities, the measured yields are in good agreement with the predictions, while for mid-peripheral and peripheral collisions corresponding to $\langle N_{\text{part}} \rangle < 200$, there is a slight excess of W^\pm bosons in data in comparison with the theory predictions. The effect grows as $\langle N_{\text{part}} \rangle$ decreases. It is largest in the most peripheral bin and amounts

to 1.7 (0.8) standard deviations for W^- (W^+) boson production. After combining the two bins with the lowest $\langle N_{\text{part}} \rangle$ values, the excess in measured normalised production yields over the theory predictions is 1.7 (0.9) standard deviations for W^- (W^+) bosons. It was checked whether the events from the lowest $\langle N_{\text{part}} \rangle$ bin could be contaminated by a contribution from photonuclear background. No significant enhancement of events with asymmetric signals in the ZDC on either side of ATLAS was seen.

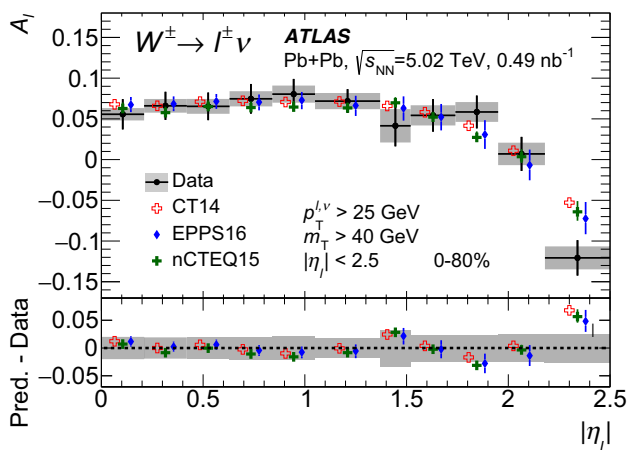


Fig. 11 Combined result for lepton charge asymmetry compared with theory predictions calculated with the CT14 NLO PDF set as well as with EPPS16 and nCTEQ15 nPDF sets. Error bars on the data points show statistical uncertainties, whereas systematic uncertainties are shown as shaded boxes. For the theory predictions, the error bars represent total uncertainties due to PDF uncertainties, scale variations and α_S variations. The lower panel shows the differences between the predicted asymmetries and the measured ones with the shaded boxes representing the total experimental uncertainties. The points for theory predictions are shifted horizontally for better visibility

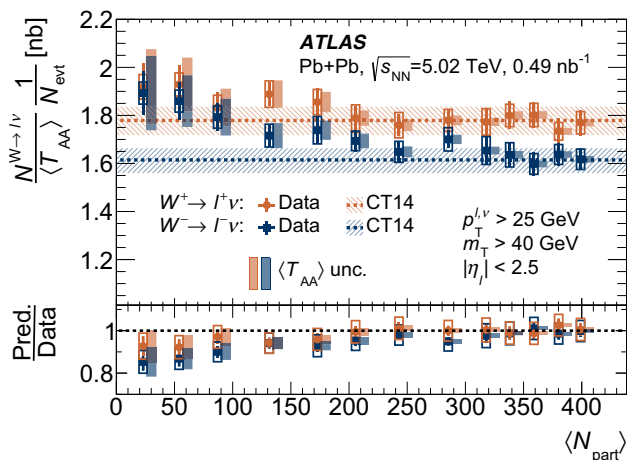


Fig. 12 Normalised production yields of W^+ and W^- bosons as a function of $\langle N_{\text{part}} \rangle$ shown for the combination of electron and muon decay channels. Predictions calculated using the CT14 NLO PDF set are shown as the horizontal bands. Error bars show statistical uncertainties, whereas systematic uncertainties are shown as the boxes around the data points. The systematic uncertainties due to $\langle T_{AA} \rangle$ are not included in those boxes, and are shown as separate shaded boxes plotted to the right of the data points for better visibility. In the lower panel the ratios of the predictions to the measured yields are displayed, and the boxes around the data points show the sum in quadrature of statistical and systematic uncertainties of the data

The measurement of normalised production yields for W^+ and W^- bosons is repeated using the alternative FCal ΣE_T ranges to define centrality classes, N_{evt} , $\langle N_{\text{part}} \rangle$ and $\langle T_{AA} \rangle$ values, extracted from the MCGLauber code v3.2. The results

obtained using the two different MCGLauber codes are compared in Fig. 13. For both the W^+ and W^- bosons, the normalised production yields extracted with geometric parameters from the MCGLauber code v3.2 are slightly closer to the constant yields expected from a scaling with the nuclear thickness. This improvement is more pronounced in peripheral events, but the MCGLauber code v3.2 results still do not fully follow a constant scaling. In addition, differences between the yields obtained using the MCGLauber code v2.4 and v3.2 are smaller than the experimental uncertainties. Theoretical predictions shown in Fig. 13 are calculated using the CT14 NLO PDF set and incorporate the neutron-skin effect [74] evaluated using the separate radial distributions for protons and neutrons provided by the MCGLauber code v3.2. The difference between the radial distributions results in an evolution of the effective proton-to-neutron ratio with centrality. The impact of the neutron skin on normalised W^\pm boson production yields is largest in the most peripheral collisions, where the predictions differ by -1.4% ($+1\%$) for W^+ (W^-) bosons relative to predictions calculated using a constant proton-to-neutron ratio.

Figure 14 shows the nuclear modification factor defined via Eq. (2) as a function of $\langle N_{\text{part}} \rangle$ for the production of W^+ and W^- bosons for the combined electron and muon channels. The pp measurements used to obtain the R_{AA} factor come from Ref. [28]. All uncertainties are assumed to be uncorrelated between the measurements in the Pb + Pb and pp systems, and, therefore, are added in quadrature. As a function of $\langle N_{\text{part}} \rangle$, the nuclear modification factors for both the W^+ and W^- bosons follow the same trend as the normalised production yields. The observed deviations of R_{AA} from unity can be mostly attributed to the isospin effect present in the Pb + Pb system, which results in an enhancement of W^- bosons and a suppression of W^+ bosons relative to the pp system. These modifications of W^\pm boson production in the Pb + Pb system arise from the larger fraction of valence d -quarks in lead nuclei than in protons, since the dominant production mode of W^\pm bosons is through $u\bar{d} \rightarrow W^+$ and $d\bar{u} \rightarrow W^-$ processes. The measured R_{AA} factors are compared with theoretical predictions calculated with the CT14 NLO PDF set. These predictions do not fully describe the R_{AA} factors despite reproducing the normalised production yields of W^+ and W^- bosons measured as a function of $|\eta_\ell|$. For peripheral collisions, the measured R_{AA} factors agree with predictions within 1.2 (0.4) standard deviations for W^- (W^+) bosons, while for central collisions the agreement is within 1.1 (1.8) standard deviations. The apparent contradiction in the theoretical description of R_{AA} factors and of the normalised production yields shown in Fig. 12 is due to the W^\pm boson production cross-sections measured in the pp system [28] being larger than the CT14 NLO theory predictions.

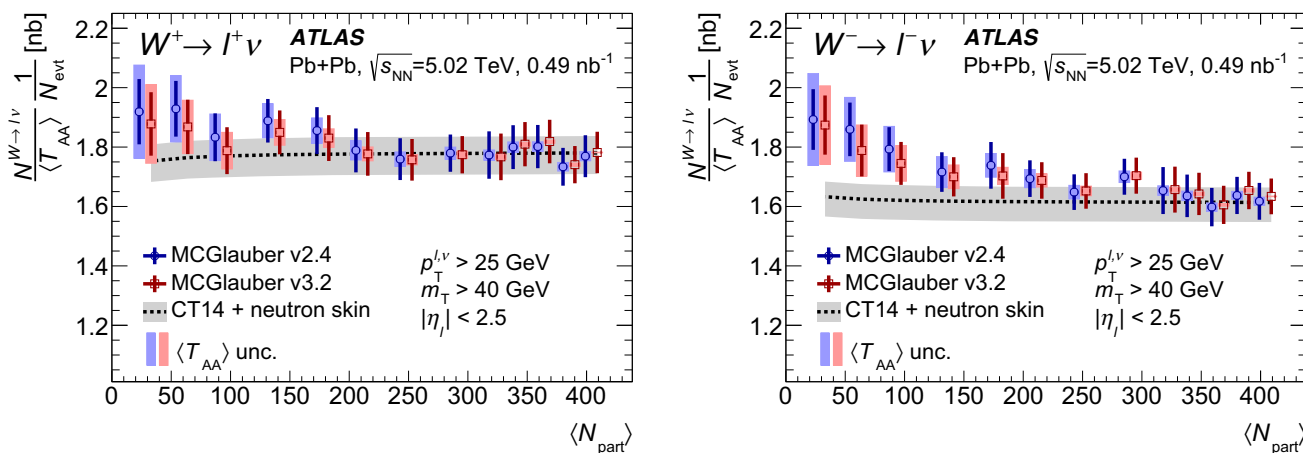


Fig. 13 Comparison of normalised production yields for W^+ (left) and W^- (right) bosons as a function of $\langle N_{\text{part}} \rangle$ for geometric parameters obtained with the MC Glauber code v2.4 and v3.2. The dashed lines show predictions calculated using the CT14 NLO PDF set which incorporate the neutron-skin effect evaluated using the separate radial distributions for protons and neutrons provided by the MC Glauber code

v3.2. Uncertainties related to the determination of radial distributions for nucleons are not included. Error bars show statistical and systematic uncertainties added in quadrature, whereas systematic uncertainties due to $\langle T_{AA} \rangle$ are shown as shaded boxes around the data points. The points for the MC Glauber code v3.2 are shifted horizontally for better visibility

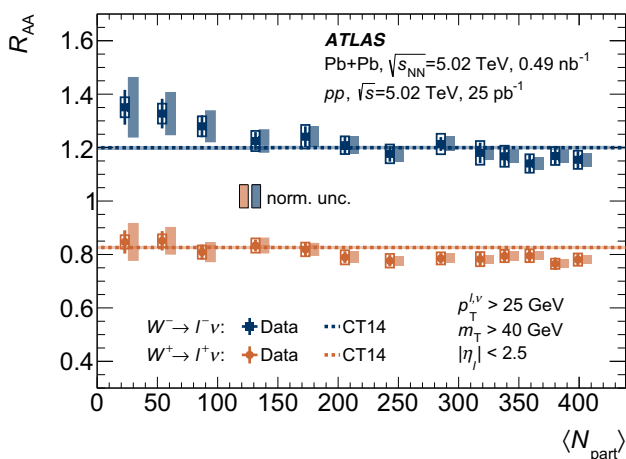


Fig. 14 Nuclear modification factor R_{AA} obtained from the fiducial W^+ and W^- boson production yields as a function of $\langle N_{\text{part}} \rangle$. Error bars show statistical uncertainties, whereas systematic uncertainties are shown as the boxes around the data points. The systematic uncertainties due to $\langle T_{AA} \rangle$ and luminosity of the pp dataset are not included in those boxes, and are shown as separate shaded boxes plotted to the right of the data points for better visibility

It was recently argued in Ref. [75] that the value of R_{AA} in peripheral A+A collisions is expected to be modified due to a biased classification of the event geometry, as specified by the centrality assignment, for events containing a hard process. In that analysis, the value of R_{AA} without any nuclear effects was determined using the HG-PYTHIA model, which describes A+A collisions using the HIJING event generator [76] and superimposes a PYTHIA 6.4 event [61] for each hard sub-interaction specified by the generator. The HG-PYTHIA prediction was demonstrated to

describe the ALICE measurement of charged-hadron R_{AA} in peripheral Pb+Pb collisions [77]. In Fig. 15, the R_{AA} factors for W^+ and W^- bosons measured as a function of centrality percentile are compared with theoretical predictions calculated with the CT14 NLO PDF set multiplied by the HG-PYTHIA prediction of the R_{AA} factor taken from Ref. [77]. The impact of re-evaluating the bias for centrality classes defined in the ATLAS centrality determination procedure is found to be negligible. Due to the different interplay of the hard process and soft production for events with jet production and EW boson production, it is not clear that the centrality bias in this analysis is expected to be the same as in the ALICE measurement. In fact, the observed trend of R_{AA} factors with centrality goes in the opposite direction to the effect of centrality bias predicted by HG-PYTHIA for charged-hadron production.

6 Summary and conclusions

Inclusive production of W^\pm bosons decaying into $\ell^\pm \nu$ measured in the electron and muon channels in Pb+Pb collisions at $\sqrt{s_{NN}} = 5.02$ TeV is reported. The measurements are based on the data collected in 2015 using the ATLAS detector at the LHC corresponding to an integrated luminosity of 0.49 nb^{-1} .

The fiducial production yields scaled by the average nuclear thickness function, $\langle T_{AA} \rangle$, and the total number of minimum-bias Pb + Pb collisions, N_{evt} , are measured in the phase-space region defined by the charged-lepton transverse momentum, $p_T^\ell > 25$ GeV, and pseudorapidity,

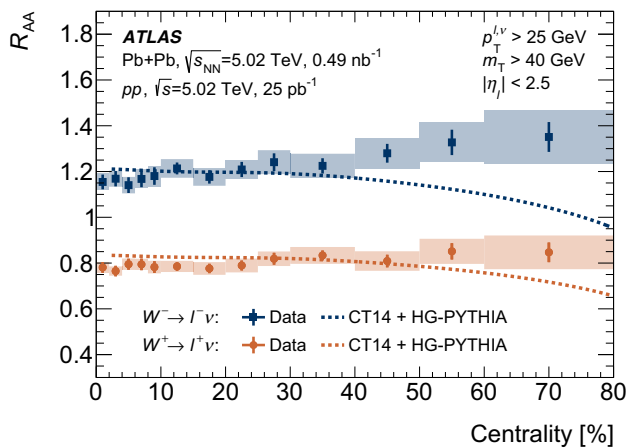


Fig. 15 Nuclear modification factor R_{AA} obtained from the fiducial W^+ and W^- boson production yields as a function of centrality percentile. Error bars show statistical uncertainties, whereas systematic uncertainties are shown as the boxes around the data points. The systematic uncertainties due to $\langle T_{AA} \rangle$ and luminosity of the pp dataset are included in those boxes. The dashed lines show predictions which incorporate the centrality bias calculated using HG-PYTHIA for the ALICE charged-hadron production measurement [77]. These predictions are corrected for the isospin effect evaluated using MCFM with the CT14 NLO PDF set

$|\eta_\ell| < 2.5$, the transverse momentum of the (anti)neutrino, $p_T^\nu > 25$ GeV, and the transverse mass of the charged-lepton–(anti)neutrino system, $m_T > 40$ GeV.

The dominant background contribution comes from multi-jet production. It is evaluated using a data-driven method and amounts to up to about 20% and 12% in the electron and muon decay channels, respectively. Other, smaller, background contributions come from EW boson decays ($Z \rightarrow \mu^+\mu^-(\tau^+\tau^-)$ and $W^\pm \rightarrow \tau^\pm\nu$) and $t\bar{t}$ production. They are estimated by normalising MC simulations to the integrated luminosity of the data sample.

After background subtraction and efficiency corrections, the normalised production yields are presented as a function of the absolute pseudorapidity of the charged lepton, $|\eta_\ell|$, and the average number of nucleons participating in the collision, $\langle N_{\text{part}} \rangle$.

The normalised production yields for W^\pm bosons are compatible in the two lepton decay channels which are combined in this analysis. The combined normalised production yields are consistent with theoretical predictions based on the CT14 NLO PDF set, while predictions obtained with the EPPS16 and nCTEQ15 nPDF sets underestimate the measured yields by 10–20%. However, measurements in the pp system have shown that CT14 NLO predictions underestimate the data by 4–5%. The measured yields for W^\pm bosons are also used to obtain the lepton charge asymmetry, which is well described by the mentioned theoretical predictions. The lepton charge asymmetry changes sign and becomes negative for $|\eta_\ell| > 2$, which is an indication of the isospin

effect yielding a larger fraction of $W^- \rightarrow \ell^-\nu$ events in Pb + Pb compared to pp collisions. The data lack sensitivity to nuclear modifications of the nucleon PDFs in the kinematic region probed by W^\pm boson production. Normalised production yields for W^\pm bosons are in agreement with the expected scaling with $\langle T_{AA} \rangle$ for mid-central and central events. In the range $\langle N_{\text{part}} \rangle < 200$, a systematic excess of the normalised production yields of W^\pm bosons is observed in the data in comparison with the theory predictions with the isospin effect included. The effect is largest in the two most peripheral bins for W^- bosons, and there, the combined excess amounts to 1.7 standard deviations. A comparison of normalised production yields for geometric parameters obtained with two versions of the MCGlauber code (v2.4 and v3.2) shows that the MCGlauber code v3.2 results are somewhat closer to the constant yields expected from the scaling with the nuclear thickness. However, the difference between the two results is smaller than the measurement uncertainties after the uncertainty in $\langle T_{AA} \rangle$ is excluded.

Nuclear modification factors, R_{AA} , for W^\pm boson production are calculated using cross-sections measured in pp collisions at the same centre-of-mass energy. As a function of $\langle N_{\text{part}} \rangle$, the measured R_{AA} factors follow the same trend as the normalised production yields. The observed deviations of R_{AA} from unity can be mostly attributed to the isospin effect. For peripheral collisions, the data agree with predictions based on the CT14 NLO PDF set within 1.2 (0.4) standard deviations for W^- (W^+) bosons, while for central collisions the agreement is within 1.1 (1.8) standard deviations. The trend observed in the data goes in the opposite direction to predictions including the centrality bias evaluated with the HG-PYTHIA model for charged-hadron production. Due to differences in the soft-particle production between events with jet production and EW boson production, it is not clear that the centrality bias should be the same for these two classes of processes. The presented measurement can be used to constrain the centrality bias in the future.

Acknowledgements We thank CERN for the very successful operation of the LHC, as well as the support staff from our institutions without whom ATLAS could not be operated efficiently. We acknowledge the support of ANPCyT, Argentina; YerPhI, Armenia; ARC, Australia; BMWFW and FWF, Austria; ANAS, Azerbaijan; SSTC, Belarus; CNPq and FAPESP, Brazil; NSERC, NRC and CFI, Canada; CERN; CONICYT, Chile; CAS, MOST and NSFC, China; COLCIENCIAS, Colombia; MSMT CR, MPO CR and VSC CR, Czech Republic; DNRF and DNSRC, Denmark; IN2P3-CNRS, CEA-DRF/IRFU, France; SRNSFG, Georgia; BMBF, HGF, and MPG, Germany; GSRT, Greece; RGC, Hong Kong SAR, China; ISF and Benozio Center, Israel; INFN, Italy; MEXT and JSPS, Japan; CNRST, Morocco; NWO, Netherlands; RCN, Norway; MNiSW and NCN, Poland; FCT, Portugal; MNE/IFA, Romania; MES of Russia and NRC KI, Russian Federation; JINR; MESTD, Serbia; MSSR, Slovakia; ARRS and MIZŠ, Slovenia; DST/NRF, South Africa; MINECO, Spain; SRC and Wallenberg Foundation, Sweden; SERI, SNSF and Cantons of Bern and Geneva, Switzerland; MOST, Taiwan; TAEK, Turkey; STFC, United Kingdom;

DOE and NSF, United States of America. In addition, individual groups and members have received support from BCKDF, CANARIE, CRC and Compute Canada, Canada; COST, ERC, ERDF, Horizon 2020, and Marie Skłodowska-Curie Actions, European Union; Investissements d’Avenir Labex and Idex, ANR, France; DFG and AvH Foundation, Germany; Herakleitos, Thales and Aristeia programmes co-financed by EU-ESF and the Greek NSRF, Greece; BSF-NSF and GIF, Israel; CERCA Programme Generalitat de Catalunya, Spain; The Royal Society and Leverhulme Trust, United Kingdom. The crucial computing support from all WLCG partners is acknowledged gratefully, in particular from CERN, the ATLAS Tier-1 facilities at TRIUMF (Canada), NDGF (Denmark, Norway, Sweden), CC-IN2P3 (France), KIT/GridKA (Germany), INFN-CNAF (Italy), NL-T1 (Netherlands), PIC (Spain), ASGC (Taiwan), RAL (UK) and BNL (USA), the Tier-2 facilities worldwide and large non-WLCG resource providers. Major contributors of computing resources are listed in Ref. [78].

Data Availability Statement This manuscript has no associated data or the data will not be deposited. [Authors’ comment: All ATLAS scientific output is published in journals, and preliminary results are made available in Conference Notes. All are openly available, without restriction on use by external parties beyond copyright law and the standard conditions agreed by CERN. Data associated with journal publications are also made available: tables and data from plots (e.g. cross section values, likelihood profiles, selection efficiencies, cross section limits, ...) are stored in appropriate repositories such as HEPDATA (<http://hepdata.cedar.ac.uk/>). ATLAS also strives to make additional material related to the paper available that allows a reinterpretation of the data in the context of new theoretical models. For example, an extended encapsulation of the analysis is often provided for measurements in the framework of RIVET (<http://rivet.hepforge.org/>).]

Open Access This article is distributed under the terms of the Creative Commons Attribution 4.0 International License (<http://creativecommons.org/licenses/by/4.0/>), which permits unrestricted use, distribution, and reproduction in any medium, provided you give appropriate credit to the original author(s) and the source, provide a link to the Creative Commons license, and indicate if changes were made. Funded by SCOAP³.

References

1. E. Shuryak, Strongly coupled quark-gluon plasma in heavy ion collisions. *Rev. Mod. Phys.* **89**, 035001 (2017). [arXiv:1412.8393](https://arxiv.org/abs/1412.8393) [hep-ph]
2. BRAHMS Collaboration, Quark-gluon plasma and color glass condensate at RHIC? The perspective from the BRAHMS experiment. *Nucl. Phys. A* **757**, 1 (2005). [arXiv:nuclex/0410020](https://arxiv.org/abs/nuclex/0410020)
3. PHOBOS Collaboration, The PHOBOS perspective on discoveries at RHIC. *Nucl. Phys. A* **757**, 28 (2005). [arXiv:nuclex/0410022](https://arxiv.org/abs/nuclex/0410022)
4. STAR Collaboration, Experimental and theoretical challenges in the search for the quark gluon plasma: The STAR Collaboration’s critical assessment of the evidence from RHIC collisions. *Nucl. Phys. A* **757**, 102 (2005). [arXiv:nuclex/0501009](https://arxiv.org/abs/nuclex/0501009)
5. PHENIX Collaboration, Formation of dense partonic matter in relativistic nucleus-nucleus collisions at RHIC: Experimental evaluation by the PHENIX collaboration. *Nucl. Phys. A* **757**, 184 (2005). [arXiv:nuclex/0410003](https://arxiv.org/abs/nuclex/0410003)
6. Y. Mehtar-Tani, J.G. Milhano, K. Tywoniuk, Jet physics in heavy-ion collisions. *Int. J. Mod. Phys. A* **28**, 1340013 (2013). [arXiv:1302.2579](https://arxiv.org/abs/1302.2579) [hep-ph]
7. G.-Y. Qin, X.-N. Wang, Jet quenching in high-energy heavy-ion collisions. *Int. J. Mod. Phys. E* **24**, 1530014 (2015). [arXiv:1511.00790](https://arxiv.org/abs/1511.00790) [hep-ph]
8. STAR Collaboration, Transverse-momentum and collision-energy dependence of high- p_T hadron suppression in Au + Au collisions at ultrarelativistic energies. *Phys. Rev. Lett.* **91**, 172302 (2003). [arXiv:nuclex/0305015](https://arxiv.org/abs/nuclex/0305015)
9. PHENIX Collaboration, High p_T charged hadron suppression in Au + Au collisions at $\sqrt{s_{NN}} = 200$ GeV. *Phys. Rev. C* **69**, 034910 (2004). [arXiv:nuclex/0308006](https://arxiv.org/abs/nuclex/0308006)
10. ATLAS Collaboration, Measurement of charged-particle spectra in Pb+Pb collisions at $\sqrt{s_{NN}} = 2.76$ TeV with the ATLAS detector at the LHC. *JHEP* **09**, 050 (2015). [arXiv:1504.04337](https://arxiv.org/abs/1504.04337) [hep-ex]
11. CMS Collaboration, Study of high- p_T charged particle suppression in PbPb compared to pp collisions at $\sqrt{s_{NN}} = 2.76$ TeV. *Eur. Phys. J. C* **72**, 1945 (2012). [arXiv:1202.2554](https://arxiv.org/abs/1202.2554) [hep-ex]
12. ALICE Collaboration, Suppression of charged particle production at large transverse momentum in central Pb–Pb collisions at $\sqrt{s_{NN}} = 2.76$ TeV. *Phys. Lett. B* **696**, 30 (2011). [arXiv:1012.1004](https://arxiv.org/abs/1012.1004) [nucl-ex]
13. ATLAS Collaboration, Measurement of the nuclear modification factor for inclusive jets in Pb+Pb collisions at $\sqrt{s_{NN}} = 5.02$ TeV with the ATLAS detector. *Phys. Lett. B* **790**, 108 (2019). [arXiv:1805.05635](https://arxiv.org/abs/1805.05635) [hep-ex]
14. CMS Collaboration, Measurement of inclusive jet cross-sections in pp and PbPb collisions at $\sqrt{s_{NN}} = 2.76$ TeV. *Phys. Rev. C* **96**, 015202 (2017). [arXiv:1609.05383](https://arxiv.org/abs/1609.05383) [hep-ex]
15. ATLAS Collaboration, Observation of a centrality-dependent dijet asymmetry in lead–lead collisions at $\sqrt{s_{NN}} = 2.76$ TeV with the ATLAS detector at the LHC. *Phys. Rev. Lett.* **105**, 252303 (2010). [arXiv:1011.6182](https://arxiv.org/abs/1011.6182) [hep-ex]
16. CMS Collaboration, Jet momentum dependence of jet quenching in PbPb collisions at $\sqrt{s_{NN}} = 2.76$ TeV. *Phys. Lett. B* **712**, 176 (2012). [arXiv:1202.5022](https://arxiv.org/abs/1202.5022) [hep-ex]
17. ATLAS Collaboration, Measurement of jet fragmentation in Pb+Pb and pp collisions at $\sqrt{s_{NN}} = 5.02$ TeV with the ATLAS detector. *Phys. Rev. C* **98**, 024908 (2018). [arXiv:1805.05424](https://arxiv.org/abs/1805.05424) [hep-ex]
18. CMS Collaboration, Jet properties in PbPb and pp collisions at $\sqrt{s_{NN}} = 5.02$ TeV. *JHEP* **05**, 006 (2018). [arXiv:1803.00042](https://arxiv.org/abs/1803.00042) [hep-ex]
19. STAR Collaboration, Direct virtual photon production in Au + Au collisions at $\sqrt{s_{NN}} = 200$ GeV. *Phys. Lett. B* **770**, 451 (2017). [arXiv:1607.01447](https://arxiv.org/abs/1607.01447) [nucl-ex]
20. PHENIX Collaboration, Measurement of direct photons in Au + Au collisions at $\sqrt{s_{NN}} = 200$ GeV. *Phys. Rev. Lett.* **109**, 152302 (2012). [arXiv:1205.5759](https://arxiv.org/abs/1205.5759) [nucl-ex]
21. ATLAS Collaboration, Centrality, rapidity and transverse momentum dependence of isolated prompt photon production in lead–lead collisions at $\sqrt{s_{NN}} = 2.76$ TeV measured with the ATLAS detector. *Phys. Rev. C* **93**, 034914 (2016). [arXiv:1506.08552](https://arxiv.org/abs/1506.08552) [hep-ex]
22. CMS Collaboration, Measurement of isolated photon production in pp and PbPb collisions at $\sqrt{s_{NN}} = 2.76$ TeV. *Phys. Lett. B* **710**, 256 (2012). [arXiv:1201.3093](https://arxiv.org/abs/1201.3093) [hep-ex]
23. ATLAS Collaboration, Measurement of Z Boson production in Pb-Pb collisions at $\sqrt{s_{NN}} = 2.76$ TeV with the ATLAS detector. *Phys. Rev. Lett.* **110**, 022301 (2013). [arXiv:1210.6486](https://arxiv.org/abs/1210.6486) [hep-ex]
24. CMS Collaboration, Study of Z Boson production in PbPb collisions at $\sqrt{s_{NN}} = 2.76$ TeV. *Phys. Rev. Lett.* **106**, 212301 (2011). [arXiv:1102.5435](https://arxiv.org/abs/1102.5435) [hep-ex]
25. ATLAS Collaboration, Measurement of the production and lepton charge asymmetry of W bosons in Pb+Pb collisions at $\sqrt{s_{NN}} = 2.76$ TeV with the ATLAS detector. *Eur. Phys. J. C* **75**, 23 (2015). [arXiv:1408.4674](https://arxiv.org/abs/1408.4674) [hep-ex]
26. CMS Collaboration, Study of W boson production in PbPb and pp collisions at $\sqrt{s_{NN}} = 2.76$ TeV. *Phys. Lett. B* **715**, 66 (2012). [arXiv:1205.6334](https://arxiv.org/abs/1205.6334) [hep-ex]
27. ALICE Collaboration, Measurement of Z^0 -boson production at large rapidities in Pb-Pb collisions at $\sqrt{s_{NN}} = 5.02$ TeV. *Phys. Lett. B* **780**, 372 (2018). [arXiv:1711.10753](https://arxiv.org/abs/1711.10753) [nucl-ex]

28. ATLAS Collaboration, Measurements of W and Z boson production in pp collisions at $\sqrt{s} = 5.02$ TeV with the ATLAS detector. *Eur. Phys. J. C* **79**, 128 (2019). [arXiv:1810.08424](#) [hep-ex]. Erratum: *Eur. Phys. J. C* **79**, 374 (2019)
29. ATLAS Collaboration, Precision measurement and interpretation of inclusive W^+ , W^- and Z/γ^* production cross sections with the ATLAS detector. *Eur. Phys. J. C* **77**, 367 (2017). [arXiv:1612.03016](#) [hep-ex]
30. ATLAS Collaboration, Measurement of the cross-section and charge asymmetry of W bosons produced in proton–proton collisions at $\sqrt{s} = 8$ TeV with the ATLAS detector. [arXiv:1904.05631](#) [hep-ex]
31. ATLAS Collaboration, Measurement of W^\pm and Z -boson production cross sections in pp collisions at $\sqrt{s} = 13$ TeV with the ATLAS detector. *Phys. Lett. B* **759**, 601 (2016). [arXiv:1603.09222](#) [hep-ex]
32. CMS Collaboration, Measurement of the inclusive W and Z production cross sections in pp collisions at $\sqrt{s} = 7$ TeV with the CMS experiment. *JHEP* **10**, 132 (2011). [arXiv:1107.4789](#) [hep-ex]
33. CMS Collaboration, Measurement of inclusive W and Z boson production cross sections in pp collisions at $\sqrt{s} = 8$ TeV. *Phys. Rev. Lett.* **112**, 191802 (2014). [arXiv:1402.0923](#) [hep-ex]
34. CDF Collaboration, Measurements of inclusive W and Z cross sections in $p\bar{p}$ collisions at $\sqrt{s} = 1.96$ TeV. *J. Phys. G* **34**, 2457 (2007). [arXiv:hep-ex/0508029](#) [hep-ex]
35. D0 Collaboration, Measurement of the W Boson production charge asymmetry in $p\bar{p} \rightarrow W + X \rightarrow e\nu + X$ events at $\sqrt{s} = 1.96$ TeV. *Phys. Rev. Lett.* **112**, 151803 (2014). [arXiv:1312.2895](#) [hep-ex]. Erratum: *Phys. Rev. Lett.* **114**, 049901 (2015)
36. A.D. Martin, R.G. Roberts, W.J. Stirling, R.S. Thorne, Parton distributions and the LHC: W and Z production. *Eur. Phys. J. C* **14**, 133 (2000). [arXiv:hep-ph/9907231](#)
37. R. Vogt, Shadowing effects on vector boson production. *Phys. Rev. C* **64**, 044901 (2001). [arXiv:hep-ph/0011242](#)
38. H. Paukkunen, C.A. Salgado, Constraints for the nuclear parton distributions from Z and W production at the LHC. *JHEP* **03**, 071 (2011). [arXiv:1010.5392](#) [hep-ph]
39. CMS Collaboration, Study of W boson production in pPb collisions at $\sqrt{s_{NN}} = 5.02$ TeV. *Phys. Lett. B* **750**, 565 (2015). [arXiv:1503.05825](#) [hep-ex]
40. CMS Collaboration, Observation of nuclear modifications in W^\pm boson production in pPb collisions at $\sqrt{s_{NN}} = 8.16$ TeV. [arXiv:1905.01486](#) [hep-ex]
41. B. Alver, M. Baker, C. Loizides, P. Steinberg, The PHOBOS Glauber Monte Carlo (2008). [arXiv:0805.4411](#) [nucl-ex]
42. M.L. Miller, K. Reygers, S.J. Sanders, P. Steinberg, Glauber modeling in high energy nuclear collisions. *Annu. Rev. Nucl. Part. Sci.* **57**, 205 (2007). [arXiv:nucl-ex/0701025](#)
43. S. Dulat et al., New parton distribution functions from a global analysis of quantum chromodynamics. *Phys. Rev. D* **93**, 033006 (2016). [arXiv:1506.07443](#) [hep-ph]
44. K.J. Eskola, P. Paakkinen, H. Paukkunen, C.A. Salgado, EPPS16: nuclear parton distributions with LHC data. *Eur. Phys. J. C* **77**, 163 (2017). [arXiv:1612.05741](#) [hep-ph]
45. K. Kovarik et al., nCTEQ15—global analysis of nuclear parton distributions with uncertainties in the CTEQ framework. *Phys. Rev. D* **93**, 085037 (2016). [arXiv:1509.00792](#) [hep-ph]
46. ATLAS Collaboration, The ATLAS experiment at the CERN large hadron collider. *JINST* **3**, S08003 (2008)
47. ATLAS Collaboration, ATLAS Insertable B-Layer Technical Design Report, ATLAS-TDR-19 (2010). <https://cds.cern.ch/record/1291633>. Addendum: ATLAS-TDR-19-ADD-1 (2012). <https://cds.cern.ch/record/1451888>
48. B. Abbott et al., Production and integration of the ATLAS insertable B-Layer. *JINST* **13**, T05008 (2018). [arXiv:1803.00844](#) [physics.ins-det]
49. ATLAS Collaboration, Performance of the ATLAS trigger system in 2015. *Eur. Phys. J. C* **77**, 317 (2017). [arXiv:1611.09661](#) [hep-ex]
50. ATLAS Collaboration, Measurement of the centrality dependence of the charged particle pseudorapidity distribution in lead–lead collisions at $\sqrt{s_{NN}} = 2.76$ TeV with the ATLAS detector. *Phys. Lett. B* **710**, 363 (2012). [arXiv:1108.6027](#) [hep-ex]
51. ATLAS Collaboration, Prompt and non-prompt J/ψ and $\psi(2S)$ suppression at high transverse momentum in 5.02 TeV Pb+Pb collisions with the ATLAS experiment. *Eur. Phys. J. C* **78**, 762 (2018). [arXiv:1805.04077](#) [hep-ex]
52. C. Loizides, J. Nagle, P. Steinberg, Improved version of the PHOBOS Glauber Monte Carlo. *SoftwareX* **1–2**, 13 (2015). [arXiv:1408.2549](#) [nucl-ex]
53. C. Loizides, J. Kamin, D. d’Enterria, Improved Monte Carlo Glauber predictions at present and future nuclear colliders. *Phys. Rev. C* **97**, 054910 (2018). [arXiv:1710.07098](#) [nucl-ex]. Erratum: *Phys. Rev. C* **99**, 019901 (2019)
54. S. Agostinelli et al., GEANT4—a simulation toolkit. *Nucl. Instrum. Methods A* **506**, 250 (2003)
55. ATLAS Collaboration, The ATLAS simulation infrastructure. *Eur. Phys. J. C* **70**, 823 (2010). [arXiv:1005.4568](#) [physics.ins-det]
56. S. Alioli, P. Nason, C. Oleari, E. Re, A general framework for implementing NLO calculations in shower Monte Carlo programs: the POWHEG BOX. *JHEP* **06**, 043 (2010). [arXiv:1002.2581](#) [hep-ph]
57. S. Alioli, P. Nason, C. Oleari, E. Re, NLO vector-boson production matched with shower in POWHEG. *JHEP* **07**, 060 (2008). [arXiv:0805.4802](#) [hep-ph]
58. T. Sjöstrand, S. Mrenna, P.Z. Skands, A brief introduction to PYTHIA 8.1. *Comput. Phys. Commun.* **178**, 852 (2008). [arXiv:0710.3820](#) [hep-ph]
59. H.-L. Lai et al., New parton distributions for collider physics. *Phys. Rev. D* **82**, 074024 (2010). [arXiv:1007.2241](#) [hep-ph]
60. S. Frixione, P. Nason, G. Ridolfi, A positive-weight next-to-leading-order Monte Carlo for heavy flavour hadroproduction. *JHEP* **09**, 126 (2007). [arXiv:0707.3088](#) [hep-ph]
61. T. Sjöstrand, S. Mrenna, P.Z. Skands, PYTHIA 6.4 physics and manual. *JHEP* **05**, 026 (2006). [arXiv:hep-ph/0603175](#)
62. S. Catani, M. Grazzini, Next-to-next-to-leading-order subtraction formalism in hadron collisions and its application to Higgs-boson production at the large hadron collider. *Phys. Rev. Lett.* **98**, 222002 (2007). [arXiv:hep-ph/0703012](#)
63. S. Catani, L. Cieri, G. Ferrera, D. Florian, M. Grazzini, Vector Boson production at hadron colliders: a fully exclusive QCD calculation at next-to-next-to-leading order. *Phys. Rev. Lett.* **103**, 082001 (2009). [arXiv:0903.2120](#) [hep-ph]
64. ATLAS Collaboration, Electron reconstruction and identification in the ATLAS experiment using the 2015 and 2016 LHC proton–proton collision data at $\sqrt{s} = 13$ TeV. [arXiv:1902.04655](#) [hep-ex]
65. ATLAS Collaboration, Measurement of the jet radius and transverse momentum dependence of inclusive jet suppression in lead–lead collisions at $\sqrt{s_{NN}} = 2.76$ TeV with the ATLAS detector. *Phys. Lett. B* **719**, 220 (2013). [arXiv:1208.1967](#) [hep-ex]
66. ATLAS Collaboration, Muon reconstruction performance of the ATLAS detector in proton–proton collision data at $\sqrt{s} = 13$ TeV. *Eur. Phys. J. C* **76**, 292 (2016). [arXiv:1603.05598](#) [hep-ex]
67. ATLAS Collaboration, Electron and photon energy calibration with the ATLAS detector using 2015–2016 LHC proton–proton collision data. *JINST* **14**, P03017 (2019). [arXiv:1812.03848](#) [hep-ex]
68. H. Abreu et al., Performance of the electronic readout of the ATLAS liquid argon calorimeters. *JINST* **5**, P09003 (2010)

69. ATLAS Collaboration, Performance of missing transverse momentum reconstruction with the ATLAS detector using proton–proton collisions at $\sqrt{s} = 13$ TeV. *Eur. Phys. J. C* **78**, 903 (2018). [arXiv:1802.08168](https://arxiv.org/abs/1802.08168) [hep-ex]
70. ATLAS Collaboration, Measurement of the W -boson mass in pp collisions at $\sqrt{s} = 7$ TeV with the ATLAS detector. *Eur. Phys. J. C* **78**, 110 (2018). [arXiv:1701.07240](https://arxiv.org/abs/1701.07240) [hep-ex]
71. A. Valassi, Combining correlated measurements of several different physical quantities. *Nucl. Instrum. Methods A* **500**, 391 (2003)
72. C.F. Berger et al., Next-to-leading order QCD predictions for $W+3$ -jet distributions at hadron colliders. *Phys. Rev. D* **80**, 074036 (2009). [arXiv:0907.1984](https://arxiv.org/abs/0907.1984) [hep-ph]
73. J.M. Campbell, R.K. Ellis, W.T. Giele, A multi-threaded version of MCFM. *Eur. Phys. J. C* **75**, 246 (2015). [arXiv:1503.06182](https://arxiv.org/abs/1503.06182) [physics.comp-ph]
74. H. Paukkunen, Neutron skin and centrality classification in high-energy heavy-ion collisions at the LHC. *Phys. Lett. B* **745**, 73 (2015). [arXiv:1503.02448](https://arxiv.org/abs/1503.02448) [hep-ph]
75. C. Loizides, A. Morsch, Absence of jet quenching in peripheral nucleus-nucleus collisions. *Phys. Lett. B* **773**, 408 (2017). [arXiv:1705.08856](https://arxiv.org/abs/1705.08856) [nucl-ex]
76. X.N. Wang, M. Gyulassy, HIJING: a Monte Carlo model for multiple jet production in pp , pA , and AA collisions. *Phys. Rev. D* **44**, 3501 (1991)
77. ALICE Collaboration, Analysis of the apparent nuclear modification in peripheral $Pb - Pb$ collisions at 5.02 TeV. *Phys. Lett. B* **793**, 420 (2019). [arXiv:1805.05212](https://arxiv.org/abs/1805.05212) [nucl-ex]
78. ATLAS Collaboration, ATLAS computing acknowledgements, ATL-GEN-PUB-2016-002. <https://cds.cern.ch/record/2202407>

ATLAS Collaboration

G. Aad¹⁰¹, B. Abbott¹²⁸, D. C. Abbott¹⁰², A. Abed Abud^{70a,70b}, K. Abeling⁵³, D. K. Abhayasinghe⁹³, S. H. Abidi¹⁶⁷, O. S. AbouZeid⁴⁰, N. L. Abraham¹⁵⁶, H. Abramowicz¹⁶¹, H. Abreu¹⁶⁰, Y. Abulaiti⁶, B. S. Acharya^{66a,66b,o}, B. Achkar⁵³, S. Adachi¹⁶³, L. Adam⁹⁹, C. Adam Bourdarios⁵, L. Adamczyk^{83a}, L. Adamek¹⁶⁷, J. Adelman¹²¹, M. Adersberger¹¹⁴, A. Adiguzel^{12c,ak}, S. Adorni⁵⁴, T. Adye¹⁴⁴, A. A. Affolder¹⁴⁶, Y. Afik¹⁶⁰, C. Agapopoulou¹³², M. N. Agarar³⁸, A. Aggarwal¹¹⁹, C. Agheorghiesei^{27c}, J. A. Aguilar-Saavedra^{140a,140f,aj}, F. Ahmadov⁷⁹, W. S. Ahmed¹⁰³, X. Ai¹⁸, G. Aielli^{73a,73b}, S. Akatsuka⁸⁵, T. P. A. Åkesson⁹⁶, E. Akilli⁵⁴, A. V. Akimov¹¹⁰, K. Al Khoury¹³², G. L. Alberghi^{23a,23b}, J. Albert¹⁷⁶, M. J. Alconada Verzini¹⁶¹, S. Alderweireldt³⁶, M. Aleksa³⁶, I. N. Aleksandrov⁷⁹, C. Alexa^{27b}, D. Alexandre¹⁹, T. Alexopoulos¹⁰, A. Alfonsi¹²⁰, M. Alhroob¹²⁸, B. Ali¹⁴², G. Alimonti^{68a}, J. Alison³⁷, S. P. Alkire¹⁴⁸, C. Allaire¹³², B. M. M. Allbrooke¹⁵⁶, B. W. Allen¹³¹, P. P. Allport²¹, A. Aloisio^{69a,69b}, A. Alonso⁴⁰, F. Alonso⁸⁸, C. Alpigiani¹⁴⁸, A. A. Alshehri⁵⁷, M. Alvarez Estevez⁹⁸, D. Álvarez Piqueras¹⁷⁴, M. G. Alviggi^{69a,69b}, Y. Amaral Coutinho^{80b}, A. Ambler¹⁰³, L. Ambroz¹³⁵, C. Amelung²⁶, D. Amidei¹⁰⁵, S. P. Amor Dos Santos^{140a}, S. Amoroso⁴⁶, C. S. Amrouche⁵⁴, F. An⁷⁸, C. Anastopoulos¹⁴⁹, N. Andari¹⁴⁵, T. Andeen¹¹, C. F. Anders^{61b}, J. K. Anders²⁰, A. Andreazza^{68a,68b}, V. Andrei^{61a}, C. R. Anelli¹⁷⁶, S. Angelidakis³⁸, A. Angerami³⁹, A. V. Anisenkov^{122a,122b}, A. Annovi^{71a}, C. Antel^{61a}, M. T. Anthony¹⁴⁹, M. Antonelli⁵¹, D. J. A. Antrim¹⁷¹, F. Anulli^{72a}, M. Aoki⁸¹, J. A. Aparisi Pozo¹⁷⁴, L. Aperio Bella³⁶, G. Arabidze¹⁰⁶, J. P. Araque^{140a}, V. Araujo Ferraz^{80b}, R. Araujo Pereira^{80b}, C. Arcangeletti⁵¹, A. T. H. Arce⁴⁹, F. A. Arduh⁸⁸, J.-F. Arguin¹⁰⁹, S. Argyropoulos⁷⁷, J.-H. Arling⁴⁶, A. J. Armbruster³⁶, A. Armstrong¹⁷¹, O. Arnaez¹⁶⁷, H. Arnold¹²⁰, A. Artamonov^{111,*}, G. Artoni¹³⁵, S. Artz⁹⁹, S. Asai¹⁶³, N. Asbah⁵⁹, E. M. Asimakopoulou¹⁷², L. Asquith¹⁵⁶, J. Assahsah^{35d}, K. Assamagan²⁹, R. Astalos^{28a}, R. J. Atkin^{33a}, M. Atkinson¹⁷³, N. B. Atlay¹⁹, H. Atmani¹³², K. Augsten¹⁴², G. Avolio³⁶, R. Avramidou^{60a}, M. K. Ayoub^{15a}, A. M. Azoulay^{168b}, G. Azuelos^{109,az}, H. Bachacou¹⁴⁵, K. Bachas^{67a,67b}, M. Backes¹³⁵, F. Backman^{45a,45b}, P. Bagnaia^{72a,72b}, M. Bahmani⁸⁴, H. Bahrasemani¹⁵², A. J. Bailey¹⁷⁴, V. R. Bailey¹⁷³, J. T. Baines¹⁴⁴, M. Bajic⁴⁰, C. Bakalis¹⁰, O. K. Baker¹⁸³, P. J. Bakker¹²⁰, D. Bakshi Gupta⁸, S. Balaji¹⁵⁷, E. M. Baldin^{122a,122b}, P. Balek¹⁸⁰, F. Balli¹⁴⁵, W. K. Balunas¹³⁵, J. Balz⁹⁹, E. Banas⁸⁴, A. Bandyopadhyay²⁴, Sw. Banerjee^{181,j}, A. A. E. Bannoura¹⁸², L. Barak¹⁶¹, W. M. Barbe³⁸, E. L. Barberio¹⁰⁴, D. Barberis^{55a,55b}, M. Barbero¹⁰¹, G. Barbour⁹⁴, T. Barillari¹¹⁵, M.-S. Barisits³⁶, J. Barkeloo¹³¹, T. Barklow¹⁵³, R. Barnea¹⁶⁰, S. L. Barnes^{60c}, B. M. Barnett¹⁴⁴, R. M. Barnett¹⁸, Z. Barnovska-Blenessy^{60a}, A. Baroncelli^{60a}, G. Barone²⁹, A. J. Barr¹³⁵, L. Barranco Navarro^{45a,45b}, F. Barreiro⁹⁸, J. Barreiro Guimarães da Costa^{15a}, S. Barsov¹³⁸, R. Bartoldus¹⁵³, G. Bartolini¹⁰¹, A. E. Barton⁸⁹, P. Bartos^{28a}, A. Basalae⁴⁶, A. Bassalat^{132,as}, M. J. Basso¹⁶⁷, R. L. Bates⁵⁷, S. Batlamous^{35e}, J. R. Batley³², B. Batool¹⁵¹, M. Battaglia¹⁴⁶, M. Baucé^{72a,72b}, F. Bauer¹⁴⁵, K. T. Bauer¹⁷¹, H. S. Bawa^{31,m}, J. B. Beacham⁴⁹, T. Beau¹³⁶, P. H. Beauchemin¹⁷⁰, F. Becherer⁵², P. Bechtel²⁴, H. C. Beck⁵³, H. P. Beck^{20,s}, K. Becker⁵², M. Becker⁹⁹, C. Becot⁴⁶, A. Beddall^{12d}, A. J. Beddall^{12a}, V. A. Bednyakov⁷⁹, M. Bedognetti¹²⁰, C. P. Bee¹⁵⁵, T. A. Beermann⁷⁶, M. Begalli^{80b}, M. Begel²⁹, A. Behera¹⁵⁵, J. K. Behr⁴⁶, F. Beisiegel²⁴, A. S. Bell⁹⁴, G. Bella¹⁶¹, L. Bellagamba^{23b}, A. Bellerive³⁴, P. Bellos⁹, K. Beloborodov^{122a,122b}, K. Belotskiy¹¹², N. L. Belyaev¹¹², D. Benchechroun^{35a}, N. Benekos¹⁰, Y. Benhammou¹⁶¹, D. P. Benjamin⁶, M. Benoit⁵⁴, J. R. Bensinger²⁶, S. Bentvelsen¹²⁰, L. Beresford¹³⁵, M. Beretta⁵¹, D. Berge⁴⁶, E. Bergeaas Kuutmann¹⁷², N. Berger⁵, B. Bergmann¹⁴², L. J. Bergsten²⁶, J. Beringer¹⁸, S. Berlendis⁷, N. R. Bernard¹⁰², G. Bernardi¹³⁶, C. Bernius¹⁵³, T. Berry⁹³, P. Berta⁹⁹, C. Bertella^{15a}, I. A. Bertram⁸⁹, O. Bessidskaia Bylund¹⁸², N. Besson¹⁴⁵, A. Bethani¹⁰⁰, S. Bethke¹¹⁵, A. Betti²⁴, A. J. Bevan⁹²,

J. Beyer¹¹⁵, R. Bi¹³⁹, R. M. Bianchi¹³⁹, O. Biebel¹¹⁴, D. Biedermann¹⁹, R. Bielski³⁶, K. Bierwagen⁹⁹, N. V. Biesuz^{71a,71b}, M. Biglietti^{74a}, T. R. V. Billoud¹⁰⁹, M. Bindi⁵³, A. Bingul^{12d}, C. Bini^{72a,72b}, S. Biondi^{23a,23b}, M. Birman¹⁸⁰, T. Bisanz⁵³, J. P. Biswal¹⁶¹, D. Biswas^{181j}, A. Bitadze¹⁰⁰, C. Bittrich⁴⁸, K. Bjørke¹³⁴, K. M. Black²⁵, T. Blazek^{28a}, I. Bloch⁴⁶, C. Blocker²⁶, A. Blue⁵⁷, U. Blumenschein⁹², G. J. Bobbink¹²⁰, V. S. Bobrovnikov^{122a,122b}, S. S. Bocchetta⁹⁶, A. Bocci⁴⁹, D. Boerner⁴⁶, D. Bogavac¹⁴, A. G. Bogdanchikov^{122a,122b}, C. Bohm^{45a}, V. Boisvert⁹³, P. Bokan^{53,172}, T. Bold^{83a}, A. S. Boldyrev¹¹³, A. E. Bolz^{61b}, M. Bomben¹³⁶, M. Bona⁹², J. S. Bonilla¹³¹, M. Boonekamp¹⁴⁵, H. M. Borecka-Bielska⁹⁰, A. Borisov¹²³, G. Borissov⁸⁹, J. Bortfeldt³⁶, D. Bortoletto¹³⁵, D. Boscherini^{23b}, M. Bosman¹⁴, J. D. Bossio Sola¹⁰³, K. Bouaouda^{35a}, J. Boudreau¹³⁹, E. V. Bouhova-Thacker⁸⁹, D. Boumediene³⁸, S. K. Boutle⁵⁷, A. Boveia¹²⁶, J. Boyd³⁶, D. Boye^{33b.at}, I. R. Boyko⁷⁹, A. J. Bozson⁹³, J. Bracini²¹, N. Brahim¹⁰¹, G. Brandt¹⁸², O. Brandt³², F. Braren⁴⁶, B. Brau¹⁰², J. E. Brau¹³¹, W. D. Breaden Madden⁵⁷, K. Brendlinger⁴⁶, L. Brenner⁴⁶, R. Brenner¹⁷², S. Bressler¹⁸⁰, B. Brickwedde⁹⁹, D. L. Briglin²¹, D. Britton⁵⁷, D. Britzger¹¹⁵, I. Brock²⁴, R. Brock¹⁰⁶, G. Brooijmans³⁹, W. K. Brooks^{147b}, E. Brost¹²¹, J. H. Broughton²¹, P. A. Bruckman de Renstrom⁸⁴, D. Bruncko^{28b}, A. Bruni^{23b}, G. Bruni^{23b}, L. S. Bruni¹²⁰, S. Bruno^{73a,73b}, B. H. Brunt³², M. Bruschi^{23b}, N. Brusino¹³⁹, P. Bryant³⁷, L. Bryngemark⁹⁶, T. Buanes¹⁷, Q. Buat³⁶, P. Buchholz¹⁵¹, A. G. Buckley⁵⁷, I. A. Budagov⁷⁹, M. K. Bugge¹³⁴, F. Bühner⁵², O. Bulekov¹¹², T. J. Burch¹²¹, S. Burdin⁹⁰, C. D. Burgard¹²⁰, A. M. Burger¹²⁹, B. Burghgrave⁸, K. Burka^{83a}, J. T. P. Burr⁴⁶, C. D. Burton¹¹, J. C. Burzynski¹⁰², V. Büscher⁹⁹, E. Buschmann⁵³, P. J. Bussey⁵⁷, J. M. Butler²⁵, C. M. Buttar⁵⁷, J. M. Butterworth⁹⁴, P. Butti³⁶, W. Buttinger³⁶, A. Buzatu¹⁵⁸, A. R. Buzykaev^{122a,122b}, G. Cabras^{23a,23b}, S. Cabrera Urbán¹⁷⁴, D. Caforio⁵⁶, H. Cai¹⁷³, V. M. M. Cairo¹⁵³, O. Cakir^{4a}, N. Calace³⁶, P. Calafiura¹⁸, A. Calandri¹⁰¹, G. Calderini¹³⁶, P. Calfayan⁶⁵, G. Callea⁵⁷, L. P. Caloba^{80b}, S. Calvente Lopez⁹⁸, D. Calvet³⁸, S. Calvet³⁸, T. P. Calvet¹⁵⁵, M. Calvetti^{71a,71b}, R. Camacho Toro¹³⁶, S. Camarda³⁶, D. Camarero Munoz⁹⁸, P. Camarri^{73a,73b}, D. Cameron¹³⁴, R. Caminal Armadans¹⁰², C. Camincher³⁶, S. Campana³⁶, M. Campanelli⁹⁴, A. Camplani⁴⁰, A. Campoverde¹⁵¹, V. Canale^{69a,69b}, A. Canesse¹⁰³, M. Cano Bret^{60c}, J. Cantero¹²⁹, T. Cao¹⁶¹, Y. Cao¹⁷³, M. D. M. Capeans Garrido³⁶, M. Capua^{41a,41b}, R. Cardarelli^{73a}, F. Cardillo¹⁴⁹, G. Carducci^{41a,41b}, I. Carli¹⁴³, T. Carli³⁶, G. Carlino^{69a}, B. T. Carlson¹³⁹, L. Carminati^{68a,68b}, R. M. D. Carney^{45a,45b}, S. Caron¹¹⁹, E. Carquin^{147b}, S. Carrá⁴⁶, J. W. S. Carter¹⁶⁷, M. P. Casado^{14e}, A. F. Casha¹⁶⁷, D. W. Casper¹⁷¹, R. Castelijin¹²⁰, F. L. Castillo¹⁷⁴, V. Castillo Gimenez¹⁷⁴, N. F. Castro^{140a,140e}, A. Catinaccio³⁶, J. R. Catmore¹³⁴, A. Cattai³⁶, J. Caudron²⁴, V. Cavaliere²⁹, E. Cavallaro¹⁴, M. Cavalli-Sforza¹⁴, V. Cavasinni^{71a,71b}, E. Celebi^{12b}, F. Ceradini^{74a,74b}, L. Cerda Alberich¹⁷⁴, K. Cerny¹³⁰, A. S. Cerqueira^{80a}, A. Cerri¹⁵⁶, L. Cerrito^{73a,73b}, F. Cerutti¹⁸, A. Cervelli^{23a,23b}, S. A. Cetin^{12b}, Z. Chadi^{35a}, D. Chakraborty¹²¹, S. K. Chan⁵⁹, W. S. Chan¹²⁰, W. Y. Chan⁹⁰, J. D. Chapman³², B. Chargeishvili^{159b}, D. G. Charlton²¹, T. P. Charman⁹², C. C. Chau³⁴, S. Che¹²⁶, A. Chegwidden¹⁰⁶, S. Chekanov⁶, S. V. Chekulaev^{168a}, G. A. Chelkov^{79.ay}, M. A. Chelstowska³⁶, B. Chen⁷⁸, C. Chen^{60a}, C. H. Chen⁷⁸, H. Chen²⁹, J. Chen^{60a}, J. Chen³⁹, S. Chen¹³⁷, S. J. Chen^{15c}, X. Chen^{15b.ax}, Y. Chen⁸², Y.-H. Chen⁴⁶, H. C. Cheng^{63a}, H. J. Cheng^{15a,15d}, A. Cheplakov⁷⁹, E. Cheremushkina¹²³, R. Cherkaoui El Moursli^{35e}, E. Cheu⁷, K. Cheung⁶⁴, T. J. A. Chevalérias¹⁴⁵, L. Chevalier¹⁴⁵, V. Chiarella⁵¹, G. Chiarelli^{71a}, G. Chiodini^{67a}, A. S. Chisholm^{21,36}, A. Chitan^{27b}, I. Chiu¹⁶³, Y. H. Chiu¹⁷⁶, M. V. Chizhov⁷⁹, K. Choi⁶⁵, A. R. Chomont^{72a,72b}, S. Chouridou¹⁶², Y. S. Chow¹²⁰, M. C. Chu^{63a}, X. Chu^{15a}, J. Chudoba¹⁴¹, A. J. Chuinard¹⁰³, J. J. Chwastowski⁸⁴, L. Chytka¹³⁰, D. Cieri¹¹⁵, K. M. Ciesla⁸⁴, D. Cinca⁴⁷, V. Cindro⁹¹, I. A. Cioară^{27b}, A. Ciocio¹⁸, F. Ciroto^{69a,69b}, Z. H. Citron^{180.k}, M. Citterio^{68a}, D. A. Ciubotaru^{27b}, B. M. Ciungu¹⁶⁷, A. Clark⁵⁴, M. R. Clark³⁹, P. J. Clark⁵⁰, C. Clement^{45a,45b}, Y. Coadou¹⁰¹, M. Cobal^{66a,66c}, A. Coccaro^{55b}, J. Cochran⁷⁸, H. Cohen¹⁶¹, A. E. C. Coimbra³⁶, L. Colasurdo¹¹⁹, B. Cole³⁹, A. P. Colijn¹²⁰, J. Collot⁵⁸, P. Conde Muñio^{140a.f}, E. Coniavitis⁵², S. H. Connell^{33b}, I. A. Connelly⁵⁷, S. Constantinescu^{27b}, F. Conventi^{69a,ba}, A. M. Cooper-Sarkar¹³⁵, F. Cormier¹⁷⁵, K. J. R. Cormier¹⁶⁷, L. D. Corpe⁹⁴, M. Corradi^{72a,72b}, E. E. Corrigan⁹⁶, F. Corriveau^{103.af}, A. Cortes-Gonzalez³⁶, M. J. Costa¹⁷⁴, F. Costanza⁵, D. Costanzo¹⁴⁹, G. Cowan⁹³, J. W. Cowley³², J. Crane¹⁰⁰, K. Cranmer¹²⁴, S. J. Crawley⁵⁷, R. A. Creager¹³⁷, S. Crépe-Renaudin⁵⁸, F. Crescioli¹³⁶, M. Cristinziani²⁴, V. Croft¹²⁰, G. Crosetti^{41a,41b}, A. Cueto⁵, T. Cuhadar Donszelmann¹⁴⁹, A. R. Cukierman¹⁵³, S. Czekerda⁸⁴, P. Czodrowski³⁶, M. J. Da Cunha Sargedas De Sousa^{60b}, J. V. Da Fonseca Pinto^{80b}, C. Da Via¹⁰⁰, W. Dabrowski^{83a}, T. Dado^{28a}, S. Dahbi^{35e}, T. Dai¹⁰⁵, C. Dallapiccola¹⁰², M. Dam⁴⁰, G. D'amen²⁹, V. D'Amico^{74a,74b}, J. Damp⁹⁹, J. R. Dandoy¹³⁷, M. F. Daneri³⁰, N. P. Dang^{181.j}, N. S. Dann¹⁰⁰, M. Danninger¹⁷⁵, V. Dao³⁶, G. Darbo^{55b}, O. Dartsis⁵, A. Dattagupta¹³¹, T. Daubney⁴⁶, S. D'Auria^{68a,68b}, W. Davey²⁴, C. David⁴⁶, T. Davidek¹⁴³, D. R. Davis⁴⁹, I. Dawson¹⁴⁹, K. De⁸, R. De Asmundis^{69a}, M. De Beurs¹²⁰, S. De Castro^{23a,23b}, S. De Cecco^{72a,72b}, N. De Groot¹¹⁹, P. de Jong¹²⁰, H. De la Torre¹⁰⁶, A. De Maria^{15c}, D. De Pedis^{72a}, A. De Salvo^{72a}, U. De Sanctis^{73a,73b}, M. De Santis^{73a,73b}, A. De Santo¹⁵⁶, K. De Vasconcelos Corga¹⁰¹, J. B. De Vivie De Regie¹³², C. Debenedetti¹⁴⁶, D. V. Dedovich⁷⁹, A. M. Deiana⁴², M. Del Gaudio^{41a,41b}, J. Del Peso⁹⁸, Y. Delabat Diaz⁴⁶, D. Delgove¹³², F. Deliot^{145.r}, C. M. Delitzsch⁷, M. Della Pietra^{69a,69b}, D. Della Volpe⁵⁴, A. Dell'Acqua³⁶, L. Dell'Asta^{73a,73b}, M. Delmastro⁵, C. Delporte¹³², P. A. Delsart⁵⁸, D. A. DeMarco¹⁶⁷, S. Demers¹⁸³, M. Demichev⁷⁹, G. Demontigny¹⁰⁹, S. P. Denisov¹²³, D. Denysiuk¹²⁰

L. D'Eramo¹³⁶, D. Derendarz⁸⁴, J. E. Derkaoui^{35d}, F. Derue¹³⁶, P. Dervan⁹⁰, K. Desch²⁴, C. Deterre⁴⁶, K. Dette¹⁶⁷, C. Deutsch²⁴, M. R. Devesa³⁰, P. O. Deviveiros³⁶, A. Dewhurst¹⁴⁴, F. A. Di Bello⁵⁴, A. Di Ciaccio^{73a,73b}, L. Di Ciaccio⁵, W. K. Di Clemente¹³⁷, C. Di Donato^{69a,69b}, A. Di Girolamo³⁶, G. Di Gregorio^{71a,71b}, B. Di Micco^{74a,74b}, R. Di Nardo¹⁰², K. F. Di Petrillo⁵⁹, R. Di Sipio¹⁶⁷, D. Di Valentino³⁴, C. Diaconu¹⁰¹, F. A. Dias⁴⁰, T. Dias Do Vale^{140a}, M. A. Diaz^{147a}, J. Dickinson¹⁸, E. B. Diehl¹⁰⁵, J. Dietrich¹⁹, S. Díez Cornell⁴⁶, A. Dimitrievska¹⁸, W. Ding^{15b}, J. Dingfelder²⁴, F. Dittus³⁶, F. Djama¹⁰¹, T. Djobava^{159b}, J. I. Djuvsland¹⁷, M. A. B. Do Vale^{80c}, M. Dobre^{27b}, D. Dodsworth²⁶, C. Dogliani⁹⁶, J. Dolejsi¹⁴³, Z. Dolezal¹⁴³, M. Donadelli^{80d}, B. Dong^{60c}, J. Donini³⁸, A. D'Onofrio⁹², M. D'Onofrio⁹⁰, J. Dopke¹⁴⁴, A. Doria^{69a}, M. T. Dova⁸⁸, A. T. Doyle⁵⁷, E. Drechsler¹⁵², E. Dreyer¹⁵², T. Dreyer⁵³, A. S. Drobac¹⁷⁰, Y. Duan^{60b}, F. Dubinin¹¹⁰, M. Dubovsky^{28a}, A. Dubreuil⁵⁴, E. Duchovni¹⁸⁰, G. Duckeck¹¹⁴, A. Ducourthial¹³⁶, O. A. Ducu¹⁰⁹, D. Duda¹¹⁵, A. Dudarev³⁶, A. C. Dudder⁹⁹, E. M. Duffield¹⁸, L. Dufflot¹³², M. Dührssen³⁶, C. Dülsen¹⁸², M. Dumancic¹⁸⁰, A. E. Dumitriu^{27b}, A. K. Duncan⁵⁷, M. Dunford^{61a}, A. Duperrin¹⁰¹, H. Duran Yildiz^{4a}, M. Düren⁵⁶, A. Durglishvili^{159b}, D. Duschinger⁴⁸, B. Dutta⁴⁶, D. Duvnjak¹, G. I. Dyckes¹³⁷, M. Dyndal³⁶, S. Dysch¹⁰⁰, B. S. Dziedzic⁸⁴, K. M. Ecker¹¹⁵, R. C. Edgar¹⁰⁵, M. G. Eggleston⁴⁹, T. Eifert³⁶, G. Eigen¹⁷, K. Einsweiler¹⁸, T. Ekelof¹⁷², H. El Jarrari^{35e}, M. El Kacimi^{35c}, R. El Kosseifi¹⁰¹, V. Ellajosyula¹⁷², M. Ellert¹⁷², F. Ellinghaus¹⁸², A. A. Elliot⁹², N. Ellis³⁶, J. Elmsheuser²⁹, M. Elsing³⁶, D. Emeliyanov¹⁴⁴, A. Emerman³⁹, Y. Enari¹⁶³, M. B. Epland⁴⁹, J. Erdmann⁴⁷, A. Ereditato²⁰, M. Errenst³⁶, M. Escalier¹³², C. Escobar¹⁷⁴, O. Estrada Pastor¹⁷⁴, E. Etzion¹⁶¹, H. Evans⁶⁵, A. Ezhilov¹³⁸, F. Fabbri⁵⁷, L. Fabbri^{23a,23b}, V. Fabiani¹¹⁹, G. Facini⁹⁴, R. M. Faisca Rodrigues Pereira^{140a}, R. M. Fakhruddinov¹²³, S. Falciano^{72a}, P. J. Falke⁵, S. Falke⁵, J. Faltova¹⁴³, Y. Fang^{15a}, Y. Fang^{15a}, G. Fanourakis⁴⁴, M. Fanti^{68a,68b}, M. Faraj^{66a,66c,v}, A. Farbin⁸, A. Farilla^{74a}, E. M. Farina^{70a,70b}, T. Farooque¹⁰⁶, S. Farrell¹⁸, S. M. Farrington⁵⁰, P. Farthouat³⁶, F. Fassi^{35e}, P. Fassnacht³⁶, D. Fassouliotis⁹, M. Fauci Giannelli⁵⁰, W. J. Fawcett³², L. Fayard¹³², O. L. Fedin^{138,p}, W. Fedorko¹⁷⁵, M. Feickert⁴², L. Felgioni¹⁰¹, A. Fell¹⁴⁹, C. Feng^{60b}, E. J. Feng³⁶, M. Feng⁴⁹, M. J. Fenton⁵⁷, A. B. Fenyuk¹²³, J. Ferrando⁴⁶, A. Ferrante¹⁷³, A. Ferrari¹⁷², P. Ferrari¹²⁰, R. Ferrari^{70a}, D. E. Ferreira de Lima^{61b}, A. Ferrer¹⁷⁴, D. Ferrere⁵⁴, C. Ferretti¹⁰⁵, F. Fiedler⁹⁹, A. Filipčić⁹¹, F. Filthaut¹¹⁹, K. D. Finelli²⁵, M. C. N. Fiolhais^{140a,140c,a}, L. Fiorini¹⁷⁴, F. Fischer¹¹⁴, W. C. Fisher¹⁰⁶, I. Fleck¹⁵¹, P. Fleischmann¹⁰⁵, R. R. M. Fletcher¹³⁷, T. Flick¹⁸², B. M. Flierl¹¹⁴, L. Flores¹³⁷, L. R. Flores Castillo^{63a}, F. M. Follega^{75a,75b}, N. Fomin¹⁷, J. H. Foo¹⁶⁷, G. T. Forcolin^{75a,75b}, A. Formica¹⁴⁵, F. A. Förster¹⁴, A. C. Forti¹⁰⁰, A. G. Foster²¹, M. G. Foti¹³⁵, D. Fournier¹³², H. Fox⁸⁹, P. Francavilla^{71a,71b}, S. Francescato^{72a,72b}, M. Franchini^{23a,23b}, S. Franchino^{61a}, D. Francis³⁶, L. Franconi²⁰, M. Franklin⁵⁹, A. N. Fray⁹², P. M. Freeman²¹, B. Freund¹⁰⁹, W. S. Freund^{80b}, E. M. Freundlich⁴⁷, D. C. Frizzell¹²⁸, D. Froidevaux³⁶, J. A. Frost¹³⁵, C. Fukunaga¹⁶⁴, E. Fullana Torregrosa¹⁷⁴, E. Fumagalli^{55a,55b}, T. Fusayasu¹¹⁶, J. Fuster¹⁷⁴, A. Gabrielli^{23a,23b}, A. Gabrielli¹⁸, G. P. Gach^{83a}, S. Gadatsch⁵⁴, P. Gadow¹¹⁵, G. Gagliardi^{55a,55b}, L. G. Gagnon¹⁰⁹, C. Galea^{27b}, B. Galhardo^{140a}, G. E. Gallardo¹³⁵, E. J. Gallas¹³⁵, B. J. Gallop¹⁴⁴, G. Galster⁴⁰, R. Gamboa Goni⁹², K. K. Gan¹²⁶, S. Ganguly¹⁸⁰, J. Gao^{60a}, Y. Gao⁵⁰, Y. S. Gao^{31,m}, C. García¹⁷⁴, J. E. García Navarro¹⁷⁴, J. A. García Pascual^{15a}, C. Garcia-Argos⁵², M. Garcia-Sciveres¹⁸, R. W. Gardner³⁷, N. Garelli¹⁵³, S. Gargiulo⁵², V. Garonne¹³⁴, A. Gaudiello^{55a,55b}, G. Gaudio^{70a}, I. L. Gavrilenko¹¹⁰, A. Gavriilyuk¹¹¹, C. Gay¹⁷⁵, G. Gaycken⁴⁶, E. N. Gazis¹⁰, A. A. Geanta^{27b}, C. N. P. Gee¹⁴⁴, J. Geisen⁵³, M. Geisen⁹⁹, M. P. Geisler^{61a}, C. Gemme^{55b}, M. H. Genest⁵⁸, C. Geng¹⁰⁵, S. Gentile^{72a,72b}, S. George⁹³, T. Gerialis⁴⁴, L. O. Gerlach⁵³, P. Gessinger-Befurt⁹⁹, G. Gessner⁴⁷, S. Ghasemi¹⁵¹, M. Ghasemi Bostanabad¹⁷⁶, A. Ghosh¹³², A. Ghosh⁷⁷, B. Giacobbe^{23b}, S. Giagu^{72a,72b}, N. Giangiacomi^{23a,23b}, P. Giannetti^{71a}, A. Giannini^{69a,69b}, G. Giannini¹⁴, S. M. Gibson⁹³, M. Gignac¹⁴⁶, D. Gillberg³⁴, G. Gilles¹⁸², D. M. Gingrich^{3,az}, M. P. Giordani^{66a,66c}, F. M. Giorgi^{23b}, P. F. Giraud¹⁴⁵, G. Giugliarelli^{66a,66c}, D. Giugni^{68a}, F. Giuli^{73a,73b}, S. Gkaitatzis¹⁶², I. Gkialas^{9,h}, E. L. Gkougkousis¹⁴, P. Gkoutoumis¹⁰, L. K. Gladilin¹¹³, C. Glasman⁹⁸, J. Glatzer¹⁴, P. C. F. Glaysheer⁴⁶, A. Glazov⁴⁶, G. R. Gledhill¹³¹, M. Goblirsch-Kolb²⁶, S. Goldfarb¹⁰⁴, T. Golling⁵⁴, D. Golubkov¹²³, A. Gomes^{140a,140b}, R. Goncalves Gama⁵³, R. Gonçalves^{140a,140b}, G. Gonella⁵², L. Gonella²¹, A. Gongadze⁷⁹, F. Gonnella²¹, J. L. Gonski⁵⁹, S. González de la Hoz¹⁷⁴, S. Gonzalez-Sevilla⁵⁴, G. R. Gonzalvo Rodriguez¹⁷⁴, L. Goossens³⁶, P. A. Gorbounov¹¹¹, H. A. Gordon²⁹, B. Gorini³⁶, E. Gorini^{67a,67b}, A. Gorišek⁹¹, A. T. Goshaw⁴⁹, M. I. Gostkin⁷⁹, C. A. Gottardo¹¹⁹, M. Gouighri^{35b}, D. Goujdami^{35c}, A. G. Goussiou¹⁴⁸, N. Govender^{33b}, C. Goy⁵, E. Gozani¹⁶⁰, I. Grabowska-Bold^{83a}, E. C. Graham⁹⁰, J. Gramling¹⁷¹, E. Gramstad¹³⁴, S. Grancagnolo¹⁹, M. Grandi¹⁵⁶, V. Gratchev¹³⁸, P. M. Gravila^{27f}, F. G. Gravili^{67a,67b}, C. Gray⁵⁷, H. M. Gray¹⁸, C. Grefe²⁴, K. Gregersen⁹⁶, I. M. Gregor⁴⁶, P. Grenier¹⁵³, K. Grevtsov⁴⁶, C. Grieco¹⁴, N. A. Grieser¹²⁸, J. Griffiths⁸, A. A. Grillo¹⁴⁶, K. Grimm^{31,l}, S. Grinstein^{14,aa}, J.-F. Grivaz¹³², S. Groh⁹⁹, E. Gross¹⁸⁰, J. Grosse-Knetter⁵³, Z. J. Grout⁹⁴, C. Grud¹⁰⁵, A. Grummer¹¹⁸, L. Guan¹⁰⁵, W. Guan¹⁸¹, J. Guenther³⁶, A. Guerguichon¹³², J. G. R. Guerrero Rojas¹⁷⁴, F. Guescini¹¹⁵, D. Guest¹⁷¹, R. Gugel⁵², T. Guillemain⁵, S. Guindon³⁶, U. Gul⁵⁷, J. Guo^{60c}, W. Guo¹⁰⁵, Y. Guo^{60a,t}, Z. Guo¹⁰¹, R. Gupta⁴⁶, S. Gurbuz^{12c}, G. Gustavino¹²⁸, P. Gutierrez¹²⁸, C. Gutsche⁹⁴, C. Guyot¹⁴⁵, C. Gwenlan¹³⁵, C. B. Gwilliam⁹⁰, A. Haas¹²⁴, C. Haber¹⁸, H. K. Hadavand⁸, N. Haddad^{35e}, A. Hadeef^{60a}, S. Hageböck³⁶, M. Haleem¹⁷⁷, J. Haley¹²⁹, G. Halladjian¹⁰⁶, G. D. Hallewell¹⁰¹, K. Hamacher¹⁸², P. Hamal¹³⁰, K. Hamano¹⁷⁶, H. Hamdaoui^{35e}, G. N. Hamity¹⁴⁹,

K. Han^{60a,am}, L. Han^{60a}, S. Han^{15a,15d}, Y. F. Han¹⁶⁷, K. Hanagaki^{81,y}, M. Hance¹⁴⁶, D. M. Handl¹¹⁴, B. Haney¹³⁷, R. Hankache¹³⁶, E. Hansen⁹⁶, J. B. Hansen⁴⁰, J. D. Hansen⁴⁰, M. C. Hansen²⁴, P. H. Hansen⁴⁰, E. C. Hanson¹⁰⁰, K. Hara¹⁶⁹, A. S. Hard¹⁸¹, T. Harenberg¹⁸², S. Harkusha¹⁰⁷, P. F. Harrison¹⁷⁸, N. M. Hartmann¹¹⁴, Y. Hasegawa¹⁵⁰, A. Hasib⁵⁰, S. Hassani¹⁴⁵, S. Haug²⁰, R. Hauser¹⁰⁶, L. B. Havener³⁹, M. Havranek¹⁴², C. M. Hawkes²¹, R. J. Hawkings³⁶, D. Hayden¹⁰⁶, C. Hayes¹⁵⁵, R. L. Hayes¹⁷⁵, C. P. Hays¹³⁵, J. M. Hays⁹², H. S. Hayward⁹⁰, S. J. Haywood¹⁴⁴, F. He^{60a}, M. P. Heath⁵⁰, V. Hedberg⁹⁶, L. Heelan⁸, S. Heer²⁴, K. K. Heidegger⁵², W. D. Heidorn⁷⁸, J. Heilman³⁴, S. Heim⁴⁶, T. Heim¹⁸, B. Heinemann^{46,au}, J. J. Heinrich¹³¹, L. Heinrich³⁶, C. Heinz⁵⁶, J. Hejbal¹⁴¹, L. Helary^{61b}, A. Held¹⁷⁵, S. Hellesund¹³⁴, C. M. Helling¹⁴⁶, S. Hellman^{45a,45b}, C. Helsen³⁶, R. C. W. Henderson⁸⁹, Y. Heng¹⁸¹, S. Henkelmann¹⁷⁵, A. M. Henriques Correia³⁶, G. H. Herbert¹⁹, H. Herde²⁶, V. Herget¹⁷⁷, Y. Hernández Jiménez^{33c}, H. Herr⁹⁹, M. G. Herrmann¹¹⁴, T. Herrmann⁴⁸, G. Herten⁵², R. Hertenberger¹¹⁴, L. Hervas³⁶, T. C. Herwig¹³⁷, G. G. Hesketh⁹⁴, N. P. Hessey^{168a}, A. Higashida¹⁶³, S. Higashino⁸¹, E. Higón-Rodríguez¹⁷⁴, K. Hildebrand³⁷, E. Hill¹⁷⁶, J. C. Hill³², K. K. Hill²⁹, K. H. Hiller⁴⁶, S. J. Hillier²¹, M. Hils⁴⁸, I. Hinchliffe¹⁸, F. Hinterkeuser²⁴, M. Hirose¹³³, S. Hirose⁵², D. Hirschbuehl¹⁸², B. Hiti⁹¹, O. Hladik¹⁴¹, D. R. Hlaluku^{33c}, X. Hoad⁵⁰, J. Hobbs¹⁵⁵, N. Hod¹⁸⁰, M. C. Hodgkinson¹⁴⁹, A. Hoecker³⁶, F. Hoenic¹¹⁴, D. Hohn⁵², D. Hohov¹³², T. R. Holmes³⁷, M. Holzbock¹¹⁴, L.B.A.H Hommels³², S. Honda¹⁶⁹, T. M. Hong¹³⁹, A. Hönle¹¹⁵, B. H. Hooberman¹⁷³, W. H. Hopkins⁶, Y. Horii¹¹⁷, P. Horn⁴⁸, L. A. Horyn³⁷, S. Hou¹⁵⁸, A. Hoummada^{35a}, J. Howarth¹⁰⁰, J. Hoya⁸⁸, M. Hrabovsky¹³⁰, J. Hrdinka⁷⁶, I. Hristova¹⁹, J. Hrivnac¹³², A. Hrynevich¹⁰⁸, T. Hryn'ova⁵, P. J. Hsu⁶⁴, S.-C. Hsu¹⁴⁸, Q. Hu²⁹, S. Hu^{60c}, D. P. Huang⁹⁴, Y. Huang^{60a}, Y. Huang^{15a}, Z. Hubacek¹⁴², F. Hubaut¹⁰¹, M. Huebner²⁴, F. Huegging²⁴, T. B. Huffman¹³⁵, M. Huhtinen³⁶, R. F. H. Hunter³⁴, P. Huo¹⁵⁵, A. M. Hupe³⁴, N. Huseynov^{79,ah}, J. Huston¹⁰⁶, J. Huth⁵⁹, R. Hyneman¹⁰⁵, S. Hyrych^{28a}, G. Iacobucci⁵⁴, G. Iakovidis²⁹, I. Ibragimov¹⁵¹, L. Iconomidou-Fayard¹³², Z. Idrissi^{35e}, P. Iengo³⁶, R. Ignazzi⁴⁰, O. Igonkina^{120,ac,*}, R. Iguchi¹⁶³, T. Iizawa⁵⁴, Y. Ikegami⁸¹, M. Ikeno⁸¹, D. Iliadis¹⁶², N. Ilic^{119,u}, F. Iltzsche⁴⁸, G. Introzzi^{70a,70b}, M. Iodice^{74a}, K. Iordanidou^{168a}, V. Ippolito^{72a,72b}, M. F. Isacson¹⁷², M. Ishino¹⁶³, W. Islam¹²⁹, C. Issever¹³⁵, S. Istin¹⁶⁰, F. Ito¹⁶⁹, J. M. Iturbe Ponce^{63a}, R. Iuppa^{75a,75b}, A. Ivina¹⁸⁰, H. Iwasaki⁸¹, J. M. Izen⁴³, V. Izzo^{69a}, P. Jacka¹⁴¹, P. Jackson¹, R. M. Jacobs²⁴, B. P. Jaeger¹⁵², V. Jain², G. Jäkel¹⁸², K. B. Jakobi⁹⁹, K. Jakobs⁵², S. Jakobsen⁷⁶, T. Jakoubek¹⁴¹, J. Jamieson⁵⁷, K. W. Janas^{83a}, R. Jansky⁵⁴, J. Janssen²⁴, M. Janus⁵³, P. A. Janus^{83a}, G. Jarlskog⁹⁶, N. Javadov^{79,ah}, T. Javůrek³⁶, M. Javurkova⁵², F. Jeanneau¹⁴⁵, L. Jeanty¹³¹, J. Jejelava^{159a,ai}, A. Jelinskas¹⁷⁸, P. Jenni^{52,b}, J. Jeong⁴⁶, N. Jeong⁴⁶, S. Jézéquel⁵, H. Ji¹⁸¹, J. Jia¹⁵⁵, H. Jiang⁷⁸, Y. Jiang^{60a}, Z. Jiang^{153,q}, S. Jiggins⁵², F. A. Jimenez Morales³⁸, J. Jimenez Pena¹¹⁵, S. Jin^{15c}, A. Jinaru^{27b}, O. Jinnouchi¹⁶⁵, H. Jivan^{33c}, P. Johansson¹⁴⁹, K. A. Johns⁷, C. A. Johnson⁶⁵, K. Jon-And^{45a,45b}, R. W. L. Jones⁸⁹, S. D. Jones¹⁵⁶, S. Jones⁷, T. J. Jones⁹⁰, J. Jongmanns^{61a}, P. M. Jorge^{140a}, J. Jovicevic³⁶, X. Ju¹⁸, J. J. Junggeburth¹¹⁵, A. Juste Rozas^{14,aa}, A. Kaczmarska⁸⁴, M. Kado^{72a,72b}, H. Kagan¹²⁶, M. Kagan¹⁵³, C. Kahra⁹⁹, T. Kaji¹⁷⁹, E. Kajomovitz¹⁶⁰, C. W. Kalderon⁹⁶, A. Kaluza⁹⁹, A. Kamenshchikov¹²³, L. Kanjir⁹¹, Y. Kano¹⁶³, V. A. Kantserov¹¹², J. Kanzaki⁸¹, L. S. Kaplan¹⁸¹, D. Kar^{33c}, K. Karava¹³⁵, M. J. Kareem^{168b}, S. N. Karpov⁷⁹, Z. M. Karpova⁷⁹, V. Kartvelishvili⁸⁹, A. N. Karyukhin¹²³, L. Kashif¹⁸¹, R. D. Kass¹²⁶, A. Kastanas^{45a,45b}, C. Kato^{60c,60d}, J. Katzy⁴⁶, K. Kawade¹⁵⁰, K. Kawagoe⁸⁷, T. Kawaguchi¹¹⁷, T. Kawamoto¹⁶³, G. Kawamura⁵³, E. F. Kay¹⁷⁶, V. F. Kazanin^{122a,122b}, R. Keeler¹⁷⁶, R. Kehoe⁴², J. S. Keller³⁴, E. Kellermann⁹⁶, D. Kelsey¹⁵⁶, J. J. Kempster²¹, J. Kendrick²¹, O. Kepka¹⁴¹, S. Kersten¹⁸², B. P. Kerševan⁹¹, S. Ketabchi Haghighat¹⁶⁷, M. Khader¹⁷³, F. Khalil-Zada¹³, M. Khandoga¹⁴⁵, A. Khanov¹²⁹, A. G. Kharlamov^{122a,122b}, T. Kharlamova^{122a,122b}, E. E. Khoda¹⁷⁵, A. Khodinov¹⁶⁶, T. J. Khoo⁵⁴, E. Khramov⁷⁹, J. Khubua^{159b}, S. Kido⁸², M. Kiehn⁵⁴, C. R. Kilby⁹³, Y. K. Kim³⁷, N. Kimura⁹⁴, O. M. Kind¹⁹, B. T. King^{90,*}, D. Kirchmeier⁴⁸, J. Kirk¹⁴⁴, A. E. Kiryunin¹¹⁵, T. Kishimoto¹⁶³, D. P. Kisiuk¹⁶⁷, V. Kitali⁴⁶, O. Kivernyk⁵, T. Klapdor-Kleingrothaus⁵², M. Klassen^{61a}, M. H. Klein¹⁰⁵, M. Klein⁹⁰, U. Klein⁹⁰, K. Kleinknecht⁹⁹, P. Klimek¹²¹, A. Klimentov²⁹, T. Klingl²⁴, T. Klioutchnikova³⁶, F. F. Klitzner¹¹⁴, P. Kluit¹²⁰, S. Kluth¹¹⁵, E. Kneringer⁷⁶, E. B. F. G. Knoops¹⁰¹, A. Knue⁵², D. Kobayashi⁸⁷, T. Kobayashi¹⁶³, M. Kobel⁴⁸, M. Kocian¹⁵³, P. Kodys¹⁴³, P. T. Koenig²⁴, T. Koffas³⁴, N. M. Köhler³⁶, T. Koi¹⁵³, M. Kolb^{61b}, I. Koletsou⁵, T. Komarek¹³⁰, T. Kondo⁸¹, N. Kondrashova^{60c}, K. Köneke⁵², A. C. König¹¹⁹, T. Kono¹²⁵, R. Konoplich^{124,ap}, V. Konstantinides⁹⁴, N. Konstantinidis⁹⁴, B. Konya⁹⁶, R. Kopeliansky⁶⁵, S. Koperny^{83a}, K. Korcyl⁸⁴, K. Kordas¹⁶², G. Koren¹⁶¹, A. Korn⁹⁴, I. Korolkov¹⁴, E. V. Korolkova¹⁴⁹, N. Korotkova¹¹³, O. Kortner¹¹⁵, S. Kortner¹¹⁵, T. Kosek¹⁴³, V. V. Kostyukhin¹⁶⁶, A. Kotwal⁴⁹, A. Koulouris¹⁰, A. Kourkouveli-Charalampidi^{70a,70b}, C. Kourkouvelis⁹, E. Kourlitis¹⁴⁹, V. Kouskoura²⁹, A. B. Kowalewska⁸⁴, R. Kowalewski¹⁷⁶, C. Kozakai¹⁶³, W. Kozanecki¹⁴⁵, A. S. Kozhin¹²³, V. A. Kramarenko¹¹³, G. Kramberger⁹¹, D. Krasnopevtsev^{60a}, M. W. Krasny¹³⁶, A. Krasznahorkay³⁶, D. Krauss¹¹⁵, J. A. Kremer^{83a}, J. Kretzschmar⁹⁰, P. Krieger¹⁶⁷, F. Krieter¹¹⁴, A. Krishnan^{61b}, K. Krizka¹⁸, K. Kroeninger⁴⁷, H. Kroha¹¹⁵, J. Kroll¹⁴¹, J. Kroll¹³⁷, J. Krstic¹⁶, U. Kruchonak⁷⁹, H. Krüger²⁴, N. Krumnack⁷⁸, M. C. Kruse⁴⁹, J. A. Krzysiak⁸⁴, T. Kubota¹⁰⁴, O. Kuchinskaja¹⁶⁶, S. Kuday^{4b}, J. T. Kuechler⁴⁶, S. Kuehn³⁶, A. Kugel^{61a}, T. Kuhl⁴⁶, V. Kukhtin⁷⁹, R. Kukla¹⁰¹, Y. Kulchitsky^{107,al}, S. Kuleshov^{147b}, Y. P. Kulinich¹⁷³, M. Kuna⁵⁸, T. Kunigo⁸⁵, A. Kupco¹⁴¹, T. Kupfer⁴⁷, O. Kuprash⁵²

H. Kurashige⁸², L. L. Kurchaninov^{168a}, Y. A. Kurochkin¹⁰⁷, A. Kurova¹¹², M. G. Kurth^{15a,15d}, E. S. Kuwertz³⁶, M. Kuze¹⁶⁵, A. K. Kvam¹⁴⁸, J. Kvita¹³⁰, T. Kwan¹⁰³, A. La Rosa¹¹⁵, L. La Rotonda^{41a,41b}, F. La Ruffa^{41a,41b}, C. Lacasta¹⁷⁴, F. Lacava^{72a,72b}, D. P. J. Lack¹⁰⁰, H. Lacker¹⁹, D. Lacour¹³⁶, E. Ladygin⁷⁹, R. Lafaye⁵, B. Laforge¹³⁶, T. Lagouri^{33c}, S. Lai⁵³, S. Lammers⁶⁵, W. Lampl⁷, C. Lampoudis¹⁶², E. Lançon²⁹, U. Landgraf⁵², M. P. J. Landon⁹², M. C. Lanfermann⁵⁴, V. S. Lang⁴⁶, J. C. Lange⁵³, R. J. Langenberg³⁶, A. J. Lankford¹⁷¹, F. Lanni²⁹, K. Lantsch²⁴, A. Lanza^{70a}, A. Lapertosa^{55a,55b}, S. Laplace¹³⁶, J. F. Laporte¹⁴⁵, T. Lari^{68a}, F. Lasagni Manghi^{23a,23b}, M. Lassnig³⁶, T. S. Lau^{63a}, A. Laudrain¹³², A. Laurier³⁴, M. Lavorgna^{69a,69b}, M. Lazzaroni^{68a,68b}, B. Le¹⁰⁴, E. Le Guirriec¹⁰¹, M. LeBlanc⁷, T. LeCompte⁶, F. Ledroit-Guillon⁵⁸, C. A. Lee²⁹, G. R. Lee¹⁷, L. Lee⁵⁹, S. C. Lee¹⁵⁸, S. J. Lee³⁴, B. Lefebvre^{168a}, M. Lefebvre¹⁷⁶, F. Legger¹¹⁴, C. Leggett¹⁸, K. Lehmann¹⁵², N. Lehmann¹⁸², G. Lehmann Miotto³⁶, W. A. Leight⁴⁶, A. Leisos^{162,z}, M. A. L. Leite^{80d}, C. E. Leitgeb¹¹⁴, R. Leitner¹⁴³, D. Lellouch^{180,*}, K. J. C. Leney⁴², T. Lenz²⁴, B. Lenzi³⁶, R. Leone⁷, S. Leone^{71a}, C. Leonidopoulos⁵⁰, A. Leopold¹³⁶, G. Lerner¹⁵⁶, C. Leroy¹⁰⁹, R. Les¹⁶⁷, C. G. Lester³², M. Levchenko¹³⁸, J. Levêque⁵, D. Levin¹⁰⁵, L. J. Levinson¹⁸⁰, D. J. Lewis²¹, B. Li^{15b}, B. Li¹⁰⁵, C.-Q. Li^{60a}, F. Li^{60c}, H. Li^{60a}, H. Li^{60b}, J. Li^{60c}, K. Li¹⁵³, L. Li^{60c}, M. Li^{15a}, Q. Li^{15a,15d}, Q. Y. Li^{60a}, S. Li^{60c,60d}, X. Li⁴⁶, Y. Li⁴⁶, Z. Li^{60b}, Z. Liang^{15a}, B. Liberti^{73a}, A. Liblong¹⁶⁷, K. Lie^{63c}, S. Liem¹²⁰, C. Y. Lin³², K. Lin¹⁰⁶, T. H. Lin⁹⁹, R. A. Linck⁶⁵, J. H. Lindon²¹, A. L. Lioni⁵⁴, E. Lipeles¹³⁷, A. Lipniacka¹⁷, M. Lisovsky^{61b}, T. M. Liss^{173,aw}, A. Lister¹⁷⁵, A. M. Litke¹⁴⁶, J. D. Little⁸, B. Liu⁷⁸, B. L. Liu⁶, H. B. Liu²⁹, H. Liu¹⁰⁵, J. B. Liu^{60a}, J. K. K. Liu¹³⁵, K. Liu¹³⁶, M. Liu^{60a}, P. Liu¹⁸, Y. Liu^{15a,15d}, Y. L. Liu¹⁰⁵, Y. W. Liu^{60a}, M. Livan^{70a,70b}, A. Lleres⁵⁸, J. Llorente Merino¹⁵², S. L. Lloyd⁹², C. Y. Lo^{63b}, F. Lo Sterzo⁴², E. M. Lobodzinska⁴⁶, P. Loch⁷, S. Loffredo^{73a,73b}, T. Lohse¹⁹, K. Lohwasser¹⁴⁹, M. Lokajicek¹⁴¹, J. D. Long¹⁷³, R. E. Long⁸⁹, L. Longo³⁶, K. A. Looper¹²⁶, J. A. Lopez^{147b}, I. Lopez Paz¹⁰⁰, A. Lopez Solis¹⁴⁹, J. Lorenz¹¹⁴, N. Lorenzo Martinez⁵, M. Losada²², P. J. Lösel¹¹⁴, A. Lösle⁵², X. Lou⁴⁶, X. Lou^{15a}, A. Lounis¹³², J. Love⁶, P. A. Love⁸⁹, J. J. Lozano Bahilo¹⁷⁴, M. Lu^{60a}, Y. J. Lu⁶⁴, H. J. Lubatti¹⁴⁸, C. Luci^{72a,72b}, A. Lucotte⁵⁸, C. Luedtke⁵², F. Luehring⁶⁵, I. Luise¹³⁶, L. Luminari^{72a}, B. Lund-Jensen¹⁵⁴, M. S. Lutz¹⁰², D. Lynn²⁹, R. Lysak¹⁴¹, E. Lytken⁹⁶, F. Lyu^{15a}, V. Lyubushkin⁷⁹, T. Lyubushkina⁷⁹, H. Ma²⁹, L. L. Ma^{60b}, Y. Ma^{60b}, G. Maccarrone⁵¹, A. Macchiolo¹¹⁵, C. M. Macdonald¹⁴⁹, J. Machado Miguens¹³⁷, D. Madaffari¹⁷⁴, R. Madar³⁸, W. F. Mader⁴⁸, N. Madysa⁴⁸, J. Maeda⁸², S. Maeland¹⁷, T. Maeno²⁹, M. Maerker⁴⁸, A. S. Maevskiy¹¹³, V. Magerl⁵², N. Magini⁷⁸, D. J. Mahon³⁹, C. Maidantchik^{80b}, T. Maier¹¹⁴, A. Maio^{140a,140b,140d}, O. Majersky^{28a}, S. Majewski¹³¹, Y. Makida⁸¹, N. Makovec¹³², B. Malaescu¹³⁶, Pa. Malecki⁸⁴, V. P. Maleev¹³⁸, F. Malek⁵⁸, U. Mallik⁷⁷, D. Malon⁶, C. Malone³², S. Maltezos¹⁰, S. Malyukov⁷⁹, J. Mamuzic¹⁷⁴, G. Mancini⁵¹, I. Mandić⁹¹, L. Manhaes de Andrade Filho^{80a}, I. M. Maniatis¹⁶², J. Manjarres Ramos⁴⁸, K. H. Mankinen⁹⁶, A. Mann¹¹⁴, A. Manousos⁷⁶, B. Mansoulie¹⁴⁵, I. Mantos¹⁶², S. Manzoni¹²⁰, A. Marantis¹⁶², G. Marceca³⁰, L. Marchese¹³⁵, G. Marchiori¹³⁶, M. Marcisovsky¹⁴¹, C. Marcon⁹⁶, C. A. Marin Tobon³⁶, M. Marjanovic³⁸, Z. Marshall¹⁸, M.U.F. Martensson¹⁷², S. Marti-Garcia¹⁷⁴, C. B. Martin¹²⁶, T. A. Martin¹⁷⁸, V. J. Martin⁵⁰, B. Martin dit Latour¹⁷, L. Martinelli^{74a,74b}, M. Martinez^{14,aa}, V. I. Martinez Outschoorn¹⁰², S. Martin-Haugh¹⁴⁴, V. S. Martoiu^{27b}, A. C. Martyniuk⁹⁴, A. Marzin³⁶, S. R. Maschek¹¹⁵, L. Masetti⁹⁹, T. Mashimo¹⁶³, R. Mashinistov¹¹⁰, J. Masik¹⁰⁰, A. L. Maslennikov^{122a,122b}, L. Massa^{73a,73b}, P. Massarotti^{69a,69b}, P. Mastrandrea^{71a,71b}, A. Mastroberardino^{41a,41b}, T. Masubuchi¹⁶³, D. Matakias¹⁰, A. Matic¹¹⁴, P. Mättig²⁴, J. Maurer^{27b}, B. Maček⁹¹, D. A. Maximov^{122a,122b}, R. Mazini¹⁵⁸, I. Maznas¹⁶², S. M. Mazza¹⁴⁶, S. P. Mc Kee¹⁰⁵, T. G. McCarthy¹¹⁵, W. P. McCormack¹⁸, E. F. McDonald¹⁰⁴, J. A. McFayden³⁶, G. Mchedlidze^{159b}, M. A. McKay⁴², K. D. McLean¹⁷⁶, S. J. McMahan¹⁴⁴, P. C. McNamara¹⁰⁴, C. J. McNicol¹⁷⁸, R. A. McPherson^{176,af}, J. E. Mdhlluli^{33c}, Z. A. Meadows¹⁰², S. Meehan³⁶, T. Megy⁵², S. Mehlhase¹¹⁴, A. Mehta⁹⁰, T. Meideck⁵⁸, B. Meirose⁴³, D. Melini¹⁷⁴, B. R. Mellado Garcia^{33c}, J. D. Mellenthin⁵³, M. Melo^{28a}, F. Meloni⁴⁶, A. Melzer²⁴, S. B. Menary¹⁰⁰, E. D. Mendes Gouveia^{140a,140e}, L. Meng³⁶, X. T. Meng¹⁰⁵, S. Menke¹¹⁵, E. Meoni^{41a,41b}, S. Mergelmeyer¹⁹, S. A. M. Merkt¹³⁹, C. Merlassino²⁰, P. Mermod⁵⁴, L. Merola^{69a,69b}, C. Meroni^{68a}, O. Meshkov^{113,110}, J. K. R. Meshreki¹⁵¹, A. Messina^{72a,72b}, J. Metcalfe⁶, A. S. Mete¹⁷¹, C. Meyer⁶⁵, J. Meyer¹⁶⁰, J.-P. Meyer¹⁴⁵, H. Meyer Zu Theenhausen^{61a}, F. Miano¹⁵⁶, M. Michetti¹⁹, R. P. Middleton¹⁴⁴, L. Mijović⁵⁰, G. Mikenberg¹⁸⁰, M. Mikesikova¹⁴¹, M. Mikuž⁹¹, H. Mildner¹⁴⁹, M. Milesi¹⁰⁴, A. Milic¹⁶⁷, D. A. Millar⁹², D. W. Miller³⁷, A. Milov¹⁸⁰, D. A. Milstead^{45a,45b}, R. A. Mina^{153,q}, A. A. Minaenko¹²³, M. Miñano Moya¹⁷⁴, I. A. Minashvili^{159b}, A. I. Mincer¹²⁴, B. Mindur^{83a}, M. Mineev⁷⁹, Y. Minegishi¹⁶³, Y. Ming¹⁸¹, L. M. Mir¹⁴, A. Mirto^{67a,67b}, K. P. Mistry¹³⁷, T. Mitani¹⁷⁹, J. Mitrevski¹¹⁴, V. A. Mitsou¹⁷⁴, M. Mittal^{60c}, O. Miu¹⁶⁷, A. Miucci²⁰, P. S. Miyagawa¹⁴⁹, A. Mizukami⁸¹, J. U. Mjörnmark⁹⁶, T. Mkrtychyan¹⁸⁴, M. Mlynarikova¹⁴³, T. Moa^{45a,45b}, K. Mochizuki¹⁰⁹, P. Mogg⁵², S. Mohapatra³⁹, R. Moles-Valls²⁴, M. C. Mondragon¹⁰⁶, K. Mönig⁴⁶, J. Monk⁴⁰, E. Monnier¹⁰¹, A. Montalbano¹⁵², J. Montejo Berlingen³⁶, M. Montella⁹⁴, F. Monticelli⁸⁸, S. Monzani^{68a}, N. Morange¹³², D. Moreno²², M. Moreno Llácer³⁶, C. Moreno Martinez¹⁴, P. Morettini^{55b}, M. Morgenstern¹²⁰, S. Morgenstern⁴⁸, D. Mori¹⁵², M. Morii⁵⁹, M. Morinaga¹⁷⁹, V. Morisbak¹³⁴, A. K. Morley³⁶, G. Mornacchi³⁶, A. P. Morris⁹⁴, L. Morvaj¹⁵⁵, P. Moschovakos³⁶, B. Moser¹²⁰, M. Mosidze^{159b}, T. Moskalets¹⁴⁵, H. J. Moss¹⁴⁹, J. Moss^{31,n}, E. J. W. Moyses¹⁰², S. Muanza¹⁰¹, J. Mueller¹³⁹,

R. S. P. Mueller¹¹⁴, D. Muenstermann⁸⁹, G. A. Mullier⁹⁶, J. L. Munoz Martinez¹⁴, F. J. Munoz Sanchez¹⁰⁰, P. Murin^{28b}, W. J. Murray^{144,178}, A. Murrone^{68a,68b}, M. Muškinja¹⁸, C. Mwewa^{33a}, A. G. Myagkov^{123,aq}, J. Myers¹³¹, M. Myska¹⁴², B. P. Nachman¹⁸, O. Nackenhorst⁴⁷, A. Nag Nag⁴⁸, K. Nagai¹³⁵, K. Nagano⁸¹, Y. Nagasaka⁶², M. Nagel⁵², E. Nagy¹⁰¹, A. M. Nairz³⁶, Y. Nakahama¹¹⁷, K. Nakamura⁸¹, T. Nakamura¹⁶³, I. Nakano¹²⁷, H. Nanjo¹³³, F. Napolitano^{61a}, R. F. Naranjo Garcia⁴⁶, R. Narayan⁴², I. Naryshkin¹³⁸, T. Naumann⁴⁶, G. Navarro²², H. A. Neal^{105,*}, P. Y. Nechaeva¹¹⁰, F. Nechansky⁴⁶, T. J. Neep²¹, A. Negri^{70a,70b}, M. Negrini^{23b}, C. Nellist⁵³, M. E. Nelson¹³⁵, S. Nemecek¹⁴¹, P. Nemethy¹²⁴, M. Nessi^{36,d}, M. S. Neubauer¹⁷³, M. Neumann¹⁸², P. R. Newman²¹, Y. S. Ng¹⁹, Y. W. Y. Ng¹⁷¹, B. Ngair^{35e}, H. D. N. Nguyen¹⁰¹, T. Nguyen Manh¹⁰⁹, E. Nibigira³⁸, R. B. Nickerson¹³⁵, R. Nicolaidou¹⁴⁵, D. S. Nielsen⁴⁰, J. Nielsen¹⁴⁶, N. Nikiforou¹¹, V. Nikolaenko^{123,aq}, I. Nikolic-Audit¹³⁶, K. Nikolopoulos²¹, P. Nilsson²⁹, H. R. Nindhito⁵⁴, Y. Ninomiya⁸¹, A. Nisati^{72a}, N. Nishu^{60c}, R. Nisius¹¹⁵, I. Nitsche⁴⁷, T. Nitta¹⁷⁹, T. Nobe¹⁶³, Y. Noguchi⁸⁵, I. Nomidis¹³⁶, M. A. Nomura²⁹, M. Nordberg³⁶, N. Norjoharuddeen¹³⁵, T. Novak⁹¹, O. Novgorodova⁴⁸, R. Novotny¹⁴², L. Nozka¹³⁰, K. Ntekas¹⁷¹, E. Nurse⁹⁴, F. G. Oakham^{34,az}, H. Oberlack¹¹⁵, J. Ocariz¹³⁶, A. Ochi⁸², I. Ochoa³⁹, J. P. Ochoa-Ricoux^{147a}, K. O'Connor²⁶, S. Oda⁸⁷, S. Odaka⁸¹, S. Oerdek⁵³, A. Ogrodnik^{83a}, A. Oh¹⁰⁰, S. H. Oh⁴⁹, C. C. Ohm¹⁵⁴, H. Oide¹⁶⁵, M. L. Ojeda¹⁶⁷, H. Okawa¹⁶⁹, Y. Okazaki⁸⁵, Y. Okumura¹⁶³, T. Okuyama⁸¹, A. Olariu^{27b}, L. F. Oleiro Seabra^{140a}, S. A. Olivares Pino^{147a}, D. Oliveira Damazio²⁹, J. L. Oliver¹, M. J. R. Olsson¹⁷¹, A. Olszewski⁸⁴, J. Olszowska⁸⁴, D. C. O'Neil¹⁵², A. P. O'Neill¹³⁵, A. Onofre^{140a,140e}, P. U. E. Onyisi¹¹, H. Oppen¹³⁴, M. J. Oreglia³⁷, G. E. Orellana⁸⁸, D. Orestano^{74a,74b}, N. Orlando¹⁴, R. S. Orr¹⁶⁷, V. O'Shea⁵⁷, R. Ospanov^{60a}, G. Otero y Garzon³⁰, H. Otono⁸⁷, P. S. Ott^{61a}, M. Ouchrif^{35d}, J. Ouellette²⁹, F. Ould-Saada¹³⁴, A. Ouraou¹⁴⁵, Q. Ouyang^{15a}, M. Owen⁵⁷, R. E. Owen²¹, V. E. Ozcan^{12c}, N. Ozturk⁸, J. Pacalt¹³⁰, H. A. Pacey³², K. Pachal⁴⁹, A. Pacheco Pages¹⁴, C. Padilla Aranda¹⁴, S. Pagan Griso¹⁸, M. Paganini¹⁸³, G. Palacino⁶⁵, S. Palazzo⁵⁰, S. Palestini³⁶, M. Palka^{83b}, D. Pallin³⁸, I. Panagoulas¹⁰, C. E. Pandini³⁶, J. G. Panduro Vazquez⁹³, P. Pani⁴⁶, G. Panizzo^{66a,66c}, L. Paolozzi⁵⁴, C. Papadatos¹⁰⁹, K. Papageorgiou^{9,h}, S. Parajuli⁴³, A. Paramonov⁶, D. Paredes Hernandez^{63b}, S. R. Paredes Saenz¹³⁵, B. Parida¹⁶⁶, T. H. Park¹⁶⁷, A. J. Parker⁸⁹, M. A. Parker³², F. Parodi^{55a,55b}, E. W. P. Parrish¹²¹, J. A. Parsons³⁹, U. Parzefall⁵², L. Pascual Dominguez¹³⁶, V. R. Pascuzzi¹⁶⁷, J. M. P. Pasner¹⁴⁶, E. Pasqualucci^{72a}, S. Passaggio^{55b}, F. Pastore⁹³, P. Pasuwan^{45a,45b}, S. Pataria⁹⁹, J. R. Pater¹⁰⁰, A. Pathak^{181,j}, T. Pauly³⁶, B. Pearson¹¹⁵, M. Pedersen¹³⁴, L. Pedraza Diaz¹¹⁹, R. Pedro^{140a}, T. Peiffer⁵³, S. V. Peleganchuk^{122a,122b}, O. Penc¹⁴¹, H. Peng^{60a}, B. S. Peralva^{80a}, M. M. Perego¹³², A. P. Pereira Peixoto^{140a}, D. V. Perepelitsa²⁹, F. Peri¹⁹, L. Perini^{68a,68b}, H. Pernegger³⁶, S. Perrella^{69a,69b}, K. Peters⁴⁶, R. F. Y. Peters¹⁰⁰, B. A. Petersen³⁶, T. C. Petersen⁴⁰, E. Petit¹⁰¹, A. Petridis¹, C. Petridou¹⁶², P. Petroff¹³², M. Petrov¹³⁵, F. Petrucci^{74a,74b}, M. Pettee¹⁸³, N. E. Pettersson¹⁰², K. Petukhova¹⁴³, A. Peyaud¹⁴⁵, R. Pezoa^{147b}, L. Pezzotti^{70a,70b}, T. Pham¹⁰⁴, F. H. Phillips¹⁰⁶, P. W. Phillips¹⁴⁴, M. W. Phipps¹⁷³, G. Piacquadio¹⁵⁵, E. Pianori¹⁸, A. Picazio¹⁰², R. H. Pickles¹⁰⁰, R. Piegaia³⁰, D. Pietreanu^{27b}, J. E. Pilcher³⁷, A. D. Pilkington¹⁰⁰, M. Pinamonti^{73a,73b}, J. L. Pinfold³, M. Pitt¹⁶¹, L. Pizzimento^{73a,73b}, M.-A. Pleier²⁹, V. Pleskot¹⁴³, E. Plotnikova⁷⁹, P. Podberezko^{122a,122b}, R. Poettgen⁹⁶, R. Poggi⁵⁴, L. Poggioli¹³², I. Pogrebnyak¹⁰⁶, D. Pohl²⁴, I. Pokharel⁵³, G. Polesello^{70a}, A. Poley¹⁸, A. Policicchio^{72a,72b}, R. Polifka¹⁴³, A. Polini^{23b}, C. S. Pollard⁴⁶, V. Polychronakos²⁹, D. Ponomarenko¹¹², L. Pontecorvo³⁶, S. Popa^{27a}, G. A. Popeneciu^{27d}, L. Portales⁵, D. M. Portillo Quintero⁵⁸, S. Pospisil¹⁴², K. Potamianos⁴⁶, I. N. Potrap⁷⁹, C. J. Potter³², H. Potti¹¹, T. Poulsen⁹⁶, J. Poveda³⁶, T. D. Powell¹⁴⁹, G. Pownall⁴⁶, M. E. Pozo Astigarraga³⁶, P. Pralavorio¹⁰¹, S. Prell⁷⁸, D. Price¹⁰⁰, M. Primavera^{67a}, S. Prince¹⁰³, M. L. Proffitt¹⁴⁸, N. Proklova¹¹², K. Prokofiev^{63c}, F. Prokoshin⁷⁹, S. Protopopescu²⁹, J. Proudfoot⁶, M. Przybycien^{83a}, D. Pudzha¹³⁸, A. Puri¹⁷³, P. Puzo¹³², J. Qian¹⁰⁵, Y. Qin¹⁰⁰, A. Quadt⁵³, M. Queitsch-Maitland⁴⁶, A. Qureshi¹, M. Racko^{28a}, P. Rados¹⁰⁴, F. Ragusa^{68a,68b}, G. Rahal⁹⁷, J. A. Raine⁵⁴, S. Rajagopalan²⁹, A. Ramirez Morales⁹², K. Ran^{15a,15d}, T. Rashid¹³², S. Raspopov⁵, D. M. Rauch⁴⁶, F. Rauscher¹¹⁴, S. Rave⁹⁹, B. Ravina¹⁴⁹, I. Ravinovitch¹⁸⁰, J. H. Rawling¹⁰⁰, M. Raymond³⁶, A. L. Read¹³⁴, N. P. Readioff⁵⁸, M. Reale^{67a,67b}, D. M. Rebuffi^{70a,70b}, A. Redelbach¹⁷⁷, G. Redlinger²⁹, K. Reeves⁴³, L. Rehnisch¹⁹, J. Reichert¹³⁷, D. Reikher¹⁶¹, A. Reiss⁹⁹, A. Rej¹⁵¹, C. Rembser³⁶, M. Renda^{27b}, M. Rescigno^{72a}, S. Resconi^{68a}, E. D. Resseguie¹³⁷, S. Rettie¹⁷⁵, E. Reynolds²¹, O. L. Rezanova^{122a,122b}, P. Reznicek¹⁴³, E. Ricci^{75a,75b}, R. Richter¹¹⁵, S. Richter⁴⁶, E. Richter-Was^{83b}, O. Ricken²⁴, M. Ridel¹³⁶, P. Rieck¹¹⁵, C. J. Riegel¹⁸², O. Rifki⁴⁶, M. Rijssenbeek¹⁵⁵, A. Rimoldi^{70a,70b}, M. Rimoldi⁴⁶, L. Rinaldi^{23b}, G. Ripellino¹⁵⁴, I. Riu¹⁴, J. C. Rivera Vergara¹⁷⁶, F. Rizatdinova¹²⁹, E. Rizvi⁹², C. Rizzi³⁶, R. T. Roberts¹⁰⁰, S. H. Robertson^{103,af}, M. Robin⁴⁶, D. Robinson³², J. E. M. Robinson⁴⁶, C. M. Robles Gajardo^{147b}, A. Robson⁵⁷, A. Rocchi^{73a,73b}, E. Rocco⁹⁹, C. Roda^{71a,71b}, S. Rodriguez Bosca¹⁷⁴, A. Rodriguez Perez¹⁴, D. Rodriguez Rodriguez¹⁷⁴, A. M. Rodríguez Vera^{168b}, S. Roe³⁶, O. Røhne¹³⁴, R. Röhrig¹¹⁵, C. P. A. Roland⁶⁵, J. Roloff⁵⁹, A. Romaniouk¹¹², M. Romano^{23a,23b}, N. Rompotis⁹⁰, M. Ronzani¹²⁴, L. Roos¹³⁶, S. Rosati^{72a}, K. Rosbach⁵², G. Rosin¹⁰², B. J. Rosser¹³⁷, E. Rossi⁴⁶, E. Rossi^{74a,74b}, E. Rossi^{69a,69b}, L. P. Rossi^{55b}, L. Rossini^{68a,68b}, R. Rosten¹⁴, M. Rotaru^{27b}, J. Rothberg¹⁴⁸, D. Rousseau¹³², G. Rovelli^{70a,70b}, A. Roy¹¹, D. Roy^{33c}, A. Rozanov¹⁰¹, Y. Rozen¹⁶⁰, X. Ruan^{33c}, F. Rubbo¹⁵³, F. Rühr⁵², A. Ruiz-Martinez¹⁷⁴, A. Rummler³⁶, Z. Rurikova⁵²

N. A. Rusakovich⁷⁹, H. L. Russell¹⁰³, L. Rustige^{38,47}, J. P. Rutherford⁷, E. M. Rüttinger¹⁴⁹, M. Rybar³⁹, G. Rybkin¹³², E. B. Rye¹³⁴, A. Ryzhov¹²³, G. F. Rzehorz⁵³, P. Sabatini⁵³, G. Sabato¹²⁰, S. Sacerdoti¹³², H.F.-W. Sadrozinski¹⁴⁶, R. Sadykov⁷⁹, F. Safai Tehrani^{72a}, B. Safarzadeh Samani¹⁵⁶, P. Saha¹²¹, S. Saha¹⁰³, M. Sahinsoy^{61a}, A. Sahu¹⁸², M. Saimpert⁴⁶, M. Saito¹⁶³, T. Saito¹⁶³, H. Sakamoto¹⁶³, A. Sakharov^{124,ap}, D. Salamani⁵⁴, G. Salamanna^{74a,74b}, J. E. Salazar Loyola^{147b}, P. H. Sales De Bruin¹⁷², A. Salnikov¹⁵³, J. Salt¹⁷⁴, D. Salvatore^{41a,41b}, F. Salvatore¹⁵⁶, A. Salvucci^{63a,63b,63c}, A. Salzburger³⁶, J. Samarati³⁶, D. Sammel⁵², D. Sampsonidis¹⁶², D. Sampsonidou¹⁶², J. Sánchez¹⁷⁴, A. Sanchez Pineda^{66a,66c}, H. Sandaker¹³⁴, C. O. Sander⁴⁶, I. G. Sanderswood⁸⁹, M. Sandhoff¹⁸², C. Sandoval²², D. P. C. Sankey¹⁴⁴, M. Sannino^{55a,55b}, Y. Sano¹¹⁷, A. Sansoni⁵¹, C. Santoni³⁸, H. Santos^{140a,140b}, S. N. Santpur¹⁸, A. Santra¹⁷⁴, A. Sapronov⁷⁹, J. G. Saraiva^{140a,140d}, O. Sasaki⁸¹, K. Sato¹⁶⁹, F. Sauerburger⁵², E. Sauvan⁵, P. Savard^{167,az}, N. Savic¹¹⁵, R. Sawada¹⁶³, C. Sawyer¹⁴⁴, L. Sawyer^{95,an}, C. Sbarra^{23b}, A. Sbrizzi^{23a}, T. Scanlon⁹⁴, J. Schaarschmidt¹⁴⁸, P. Schacht¹¹⁵, B. M. Schachtner¹¹⁴, D. Schaefer³⁷, L. Schaefer¹³⁷, J. Schaeffer⁹⁹, S. Schaepe³⁶, U. Schäfer⁹⁹, A. C. Schaffer¹³², D. Schaile¹¹⁴, R. D. Schamberger¹⁵⁵, N. Scharmberg¹⁰⁰, V. A. Schegelsky¹³⁸, D. Scheirich¹⁴³, F. Schenck¹⁹, M. Schernau¹⁷¹, C. Schiavi^{55a,55b}, S. Schier¹⁴⁶, L. K. Schildgen²⁴, Z. M. Schillaci²⁶, E. J. Schioppa³⁶, M. Schioppa^{41a,41b}, K. E. Schleicher⁵², S. Schlenker³⁶, K. R. Schmidt-Sommerfeld¹¹⁵, K. Schmieden³⁶, C. Schmitt⁹⁹, S. Schmitt⁴⁶, S. Schmitz⁹⁹, J. C. Schmoedel⁴⁶, U. Schnoor⁵², L. Schoeffel¹⁴⁵, A. Schoening^{61b}, P. G. Scholer⁵², E. Schopf¹³⁵, M. Schott⁹⁹, J. F. P. Schouwenberg¹¹⁹, J. Schovancova³⁶, S. Schramm⁵⁴, F. Schroeder¹⁸², A. Schulte⁹⁹, H.-C. Schultz-Coulon^{61a}, M. Schumacher⁵², B. A. Schumm¹⁴⁶, Ph. Schune¹⁴⁵, A. Schwartzman¹⁵³, T. A. Schwarz¹⁰⁵, Ph. Schwemling¹⁴⁵, R. Schwienhorst¹⁰⁶, A. Sciandra¹⁴⁶, G. Sciolla²⁶, M. Scodreggio⁴⁶, M. Scornajenghi^{41a,41b}, F. Scuri^{71a}, F. Scutti¹⁰⁴, L. M. Scyboz¹¹⁵, C. D. Sebastiani^{72a,72b}, P. Seema¹⁹, S. C. Seidel¹¹⁸, A. Seiden¹⁴⁶, B. D. Seidlitz²⁹, T. Seiss³⁷, J. M. Seixas^{80b}, G. Sekhniaidze^{69a}, K. Sekhon¹⁰⁵, S. J. Sekula⁴², N. Semprini-Cesari^{23a,23b}, S. Sen⁴⁹, S. Senkin³⁸, C. Serfon⁷⁶, L. Serin¹³², L. Serkin^{66a,66b}, M. Sessa^{60a}, H. Severini¹²⁸, T. Šfiligoj⁹¹, F. Sforza^{55a,55b}, A. Sfyrla⁵⁴, E. Shabalina⁵³, J. D. Shahinian¹⁴⁶, N. W. Shaikh^{45a,45b}, D. Shaked Renous¹⁸⁰, L. Y. Shan^{15a}, R. Shang¹⁷³, J. T. Shank²⁵, M. Shapiro¹⁸, A. Sharma¹³⁵, A. S. Sharma¹, P. B. Shatalov¹¹¹, K. Shaw¹⁵⁶, S. M. Shaw¹⁰⁰, A. Shcherbakova¹³⁸, M. Shehade¹⁸⁰, Y. Shen¹²⁸, N. Sherafati³⁴, A. D. Sherman²⁵, P. Sherwood⁹⁴, L. Shi^{158,av}, S. Shimizu⁸¹, C. O. Shimmin¹⁸³, Y. Shimogama¹⁷⁹, M. Shimojima¹¹⁶, I. P. J. Shipsey¹³⁵, S. Shirabe⁸⁷, M. Shiyakova^{79,ad}, J. Shlomi¹⁸⁰, A. Shmeleva¹¹⁰, M. J. Shochet³⁷, J. Shojaii¹⁰⁴, D. R. Shope¹²⁸, S. Shrestha¹²⁶, E. M. Shrif^{33c}, E. Shulga¹⁸⁰, P. Sicho¹⁴¹, A. M. Sickles¹⁷³, P. E. Sidebo¹⁵⁴, E. Sideras Haddad^{33c}, O. Sidiropoulou³⁶, A. Sidoti^{23a,23b}, F. Siegert⁴⁸, Dj. Sijacki¹⁶, M. Jr. Silva¹⁸¹, M. V. Silva Oliveira^{80a}, S. B. Silverstein^{45a}, S. Simion¹³², E. Simioni⁹⁹, R. Simoniello⁹⁹, S. Simsek^{12b}, P. Sinervo¹⁶⁷, V. Sinetckii^{113,110}, N. B. Sinev¹³¹, M. Sioli^{23a,23b}, I. Siral¹⁰⁵, S. Yu. Sivoklov¹¹³, J. Sjölin^{45a,45b}, E. Skorda⁹⁶, P. Skubic¹²⁸, M. Slawinska⁸⁴, K. Sliwa¹⁷⁰, R. Slovak¹⁴³, V. Smakhtin¹⁸⁰, B. H. Smart¹⁴⁴, J. Smiesko^{28a}, N. Smirnov¹¹², S. Yu. Smirnov¹¹², Y. Smirnov¹¹², L. N. Smirnova^{113,w}, O. Smirnova⁹⁶, J. W. Smith⁵³, M. Smizanska⁸⁹, K. Smolek¹⁴², A. Smykiewicz⁸⁴, A. A. Snesarev¹¹⁰, H. L. Snoek¹²⁰, I. M. Snyder¹³¹, S. Snyder²⁹, R. Sobie^{176,af}, A. Soffer¹⁶¹, A. Sogaard⁵⁰, F. Sohns⁵³, C. A. Solans Sanchez³⁶, E. Yu. Soldatov¹¹², U. Soldevila¹⁷⁴, A. A. Solodkov¹²³, A. Soloshenko⁷⁹, O. V. Solovyanov¹²³, V. Solovyev¹³⁸, P. Sommer¹⁴⁹, H. Son¹⁷⁰, W. Song¹⁴⁴, W. Y. Song^{168b}, A. Sopczak¹⁴², F. Sopkova^{28b}, C. L. Sotiropoulou^{71a,71b}, S. Sottocornola^{70a,70b}, R. Soualah^{66a,66c,g}, A. M. Soukharev^{122a,122b}, D. South⁴⁶, S. Spagnolo^{67a,67b}, M. Spalla¹¹⁵, M. Spangenberg¹⁷⁸, F. Spanò⁹³, D. Sperlich⁵², T. M. Spieker^{61a}, R. Spighi^{23b}, G. Spigo³⁶, M. Spina¹⁵⁶, D. P. Spiteri⁵⁷, M. Spousta¹⁴³, A. Stabile^{68a,68b}, B. L. Stamas¹²¹, R. Stamen^{61a}, M. Stamenkovic¹²⁰, E. Stanecka⁸⁴, B. Stanislaus¹³⁵, M. M. Stanitzki⁴⁶, M. Stankaityte¹³⁵, B. Stapf¹²⁰, E. A. Starchenko¹²³, G. H. Stark¹⁴⁶, J. Stark⁵⁸, S. H. Stark⁴⁰, P. Staroba¹⁴¹, P. Starovoitov^{61a}, S. Stärz¹⁰³, R. Staszewski⁸⁴, G. Stavropoulos⁴⁴, M. Stegler⁴⁶, P. Steinberg²⁹, A. L. Steinhebel¹³¹, B. Stelzer¹⁵², H. J. Stelzer¹³⁹, O. Stelzer-Chilton^{168a}, H. Stenzel⁵⁶, T. J. Stevenson¹⁵⁶, G. A. Stewart³⁶, M. C. Stockton³⁶, G. Stoicea^{27b}, M. Stolarski^{140a}, S. Stonjek¹¹⁵, A. Straessner⁴⁸, J. Strandberg¹⁵⁴, S. Strandberg^{45a,45b}, M. Strauss¹²⁸, P. Strizenc^{28b}, R. Ströhmer¹⁷⁷, D. M. Strom¹³¹, R. Stroynowski⁴², A. Strubig⁵⁰, S. A. Stucci²⁹, B. Stugu¹⁷, J. Stupak¹²⁸, N. A. Styles⁴⁶, D. Su¹⁵³, S. Suchek^{61a}, V. V. Sulin¹¹⁰, M. J. Sullivan⁹⁰, D. M. S. Sultan⁵⁴, S. Sultansoy^{4c}, T. Sumida⁸⁵, S. Sun¹⁰⁵, X. Sun³, K. Suruliz¹⁵⁶, C. J. E. Suster¹⁵⁷, M. R. Sutton¹⁵⁶, S. Suzuki⁸¹, M. Svatos¹⁴¹, M. Swiatlowski³⁷, S. P. Swift², T. Swirski¹⁷⁷, A. Sydorenko⁹⁹, I. Sykora^{28a}, M. Sykora¹⁴³, T. Sykora¹⁴³, D. Ta⁹⁹, K. Tackmann^{46,ab}, J. Taenzer¹⁶¹, A. Taffard¹⁷¹, R. Tafirout^{168a}, H. Takai²⁹, R. Takashima⁸⁶, K. Takeda⁸², T. Takeshita¹⁵⁰, E. P. Takeva⁵⁰, Y. Takubo⁸¹, M. Talby¹⁰¹, A. A. Talyshev^{122a,122b}, N. M. Tamir¹⁶¹, J. Tanaka¹⁶³, M. Tanaka¹⁶⁵, R. Tanaka¹³², S. Tapia Araya¹⁷³, S. Tapprogge⁹⁹, A. Tarek Abouelfadl Mohamed¹³⁶, S. Tarem¹⁶⁰, G. Tarna^{27b,c}, G. F. Tartarelli^{68a}, P. Tas¹⁴³, M. Tasevsky¹⁴¹, T. Tashiro⁸⁵, E. Tassi^{41a,41b}, A. Tavares Delgado^{140a,140b}, Y. Tayalati^{35e}, A. J. Taylor⁵⁰, G. N. Taylor¹⁰⁴, W. Taylor^{168b}, A. S. Tee⁸⁹, R. Teixeira De Lima¹⁵³, P. Teixeira-Dias⁹³, H. Ten Kate³⁶, J. J. Teoh¹²⁰, S. Terada⁸¹, K. Terashi¹⁶³, J. Terron⁹⁸, S. Terzo¹⁴, M. Testa⁵¹, R. J. Teuscher^{167,af}, S. J. Thais¹⁸³, T. Theveneaux-Pelzer⁴⁶, F. Thiele⁴⁰, D. W. Thomas⁹³, J. O. Thomas⁴², J. P. Thomas²¹, A. S. Thompson⁵⁷, P. D. Thompson²¹, L. A. Thomsen¹⁸³, E. Thomson¹³⁷, E. J. Thorpe⁹², Y. Tian³⁹,

R. E. Tisce Torres⁵³, V. O. Tikhomirov^{110,ar}, Yu. A. Tikhonov^{122a,122b}, S. Timoshenko¹¹², P. Tipton¹⁸³, S. Tisserant¹⁰¹, K. Todome^{23a,23b}, S. Todorova-Nova⁵, S. Todt⁴⁸, J. Tojo⁸⁷, S. Tokár^{28a}, K. Tokushuku⁸¹, E. Tolley¹²⁶, K. G. Tomiwa^{33c}, M. Tomoto¹¹⁷, L. Tompkins^{153,q}, B. Tong⁵⁹, P. Tornambe¹⁰², E. Torrence¹³¹, H. Torres⁴⁸, E. Torró Pastor¹⁴⁸, C. Toscirri¹³⁵, J. Toth^{101,ae}, D. R. Tovey¹⁴⁹, A. Traeet¹⁷, C. J. Treado¹²⁴, T. Trefzger¹⁷⁷, F. Tresoldi¹⁵⁶, A. Tricoli²⁹, I. M. Trigger^{168a}, S. Trincaz-Duvoid¹³⁶, W. Trischuk¹⁶⁷, B. Trocme⁵⁸, A. Trofymov¹⁴⁵, C. Troncon^{68a}, M. Trovatelli¹⁷⁶, F. Trovato¹⁵⁶, L. Truong^{33b}, M. Trzebinski⁸⁴, A. Trzuppek⁸⁴, F. Tsai⁴⁶, J.C.-L. Tseng¹³⁵, P. V. Tsiarshka^{107,al}, A. Tsirigotis¹⁶², N. Tsirintanis⁹, V. Tsiskaridze¹⁵⁵, E. G. Tskhadadze^{159a}, M. Tsopoulou¹⁶², I. I. Tsukerman¹¹¹, V. Tsulaia¹⁸, S. Tsuno⁸¹, D. Tsybychev¹⁵⁵, Y. Tu^{63b}, A. Tudorache^{27b}, V. Tudorache^{27b}, T. T. Tulbure^{27a}, A. N. Tuna⁵⁹, S. Turchikhin⁷⁹, D. Turgeman¹⁸⁰, I. Turk Cakir^{4b,x}, R. J. Turner²¹, R. T. Turra^{68a}, P. M. Tuts³⁹, S. Tzamarias¹⁶², E. Tzovara⁹⁹, G. Uccielli⁴⁷, K. Uchida¹⁶³, I. Ueda⁸¹, M. Ughetto^{45a,45b}, F. Ukegawa¹⁶⁹, G. Unal³⁶, A. Undrus²⁹, G. Unel¹⁷¹, F. C. Ungaro¹⁰⁴, Y. Unno⁸¹, K. Uno¹⁶³, J. Urban^{28b}, P. Urquijo¹⁰⁴, G. Usai⁸, Z. Uysal^{12d}, L. Vacavant¹⁰¹, V. Vacek¹⁴², B. Vachon¹⁰³, K. O. H. Vadla¹³⁴, A. Vaidya⁹⁴, C. Valderanis¹¹⁴, E. Valdes Santurio^{45a,45b}, M. Valente⁵⁴, S. Valentinetti^{23a,23b}, A. Valero¹⁷⁴, L. Valéry⁴⁶, R. A. Vallance²¹, A. Vallier³⁶, J. A. Valls Ferrer¹⁷⁴, T. R. Van Daalen¹⁴, P. Van Gemmeren⁶, I. Van Vulpen¹²⁰, M. Vanadia^{73a,73b}, W. Vandelli³⁶, A. Vaniachine¹⁶⁶, D. Vannicola^{72a,72b}, R. Vari^{72a}, E. W. Varnes⁷, C. Varni^{55a,55b}, T. Varol⁴², D. Varouchas¹³², K. E. Varvell¹⁵⁷, M. E. Vasile^{27b}, G. A. Vasquez¹⁷⁶, J. G. Vasquez¹⁸³, F. Vazeille³⁸, D. Vazquez Furelos¹⁴, T. Vazquez Schroeder³⁶, J. Veatch⁵³, V. Vecchio^{74a,74b}, M. J. Veen¹²⁰, L. M. Veloce¹⁶⁷, F. Veloso^{140a,140c}, S. Veneziano^{72a}, A. Ventura^{67a,67b}, N. Venturi³⁶, A. Verbytskyi¹¹⁵, V. Vercesi^{70a}, M. Verducci^{71a,71b}, C. M. Vergel Infante⁷⁸, C. Vergis²⁴, W. Verkerke¹²⁰, A. T. Vermeulen¹²⁰, J. C. Vermeulen¹²⁰, M. C. Vetterli^{152,az}, N. Viaux Maira^{147b}, M. Vicente Barreto Pinto⁵⁴, T. Vickey¹⁴⁹, O. E. Vickey Boeriu¹⁴⁹, G. H. A. Viehhauser¹³⁵, L. Vigani^{61b}, M. Villa^{23a,23b}, M. Villaplana Perez^{68a,68b}, E. Vilucchi⁵¹, M. G. Vincter³⁴, G. S. Virdee²¹, A. Vishwakarma⁴⁶, C. Vittori^{23a,23b}, I. Vivarelli¹⁵⁶, M. Vogel¹⁸², P. Vokac¹⁴², S. E. von Buddenbrock^{33c}, E. Von Toerne²⁴, V. Vorobel¹⁴³, K. Vorobev¹¹², M. Vos¹⁷⁴, J. H. Vosseveld⁹⁰, M. Vozak¹⁰⁰, N. Vranjes¹⁶, M. Vranjes Milosavljevic¹⁶, V. Vrba¹⁴², M. Vreeswijk¹²⁰, R. Vuillermet³⁶, I. Vukotic³⁷, P. Wagner²⁴, W. Wagner¹⁸², J. Wagner-Kuhr¹¹⁴, S. Wahdan¹⁸², H. Wahlberg⁸⁸, V. M. Walbrecht¹¹⁵, J. Walder⁸⁹, R. Walker¹¹⁴, S. D. Walker⁹³, W. Walkowiak¹⁵¹, V. Wallangen^{45a,45b}, A. M. Wang⁵⁹, C. Wang^{60c}, C. Wang^{60b}, F. Wang¹⁸¹, H. Wang¹⁸, H. Wang³, J. Wang¹⁵⁷, J. Wang^{61b}, P. Wang⁴², Q. Wang¹²⁸, R.-J. Wang⁹⁹, R. Wang^{60a}, R. Wang⁶, S. M. Wang¹⁵⁸, W. T. Wang^{60a}, W. Wang^{15c,ag}, W. X. Wang^{60a,ag}, Y. Wang^{60a,ao}, Z. Wang^{60c}, C. Wanotayaroj⁴⁶, A. Warburton¹⁰³, C. P. Ward³², D. R. Wardrope⁹⁴, N. Warrack⁵⁷, A. Washbrook⁵⁰, A. T. Watson²¹, M. F. Watson²¹, G. Watts¹⁴⁸, B. M. Waugh⁹⁴, A. F. Webb¹¹, S. Webb⁹⁹, C. Weber¹⁸³, M. S. Weber²⁰, S. A. Weber³⁴, S. M. Weber^{61a}, A. R. Weidberg¹³⁵, J. Weingarten⁴⁷, M. Weirich⁹⁹, C. Weiser⁵², P. S. Wells³⁶, T. Wenaus²⁹, T. Wengler³⁶, S. Wenig³⁶, N. Wermes²⁴, M. D. Werner⁷⁸, M. Wessels^{61a}, T. D. Weston²⁰, K. Whalen¹³¹, N. L. Whallon¹⁴⁸, A. M. Wharton⁸⁹, A. S. White¹⁰⁵, A. White⁸, M. J. White¹, D. Whiteson¹⁷¹, B. W. Whitmore⁸⁹, W. Wiedenmann¹⁸¹, M. Wielers¹⁴⁴, N. Wieseotte⁹⁹, C. Wiglesworth⁴⁰, L. A. M. Wiik-Fuchs⁵², F. Wilk¹⁰⁰, H. G. Wilkens³⁶, L. J. Wilkins⁹³, H. H. Williams¹³⁷, S. Williams³², C. Willis¹⁰⁶, S. Willocq¹⁰², J. A. Wilson²¹, I. Wingerter-Seez⁵, E. Winkels¹⁵⁶, F. Winklmeier¹³¹, O. J. Winston¹⁵⁶, B. T. Winter⁵², M. Wittgen¹⁵³, M. Wobisch⁹⁵, A. Wolf⁹⁹, T. M. H. Wolf¹²⁰, R. Wolff¹⁰¹, R. W. Wölker¹³⁵, J. Wollrath⁵², M. W. Wolter⁸⁴, H. Wolters^{140a,140c}, V. W. S. Wong¹⁷⁵, N. L. Woods¹⁴⁶, S. D. Worm²¹, B. K. Wosiek⁸⁴, K. W. Woźniak⁸⁴, K. Wraight⁵⁷, S. L. Wu¹⁸¹, X. Wu⁵⁴, Y. Wu^{60a}, T. R. Wyatt¹⁰⁰, B. M. Wynne⁵⁰, S. Xella⁴⁰, Z. Xi¹⁰⁵, L. Xia¹⁷⁸, X. Xiao¹⁰⁵, D. Xu^{15a}, H. Xu^{60a,c}, L. Xu²⁹, T. Xu¹⁴⁵, W. Xu¹⁰⁵, Z. Xu^{60b}, Z. Xu¹⁵³, B. Yabsley¹⁵⁷, S. Yacoob^{33a}, K. Yajima¹³³, D. P. Yallup⁹⁴, D. Yamaguchi¹⁶⁵, Y. Yamaguchi¹⁶⁵, A. Yamamoto⁸¹, M. Yamatani¹⁶³, T. Yamazaki¹⁶³, Y. Yamazaki⁸², Z. Yan²⁵, H. J. Yang^{60c,60d}, H. T. Yang¹⁸, S. Yang⁷⁷, X. Yang^{58,60b}, Y. Yang¹⁶³, W.-M. Yao¹⁸, Y. C. Yap⁴⁶, Y. Yasu⁸¹, E. Yatsenko^{60c,60d}, J. Ye⁴², S. Ye²⁹, I. Yeletsikh⁷⁹, M. R. Yexley⁸⁹, E. Yigitbasi²⁵, K. Yorita¹⁷⁹, K. Yoshihara¹³⁷, C. J. S. Young³⁶, C. Young¹⁵³, J. Yu⁷⁸, R. Yuan^{60b,i}, X. Yue^{61a}, S. P. Y. Yuen²⁴, M. Zaazoua^{35e}, B. Zabinski⁸⁴, G. Zacharis¹⁰, E. Zaffaroni⁵⁴, J. Zahreddine¹³⁶, A. M. Zaitsev^{123,aq}, T. Zakareishvili^{159b}, N. Zakharchuk³⁴, S. Zambito⁵⁹, D. Zanzi³⁶, D. R. Zaripovas⁵⁷, S. V. Zeiβner⁴⁷, C. Zeitnitz¹⁸², G. Zemaityte¹³⁵, J. C. Zeng¹⁷³, O. Zenin¹²³, T. Ženiš^{28a}, D. Zerwas¹³², M. Zgubič¹³⁵, D. F. Zhang^{15b}, F. Zhang¹⁸¹, G. Zhang^{15b}, H. Zhang^{15c}, J. Zhang⁶, L. Zhang^{15c}, L. Zhang^{60a}, M. Zhang¹⁷³, R. Zhang²⁴, X. Zhang^{60b}, Y. Zhang^{15a,15d}, Z. Zhang^{63a}, Z. Zhang¹³², P. Zhao⁴⁹, Y. Zhao^{60b}, Z. Zhao^{60a}, A. Zhemchugov⁷⁹, Z. Zheng¹⁰⁵, D. Zhong¹⁷³, B. Zhou¹⁰⁵, C. Zhou¹⁸¹, M. S. Zhou^{15a,15d}, M. Zhou¹⁵⁵, N. Zhou^{60c}, Y. Zhou⁷, C. G. Zhu^{60b}, H. L. Zhu^{60a}, H. Zhu^{15a}, J. Zhu¹⁰⁵, Y. Zhu^{60a}, X. Zhuang^{15a}, K. Zhukov¹¹⁰, V. Zhulanov^{122a,122b}, D. Zieminska⁶⁵, N. I. Zimine⁷⁹, S. Zimmermann⁵², Z. Zinonos¹¹⁵, M. Ziolkowski¹⁵¹, L. Živković¹⁶, G. Zobernig¹⁸¹, A. Zoccoli^{23a,23b}, K. Zoch⁵³, T. G. Zorbas¹⁴⁹, R. Zou³⁷, L. Zwalinski³⁶

¹ Department of Physics, University of Adelaide, Adelaide, Australia

² Physics Department, SUNY Albany, Albany, NY, USA

³ Department of Physics, University of Alberta, Edmonton, AB, Canada

- ⁴ (a)Department of Physics, Ankara University, Ankara, Turkey; (b)Istanbul Aydin University, Istanbul, Turkey; (c)Division of Physics, TOBB University of Economics and Technology, Ankara, Turkey
- ⁵ LAPP, Université Grenoble Alpes, Université Savoie Mont Blanc, CNRS/IN2P3, Annecy, France
- ⁶ High Energy Physics Division, Argonne National Laboratory, Argonne, IL, USA
- ⁷ Department of Physics, University of Arizona, Tucson, AZ, USA
- ⁸ Department of Physics, University of Texas at Arlington, Arlington, TX, USA
- ⁹ Physics Department, National and Kapodistrian University of Athens, Athens, Greece
- ¹⁰ Physics Department, National Technical University of Athens, Zografou, Greece
- ¹¹ Department of Physics, University of Texas at Austin, Austin, TX, USA
- ¹² (a)Faculty of Engineering and Natural Sciences, Bahcesehir University, Istanbul, Turkey; (b)Faculty of Engineering and Natural Sciences, Istanbul Bilgi University, Istanbul, Turkey; (c)Department of Physics, Bogazici University, Istanbul, Turkey; (d)Department of Physics Engineering, Gaziantep University, Gaziantep, Turkey
- ¹³ Institute of Physics, Azerbaijan Academy of Sciences, Baku, Azerbaijan
- ¹⁴ Institut de Física d'Altes Energies (IFAE), Barcelona Institute of Science and Technology, Barcelona, Spain
- ¹⁵ (a)Institute of High Energy Physics, Chinese Academy of Sciences, Beijing, China; (b)Physics Department, Tsinghua University, Beijing, China; (c)Department of Physics, Nanjing University, Nanjing, China; (d)University of Chinese Academy of Science (UCAS), Beijing, China
- ¹⁶ Institute of Physics, University of Belgrade, Belgrade, Serbia
- ¹⁷ Department for Physics and Technology, University of Bergen, Bergen, Norway
- ¹⁸ Physics Division, Lawrence Berkeley National Laboratory and University of California, Berkeley, CA, USA
- ¹⁹ Institut für Physik, Humboldt Universität zu Berlin, Berlin, Germany
- ²⁰ Albert Einstein Center for Fundamental Physics and Laboratory for High Energy Physics, University of Bern, Bern, Switzerland
- ²¹ School of Physics and Astronomy, University of Birmingham, Birmingham, UK
- ²² Facultad de Ciencias y Centro de Investigaciones, Universidad Antonio Nariño, Bogotá, Colombia
- ²³ (a)Dipartimento di Fisica, INFN Bologna and Università di Bologna, Bologna, Italy; (b)INFN Sezione di Bologna, Bologna, Italy
- ²⁴ Physikalisches Institut, Universität Bonn, Bonn, Germany
- ²⁵ Department of Physics, Boston University, Boston, MA, USA
- ²⁶ Department of Physics, Brandeis University, Waltham, MA, USA
- ²⁷ (a)Transilvania University of Brasov, Brasov, Romania; (b)Horia Hulubei National Institute of Physics and Nuclear Engineering, Bucharest, Romania; (c)Department of Physics, Alexandru Ioan Cuza University of Iasi, Iasi, Romania; (d)Physics Department, National Institute for Research and Development of Isotopic and Molecular Technologies, Cluj-Napoca, Romania; (e)University Politehnica Bucharest, Bucharest, Romania; (f)West University in Timisoara, Timisoara, Romania
- ²⁸ (a)Faculty of Mathematics, Physics and Informatics, Comenius University, Bratislava, Slovak Republic; (b)Department of Subnuclear Physics, Institute of Experimental Physics of the Slovak Academy of Sciences, Kosice, Slovak Republic
- ²⁹ Physics Department, Brookhaven National Laboratory, Upton, NY, USA
- ³⁰ Departamento de Física, Universidad de Buenos Aires, Buenos Aires, Argentina
- ³¹ California State University, CA, USA
- ³² Cavendish Laboratory, University of Cambridge, Cambridge, UK
- ³³ (a)Department of Physics, University of Cape Town, Cape Town, South Africa; (b)Department of Mechanical Engineering Science, University of Johannesburg, Johannesburg, South Africa; (c)School of Physics, University of the Witwatersrand, Johannesburg, South Africa
- ³⁴ Department of Physics, Carleton University, Ottawa, ON, Canada
- ³⁵ (a)Faculté des Sciences Ain Chock, Réseau Universitaire de Physique des Hautes Energies-Université Hassan II, Casablanca, Morocco; (b)Faculté des Sciences, Université Ibn-Tofail, Kenitra, Morocco; (c)Faculté des Sciences Semlalia, Université Cadi Ayyad, LPHEA, Marrakech, Morocco; (d)Faculté des Sciences, Université Mohamed Premier and LPTPM, Oujda, Morocco; (e)Faculté des sciences, Université Mohammed V, Rabat, Morocco
- ³⁶ CERN, Geneva, Switzerland
- ³⁷ Enrico Fermi Institute, University of Chicago, Chicago, IL, USA
- ³⁸ LPC, Université Clermont Auvergne, CNRS/IN2P3, Clermont-Ferrand, France
- ³⁹ Nevis Laboratory, Columbia University, Irvington, NY, USA

- 40 Niels Bohr Institute, University of Copenhagen, Copenhagen, Denmark
- 41 (a)Dipartimento di Fisica, Università della Calabria, Rende, Italy; (b)INFN Gruppo Collegato di Cosenza, Laboratori Nazionali di Frascati, Italy
- 42 Physics Department, Southern Methodist University, Dallas, TX, USA
- 43 Physics Department, University of Texas at Dallas, Richardson, TX, USA
- 44 National Centre for Scientific Research “Demokritos”, Agia Paraskevi, Greece
- 45 (a)Department of Physics, Stockholm University, Stockholm, Sweden; (b)Oskar Klein Centre, Stockholm, Sweden
- 46 Deutsches Elektronen-Synchrotron DESY, Hamburg and Zeuthen, Germany
- 47 Lehrstuhl für Experimentelle Physik IV, Technische Universität Dortmund, Dortmund, Germany
- 48 Institut für Kern- und Teilchenphysik, Technische Universität Dresden, Dresden, Germany
- 49 Department of Physics, Duke University, Durham, NC, USA
- 50 SUPA-School of Physics and Astronomy, University of Edinburgh, Edinburgh, UK
- 51 INFN e Laboratori Nazionali di Frascati, Frascati, Italy
- 52 Physikalisches Institut, Albert-Ludwigs-Universität Freiburg, Freiburg, Germany
- 53 II. Physikalisches Institut, Georg-August-Universität Göttingen, Göttingen, Germany
- 54 Département de Physique Nucléaire et Corpusculaire, Université de Genève, Geneva, Switzerland
- 55 (a)Dipartimento di Fisica, Università di Genova, Genoa, Italy; (b)INFN Sezione di Genova, Genoa, Italy
- 56 II. Physikalisches Institut, Justus-Liebig-Universität Giessen, Giessen, Germany
- 57 SUPA-School of Physics and Astronomy, University of Glasgow, Glasgow, UK
- 58 LPSC, Université Grenoble Alpes, CNRS/IN2P3, Grenoble INP, Grenoble, France
- 59 Laboratory for Particle Physics and Cosmology, Harvard University, Cambridge, MA, USA
- 60 (a)Department of Modern Physics and State Key Laboratory of Particle Detection and Electronics, University of Science and Technology of China, Hefei, China; (b)Institute of Frontier and Interdisciplinary Science and Key Laboratory of Particle Physics and Particle Irradiation (MOE), Shandong University, Qingdao, China; (c)School of Physics and Astronomy, KLPPAC-MoE, SKLPPC, Shanghai Jiao Tong University, Shanghai, China; (d)Tsung-Dao Lee Institute, Shanghai, China
- 61 (a)Kirchhoff-Institut für Physik, Ruprecht-Karls-Universität Heidelberg, Heidelberg, Germany; (b)Physikalisches Institut, Ruprecht-Karls-Universität Heidelberg, Heidelberg, Germany
- 62 Faculty of Applied Information Science, Hiroshima Institute of Technology, Hiroshima, Japan
- 63 (a)Department of Physics, Chinese University of Hong Kong, Shatin, N.T., Hong Kong; (b)Department of Physics, University of Hong Kong, Pok Fu Lam, Hong Kong; (c)Department of Physics and Institute for Advanced Study, Hong Kong University of Science and Technology, Clear Water Bay, Kowloon, Hong Kong, China
- 64 Department of Physics, National Tsing Hua University, Hsinchu, Taiwan
- 65 Department of Physics, Indiana University, Bloomington, IN, USA
- 66 (a)INFN Gruppo Collegato di Udine, Sezione di Trieste, Udine, Italy; (b)ICTP, Trieste, Italy; (c)Dipartimento Politecnico di Ingegneria e Architettura, Università di Udine, Udine, Italy
- 67 (a)INFN Sezione di Lecce, Lecce, Italy; (b)Dipartimento di Matematica e Fisica, Università del Salento, Lecce, Italy
- 68 (a)INFN Sezione di Milano, Milan, Italy; (b)Dipartimento di Fisica, Università di Milano, Milan, Italy
- 69 (a)INFN Sezione di Napoli, Naples, Italy; (b)Dipartimento di Fisica, Università di Napoli, Naples, Italy
- 70 (a)INFN Sezione di Pavia, Pavia, Italy; (b)Dipartimento di Fisica, Università di Pavia, Pavia, Italy
- 71 (a)INFN Sezione di Pisa, Pisa, Italy; (b)Dipartimento di Fisica E. Fermi, Università di Pisa, Pisa, Italy
- 72 (a)INFN Sezione di Roma, Rome, Italy; (b)Dipartimento di Fisica, Sapienza Università di Roma, Rome, Italy
- 73 (a)INFN Sezione di Roma Tor Vergata, Rome, Italy; (b)Dipartimento di Fisica, Università di Roma Tor Vergata, Rome, Italy
- 74 (a)INFN Sezione di Roma Tre, Rome, Italy; (b)Dipartimento di Matematica e Fisica, Università Roma Tre, Rome, Italy
- 75 (a)INFN-TIFPA, Trento, Italy; (b)Università degli Studi di Trento, Trento, Italy
- 76 Institut für Astro- und Teilchenphysik, Leopold-Franzens-Universität, Innsbruck, Austria
- 77 University of Iowa, Iowa City, IA, USA
- 78 Department of Physics and Astronomy, Iowa State University, Ames, IA, USA
- 79 Joint Institute for Nuclear Research, Dubna, Russia
- 80 (a)Departamento de Engenharia Elétrica, Universidade Federal de Juiz de Fora (UFJF), Juiz de Fora, Brazil; (b)Universidade Federal do Rio De Janeiro COPPE/EE/IF, Rio de Janeiro, Brazil; (c)Universidade Federal de São João del Rei (UFSJ), São João del Rei, Brazil; (d)Instituto de Física, Universidade de São Paulo, São Paulo, Brazil

- 81 KEK, High Energy Accelerator Research Organization, Tsukuba, Japan
- 82 Graduate School of Science, Kobe University, Kobe, Japan
- 83 (a) AGH University of Science and Technology, Faculty of Physics and Applied Computer Science, Krakow, Poland; (b) Marian Smoluchowski Institute of Physics, Jagiellonian University, Kraków, Poland
- 84 Institute of Nuclear Physics Polish Academy of Sciences, Kraków, Poland
- 85 Faculty of Science, Kyoto University, Kyoto, Japan
- 86 Kyoto University of Education, Kyoto, Japan
- 87 Research Center for Advanced Particle Physics and Department of Physics, Kyushu University, Fukuoka, Japan
- 88 Instituto de Física La Plata, Universidad Nacional de La Plata and CONICET, La Plata, Argentina
- 89 Physics Department, Lancaster University, Lancaster, UK
- 90 Oliver Lodge Laboratory, University of Liverpool, Liverpool, UK
- 91 Department of Experimental Particle Physics, Jožef Stefan Institute and Department of Physics, University of Ljubljana, Ljubljana, Slovenia
- 92 School of Physics and Astronomy, Queen Mary University of London, London, UK
- 93 Department of Physics, Royal Holloway University of London, Egham, UK
- 94 Department of Physics and Astronomy, University College London, London, UK
- 95 Louisiana Tech University, Ruston, LA, USA
- 96 Fysiska institutionen, Lunds universitet, Lund, Sweden
- 97 Centre de Calcul de l'Institut National de Physique Nucléaire et de Physique des Particules (IN2P3), Villeurbanne, France
- 98 Departamento de Física Teórica C-15 and CIAFF, Universidad Autónoma de Madrid, Madrid, Spain
- 99 Institut für Physik, Universität Mainz, Mainz, Germany
- 100 School of Physics and Astronomy, University of Manchester, Manchester, UK
- 101 CPPM, Aix-Marseille Université, CNRS/IN2P3, Marseille, France
- 102 Department of Physics, University of Massachusetts, Amherst, MA, USA
- 103 Department of Physics, McGill University, Montreal, QC, Canada
- 104 School of Physics, University of Melbourne, Victoria, Australia
- 105 Department of Physics, University of Michigan, Ann Arbor, MI, USA
- 106 Department of Physics and Astronomy, Michigan State University, East Lansing, MI, USA
- 107 B.I. Stepanov Institute of Physics, National Academy of Sciences of Belarus, Minsk, Belarus
- 108 Research Institute for Nuclear Problems of Byelorussian State University, Minsk, Belarus
- 109 Group of Particle Physics, University of Montreal, Montreal, QC, Canada
- 110 P.N. Lebedev Physical Institute of the Russian Academy of Sciences, Moscow, Russia
- 111 Institute for Theoretical and Experimental Physics of the National Research Centre Kurchatov Institute, Moscow, Russia
- 112 National Research Nuclear University MEPhI, Moscow, Russia
- 113 D.V. Skobel'syn Institute of Nuclear Physics, M.V. Lomonosov Moscow State University, Moscow, Russia
- 114 Fakultät für Physik, Ludwig-Maximilians-Universität München, Munich, Germany
- 115 Max-Planck-Institut für Physik (Werner-Heisenberg-Institut), Munich, Germany
- 116 Nagasaki Institute of Applied Science, Nagasaki, Japan
- 117 Graduate School of Science and Kobayashi-Maskawa Institute, Nagoya University, Nagoya, Japan
- 118 Department of Physics and Astronomy, University of New Mexico, Albuquerque, NM, USA
- 119 Institute for Mathematics, Astrophysics and Particle Physics, Radboud University Nijmegen/Nikhef, Nijmegen, The Netherlands
- 120 Nikhef National Institute for Subatomic Physics and University of Amsterdam, Amsterdam, The Netherlands
- 121 Department of Physics, Northern Illinois University, DeKalb, IL, USA
- 122 (a) Budker Institute of Nuclear Physics and NSU, SB RAS, Novosibirsk, Russia; (b) Novosibirsk State University Novosibirsk, Novosibirsk, Russia
- 123 Institute for High Energy Physics of the National Research Centre Kurchatov Institute, Protvino, Russia
- 124 Department of Physics, New York University, New York, NY, USA
- 125 Ochanomizu University, Otsuka, Bunkyo-ku, Tokyo, Japan
- 126 Ohio State University, Columbus, OH, USA
- 127 Faculty of Science, Okayama University, Okayama, Japan
- 128 Homer L. Dodge Department of Physics and Astronomy, University of Oklahoma, Norman, OK, USA

- 129 Department of Physics, Oklahoma State University, Stillwater, OK, USA
- 130 Palacký University, RCPTM, Joint Laboratory of Optics, Olomouc, Czech Republic
- 131 Center for High Energy Physics, University of Oregon, Eugene, OR, USA
- 132 LAL, Université Paris-Sud, CNRS/IN2P3, Université Paris-Saclay, Orsay, France
- 133 Graduate School of Science, Osaka University, Osaka, Japan
- 134 Department of Physics, University of Oslo, Oslo, Norway
- 135 Department of Physics, Oxford University, Oxford, UK
- 136 LPNHE, Sorbonne Université, Université de Paris, CNRS/IN2P3, Paris, France
- 137 Department of Physics, University of Pennsylvania, Philadelphia, PA, USA
- 138 Konstantinov Nuclear Physics Institute of National Research Centre “Kurchatov Institute”, PNPI, St. Petersburg, Russia
- 139 Department of Physics and Astronomy, University of Pittsburgh, Pittsburgh, PA, USA
- 140 (a) Laboratório de Instrumentação e Física Experimental de Partículas-LIP, Lisbon, Portugal; (b) Departamento de Física, Faculdade de Ciências, Universidade de Lisboa, Lisbon, Portugal; (c) Departamento de Física, Universidade de Coimbra, Coimbra, Portugal; (d) Centro de Física Nuclear da Universidade de Lisboa, Lisbon, Portugal; (e) Departamento de Física, Universidade do Minho, Braga, Portugal; (f) Universidad de Granada, Granada, Spain; (g) Dep Física and CEFITEC of Faculdade de Ciências e Tecnologia, Universidade Nova de Lisboa, Caparica, Portugal; (h) Av. Rovisco Pais, 1, 1049-001 Lisbon, Portugal
- 141 Institute of Physics of the Czech Academy of Sciences, Prague, Czech Republic
- 142 Czech Technical University in Prague, Prague, Czech Republic
- 143 Charles University, Faculty of Mathematics and Physics, Prague, Czech Republic
- 144 Particle Physics Department, Rutherford Appleton Laboratory, Didcot, UK
- 145 IRFU, CEA, Université Paris-Saclay, Gif-sur-Yvette, France
- 146 Santa Cruz Institute for Particle Physics, University of California Santa Cruz, Santa Cruz, CA, USA
- 147 (a) Departamento de Física, Pontificia Universidad Católica de Chile, Santiago, Chile; (b) Departamento de Física, Universidad Técnica Federico Santa María, Valparaíso, Chile
- 148 Department of Physics, University of Washington, Seattle, WA, USA
- 149 Department of Physics and Astronomy, University of Sheffield, Sheffield, UK
- 150 Department of Physics, Shinshu University, Nagano, Japan
- 151 Department Physik, Universität Siegen, Siegen, Germany
- 152 Department of Physics, Simon Fraser University, Burnaby, BC, Canada
- 153 SLAC National Accelerator Laboratory, Stanford, CA, USA
- 154 Physics Department, Royal Institute of Technology, Stockholm, Sweden
- 155 Departments of Physics and Astronomy, Stony Brook University, Stony Brook, NY, USA
- 156 Department of Physics and Astronomy, University of Sussex, Brighton, UK
- 157 School of Physics, University of Sydney, Sydney, Australia
- 158 Institute of Physics, Academia Sinica, Taipei, Taiwan
- 159 (a) E. Andronikashvili Institute of Physics, Iv. Javakhishvili Tbilisi State University, Tbilisi, Georgia; (b) High Energy Physics Institute, Tbilisi State University, Tbilisi, Georgia
- 160 Department of Physics, Technion, Israel Institute of Technology, Haifa, Israel
- 161 Raymond and Beverly Sackler School of Physics and Astronomy, Tel Aviv University, Tel Aviv, Israel
- 162 Department of Physics, Aristotle University of Thessaloniki, Thessaloníki, Greece
- 163 International Center for Elementary Particle Physics and Department of Physics, University of Tokyo, Tokyo, Japan
- 164 Graduate School of Science and Technology, Tokyo Metropolitan University, Tokyo, Japan
- 165 Department of Physics, Tokyo Institute of Technology, Tokyo, Japan
- 166 Tomsk State University, Tomsk, Russia
- 167 Department of Physics, University of Toronto, Toronto, ON, Canada
- 168 (a) TRIUMF, Vancouver, BC, Canada; (b) Department of Physics and Astronomy, York University, Toronto, ON, Canada
- 169 Division of Physics, Tomonaga Center for the History of the Universe, Faculty of Pure and Applied Sciences, University of Tsukuba, Tsukuba, Japan
- 170 Department of Physics and Astronomy, Tufts University, Medford, MA, USA
- 171 Department of Physics and Astronomy, University of California Irvine, Irvine, CA, USA
- 172 Department of Physics and Astronomy, University of Uppsala, Uppsala, Sweden
- 173 Department of Physics, University of Illinois, Urbana, IL, USA

- 174 Instituto de Física Corpuscular (IFIC), Centro Mixto Universidad de Valencia-CSIC, Valencia, Spain
- 175 Department of Physics, University of British Columbia, Vancouver, BC, Canada
- 176 Department of Physics and Astronomy, University of Victoria, Victoria, BC, Canada
- 177 Fakultät für Physik und Astronomie, Julius-Maximilians-Universität Würzburg, Würzburg, Germany
- 178 Department of Physics, University of Warwick, Coventry, UK
- 179 Waseda University, Tokyo, Japan
- 180 Department of Particle Physics, Weizmann Institute of Science, Rehovot, Israel
- 181 Department of Physics, University of Wisconsin, Madison, WI, USA
- 182 Fakultät für Mathematik und Naturwissenschaften, Fachgruppe Physik, Bergische Universität Wuppertal, Wuppertal, Germany
- 183 Department of Physics, Yale University, New Haven, CT, USA
- 184 Yerevan Physics Institute, Yerevan, Armenia
- ^a Also at Borough of Manhattan Community College, City University of New York, New York NY, USA
- ^b Also at CERN, Geneva, Switzerland
- ^c Also at CPPM, Aix-Marseille Université, CNRS/IN2P3, Marseille, France
- ^d Also at Département de Physique Nucléaire et Corpusculaire, Université de Genève, Genève, Switzerland
- ^e Also at Departament de Física de la Universitat Autònoma de Barcelona, Barcelona, Spain
- ^f Also at Departamento de Física, Instituto Superior Técnico, Universidade de Lisboa, Lisboa, Portugal
- ^g Also at Department of Applied Physics and Astronomy, University of Sharjah, Sharjah, United Arab Emirates
- ^h Also at Department of Financial and Management Engineering, University of the Aegean, Chios, Greece
- ⁱ Also at Department of Physics and Astronomy, Michigan State University, East Lansing MI, USA
- ^j Also at Department of Physics and Astronomy, University of Louisville, Louisville, KY, USA
- ^k Also at Department of Physics, Ben Gurion University of the Negev, Beer Sheva, Israel
- ^l Also at Department of Physics, California State University, East Bay, USA
- ^m Also at Department of Physics, California State University, Fresno, USA
- ⁿ Also at Department of Physics, California State University, Sacramento, USA
- ^o Also at Department of Physics, King's College London, London, UK
- ^p Also at Department of Physics, St. Petersburg State Polytechnical University, St. Petersburg, Russia
- ^q Also at Department of Physics, Stanford University, Stanford CA, USA
- ^r Also at Department of Physics, University of Adelaide, Adelaide, Australia
- ^s Also at Department of Physics, University of Fribourg, Fribourg, Switzerland
- ^t Also at Department of Physics, University of Michigan, Ann Arbor MI, USA
- ^u Also at Department of Physics, University of Toronto, Toronto ON, Canada
- ^v Also at Dipartimento di Matematica, Informatica e Fisica, Università di Udine, Udine, Italy
- ^w Also at Faculty of Physics, M.V. Lomonosov Moscow State University, Moscow, Russia
- ^x Also at Giresun University, Faculty of Engineering, Giresun, Turkey
- ^y Also at Graduate School of Science, Osaka University, Osaka, Japan
- ^z Also at Hellenic Open University, Patras, Greece
- ^{aa} Also at Institutio Catalana de Recerca i Estudis Avancats, ICREA, Barcelona, Spain
- ^{ab} Also at Institut für Experimentalphysik, Universität Hamburg, Hamburg, Germany
- ^{ac} Also at Institute for Mathematics, Astrophysics and Particle Physics, Radboud University Nijmegen/Nikhef, Nijmegen, The Netherlands
- ^{ad} Also at Institute for Nuclear Research and Nuclear Energy (INRNE) of the Bulgarian Academy of Sciences, Sofia, Bulgaria
- ^{ae} Also at Institute for Particle and Nuclear Physics, Wigner Research Centre for Physics, Budapest, Hungary
- ^{af} Also at Institute of Particle Physics (IPP), Vancouver, Canada
- ^{ag} Also at Institute of Physics, Academia Sinica, Taipei, Taiwan
- ^{ah} Also at Institute of Physics, Azerbaijan Academy of Sciences, Baku, Azerbaijan
- ^{ai} Also at Institute of Theoretical Physics, Ilia State University, Tbilisi, Georgia
- ^{aj} Also at Instituto de Física Teórica, IFT-UAM/CSIC, Madrid, Spain
- ^{ak} Also at Istanbul University, Dept. of Physics, Istanbul, Turkey
- ^{al} Also at Joint Institute for Nuclear Research, Dubna, Russia

- ^{am} Also at LAL, Université Paris-Sud, CNRS/IN2P3, Université Paris-Saclay, Orsay, France
- ^{an} Also at Louisiana Tech University, Ruston LA, USA
- ^{ao} Also at LPNHE, Sorbonne Université, Université de Paris, CNRS/IN2P3, Paris, France
- ^{ap} Also at Manhattan College, New York NY, USA
- ^{aq} Also at Moscow Institute of Physics and Technology State University, Dolgoprudny, Russia
- ^{ar} Also at National Research Nuclear University MEPhI, Moscow, Russia
- ^{as} Also at Physics Department, An-Najah National University, Nablus, Palestine
- ^{at} Also at Physics Dept, University of South Africa, Pretoria, South Africa
- ^{au} Also at Physikalisches Institut, Albert-Ludwigs-Universität Freiburg, Freiburg, Germany
- ^{av} Also at School of Physics, Sun Yat-sen University, Guangzhou, China
- ^{aw} Also at The City College of New York, New York NY, USA
- ^{ax} Also at The Collaborative Innovation Center of Quantum Matter (CICQM), Beijing, China
- ^{ay} Also at Tomsk State University, Tomsk, and Moscow Institute of Physics and Technology State University, Dolgoprudny, Russia
- ^{az} Also at TRIUMF, Vancouver BC, Canada
- ^{ba} Also at Università di Napoli Parthenope, Napoli, Italy
- * Deceased